Spring 5-2009

Design, Synthesis, and Film Formation of Fluorine Containing Colloidal Dispersions

Anuradha Misra
University of Southern Mississippi

The University of Southern Mississippi

DESIGN, SYNTHESIS, AND FILM FORMATION OF FLUORINE CONTAINING COLLOIDAL DISPERSIONS

by

Anuradha Misra

Abstract of a Dissertation
Submitted to the Graduate Studies Office
of The University of Southern Mississippi
in Partial Fulfillment of the Requirements
for the Degree of Doctor of Philosophy

May 2009

The University of Southern Mississippi

DESIGN, SYNTHESIS, AND FILM FORMATION OF FLUORINE CONTAINING COLLOIDAL DISPERSIONS

by

Anuradha Misra

A Dissertation
Submitted to the Graduate Studies Office
of The University of Southern Mississippi
in Partial Fulfillment of the Requirements
for the Degree of Doctor of Philosophy

Approved:

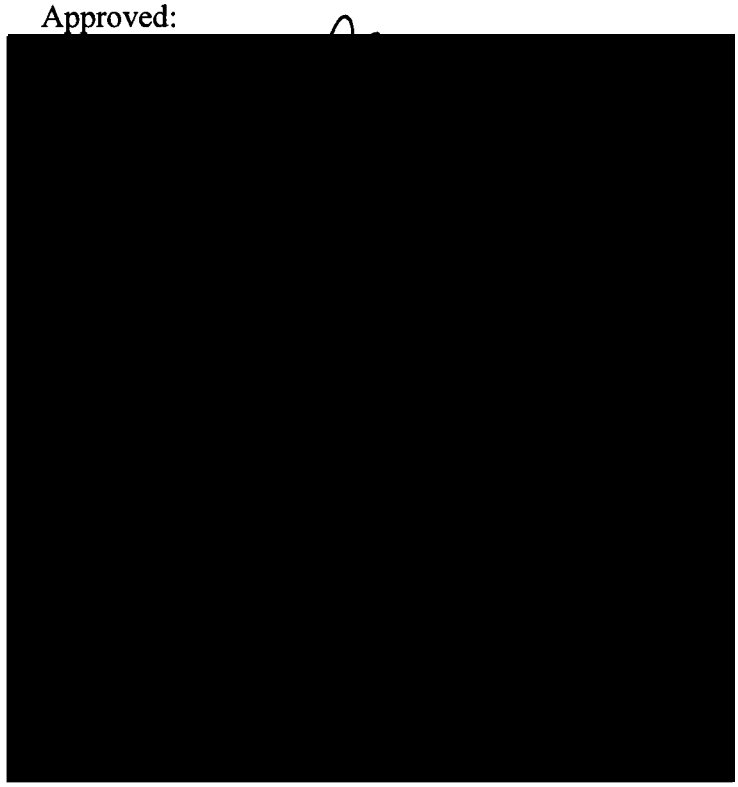

May 2009

ABSTRACT

DESIGN, SYNTHESIS, AND FILM FORMATION OF FLUORINE CONTAINING COLLOIDAL DISPERSIONS

by Anuradha Misra

May 2009

Fluoropolymers (FPs) have been subject of interest for many years, however due to extreme synthetic and processing conditions their applications have been limited. This dissertation focuses on design and synthesis of fluorine containing colloidal dispersions to advance limited knowledge and to gain further understanding of fluorine containing colloidal dispersions. Fluoroacrylates and fluoro methacrylates consisting of varying chain length of perfluoroalkyl side chain were copolymerized with methylmethacrylate (MMA) and n-butylacrylate (n-BA) under aqueous environment utilizing phospholipids (PLs) as dispersing agent. Morphologies of colloids, coalescence, and film formation processes after water evaporation was investigated using various microscopic probes such as transmission electron microscope (TEM), atomic force microscopy (AFM), nuclear magnetic resonance (NMR), infrared (IR), and internal reflection infrared imaging (IRIRI). These studies showed that FPs exist as phase-separated domains within colloidal particles leading to unique non-spherical morphologies where blocky phase of FPs exists on the p-MMA/nBA core. Upon coalescence FPs migrates to the film-air (F-A) interface, generating highly hydrophobic and ultra low coefficient of friction surfaces. Further studies focused on utilization of pentafluorostyrene (PFS) as fluorinated component incorporated into p-MMA/nBA colloids, which upon copolymerization with polyethyleneglycol (PEG) molecules leads

to surfaces that repel proteins. Copolymerizing PFS in two step synthetic processes, resulted in unique acorn-shaped colloids that consist of two phases p-MMA/nBA and p-nBA/PFS. These acorn-shaped colloids are able to self-assemble which is driven by the surface energies of substrates. For high surface energy substrates, such as glass, fluorinated phase is observed at the F-A interface, but for low surface energy substrates, such as polytetrafluoroethylene (PTFE), hydrogenated phase is exposed at the F-A interface. Using a number of spectroscopic and morphological analytical approaches combined with contact angle analysis as well as thermodynamic modeling aspects of acorn-shaped particles, morphologies and film formations were examined and confirmed the self-assembly of acorn-shaped colloidal particles.

ACKNOWLEDGEMENTS

I would like to thank my research advisor, Dr. Marek Urban, for his guidance, support, and encouragement throughout my graduate career. Through his leadership, he empowered me with the ability to question thoughts and generate creative ideas. His insightful comments and technical advice at different stages of research helped me gain the level of intelligence that I feel will remain with me throughout my professional career. I would also like to thank him for acquiring the funding necessary to pursue my graduate degree in Polymer Science and Engineering.

I would also like to thank my graduate committee members Dr. Robert Lochhead, Dr. Kenneth Mauritz, Dr. William Jarrett, and Dr. Jeffrey Wiggins for their advice and support throughout the duration of these studies. Special gratitude to Dr. William Jarrett for helping me develop a deep understanding and appreciation of NMR spectroscopy while assisting with numerous NMR experiments conducted for this research.

Special appreciation goes to the Urban Research Group both past and present, for their continuous friendship and support. Irene Gorman is also acknowledged for the efforts in molecular weight studies. Financially, this work was supported primarily by the National Science Foundation Materials Research Science Engineering Center (NSF MRSEC) program under award number DMR 0213883.

TABLE OF CONTENTS

LIST OF ILLUSTRATIONS

Figure

LIST OF SCHEMES

Scheme

LIST OF TABLES

INTRODUCTION

This dissertation is concerned with the synthesis and film formation mechanism of fluorine containing colloidal dispersions. The goal is to advance limited synthetic knowledge of fluoro colloids pertaining to molecular level processes governing phase-separation within colloidal particles, morphologies of colloids, coalesce of particles and surface interfacial properties. A major portion of this work is focused on the environmental compliant synthesis resulting in asymmetric nano-colloids, and understanding coalescence mechanisms via molecular level spectroscopic and microscopic approaches which have been used in these studies.

Chapter I provides background information on fluoropolymers (FPs), along with an overview of relevant literature. Various synthetic approaches utilized for obtaining FPs and fluorine colloids have been discussed along with the surface-interfacial properties after film formation. This chapter also outline existing shortcomings of existing synthetic aspects of FPs and limited knowledge of their coalesce.

Chapter II addresses the formation of non-spherical colloidal particles in which up to 15% w/w heptadecafluorodecylmethacrylate (FMA) have been copolymerized with methylmethacrylate (MMA) and n-butylacrylate (nBA) by utilizing bio-active dispersing agent phospholipids (PLs). The non-spherical morphologies of p-MMA/nBA/FMA colloidal particles is addressed. The role of PLs will be discussed in the context of stability as well as facilitating polymerization of FMA. Coalescence mechanism of non-spherical colloids is reported by capturing different stages of coalescence via transmission electron microscope (TEM). Surface properties and chemical makeup in which p-FMA migrates to the F-A Interface are reported.

Chapter III further elaborates on the origin of non-spherical morphologies of p-MMA/nBA/FMA colloidal particles synthesized in an aqueous phase in the presence of bio-active dispersing agents. The morphologies of colloids depend upon MMA/nBA ratios and lead to significantly different coalescence mechanisms and consequently surface properties. For higher MMA content, the particles are spherical, but at higher nBA contents, non-spherical morphologies are observed. This behavior is attributed to monomer starved conditions and the differences in reactivity ratios which force copolymerization of FMA on the surface of p-MMA/n-BA particles, giving rise to non-spherical morphologies in the presence of biologically active PLs. Surface properties such as coefficients of frictions and thermo-responsiveness of p-FMA are addressed.

Chapter IV illustrate copolymerization of fluoromonomers with various chain lengths of perfluoroalkyl side chain such as heptafluorobutylmethacrylate (FBMA), heptafluorobutylacrylate (FBA), FMA, and heptadecafluorodecylacrylate (FA) with MMA and n-BA monomers which resulted in the formation of stable non-spherical colloidal dispersions that contain up to 15% (w/w) of the fluoropolymer (FP) phase. These studies report for the first time an aqueous phase FP colloidal dispersion synthesis without the use of fluoro-dispersing agents. Thermodynamic molecular modeling simulations show that the co-existence of fluorinated and non-fluorinated segments is energetically favorable and the presence of FP phase decreases the cohesive energy density of macromolecular chains. These predictions are in agreement with the experimental results. Non-spherical FP containing colloidal particles coalesce to form stable films with ultra low static and kinetic coefficients of friction as well as the low surface energy which result from stratification of the FP phase near the film-air (F-A)

interface and surface properties are proportional to the perfluoroalkyl side chain length of FP segment.

Chapter V describes a new family of water dispersible colloidal particles composed of p-MMA/nBA/Pentafluorostyrene (PFS)/poly (ethylene glycol) dimethacrylate (PEG) copolymers which coalesce at room temperature. These stable colloidal dispersions contain up to 30% w/w PEG and 35% w/w PFS, and exhibit core-shell morphologies that consist of the p-MMA/nBA/PFS core and the PEG shell. Solid state 2D NMR, internal reflection infrared imaging (IRIRI), and atomic force microscopy (AFM) analysis showed that after coalescence the surface contains PEG-rich component which, combined with fluorinated domains result in hydrophobic and hydrophilic segments that inhibit protein adsorption. Adsorption of bovine serum albumin (BSA), lipopolysacharide (Lipopoly), and fibrinogen (Fib) on p-MMA/nBA/PFS, and p-MMA/nBA/PFS/PEG (5, 10, 20, and 30 %) film surfaces revealed that the proteins exhibit higher affinity towards p-MMA/nBA/PFS surfaces, but the presence of PEG incorporated into p-MMA/nBA/PFS colloidal particles results in significantly reduced protein adsorption and compositional heterogeneity of the PFS and PEG phases is believed to be responsible for a minimal affinity for the protein adsorption.

Chapter VI illustrates the synthesis of phase separated two distinct phases within one colloidal particle which consist of p-MMA/nBA and p-nBA/PFS phases and exhibit a unique acorn-shaped morphologies. These colloidal particles are capable of self-assembling on surfaces, and depending on the surface energy of a substrate, create hydrophobic or hydrophilic F-A interfaces, such that when coalesced on a high surface

tension substrate, the p-PFS phase expresses itself near the F-A interface, whereas for low surface energy substrates the p-PFS phase is near the film-substrate (F-S) interface. Using a number of spectroscopic and morphological analytical approaches combined with contact angle analysis this phenomenon is reported.

CHAPTER I

FLUORINE CONTAINING COLLOIDS AND FILM FORMATION

Introduction

Due to high thermal stability, superb chemical resistance, excellent mechanical properties and weatherability, low flammability as well as low refractive index, fluorinated polymers have attracted significant scientific and commercial attention.[1] The development of fluoropolymers (FPs) began with the invention of polytetrafluoroethylene (PTFE) in 1938. While working with chlorofluorocarbon (CFC) refrigerants, Roy J. Plunkett (1910–1994) of DuPont observed that tetrafluoroethylene gas (TFE) stored at low temperatures turned into a white powder. Upon further characterization he determined that the substance was heat resistant, chemically inert, and possessed low surface friction properties. As it turned out, TFE gas had spontaneously polymerized to form PTFE, later designated by the trade name of Teflon.[1] Since that discovery FPs have been widely used as thermoplastics, elastomers, textile finishes, coatings, and due to their unique physical and chemical properties, as functional materials.

Although the unique properties due to presence of fluorine atom in the polymer backbone of FPs are attractive, there exist a number of synthetic and processing challenges due to their poor solubility, enhanced crystallinty, elevated melting points (T_m), and glass transition temperatures (T_g). In an effort to overcome these problems, chemical and structural modifications of FPs have been employed. For example, incorporation of hexafluoropropylene and perfluoro(propyl vinyl ether) into the polymer backbone alter properties,[1] such as soluble fluoroolefin-vinyl ether copolymers

(Lumiflon®) have been developed which allow less stringent application methods while obtaining good compatibility, and crosslinking along with hardness and adhesion. As illustrated in Figure I-1, altering functional groups along the polymer backbone allow for tailoring of specific properties. When R_1 is n-butyl acrylate (nBA), the T_g of the copolymer will be lowered, but by the incorporation of $-CF_3$ end groups on alkyl side chains of fluoro-acrylates lower surface energies will be achieved, and improvements in properties such as weather and chemical resistance may be obtained relative to PTFE-like materials containing the $-CF_2-$ moiety in the polymer backbone.[2] Furthermore, incorporation of R_3-COOH and R_4-OH functionalities will provide an opportunity for compatibility and crosslinking enhancements. It should be also noted that latex blends consisting of fluorinated and fluorine-free acrylates have been shown to give superior performance compared to those derived from corresponding random copolymers.[9-11] For example, fluorine-containing acrylic copolymer latexes were prepared by emulsion polymerization of styrene and n-butyl acrylate with different compositions of a fluorinated acrylic monomer. In essence, by incorporating appropriate $R_1 - R_4$ groups, such as alkyl, cycloalkyl, alkene, and cycloalkene, numerous properties may be altered, including crosslinking and water solubility via OH or COOH functionalities.

Synthetic Aspects of Fluoro-Polymerization

Various synthetic approaches previously utilized to synthesize FPs are free radical bulk, solution, suspension and emulsion polymerization.[3, 4] Due to low intermolecular attractive forces and insolubility of FPs in most polar and nonpolar solvents halogenated solvents are utilized in their free radical synthesis as organic solvents.[5, 6] Bulk and solution polymerization of fluoromonomers are limited because

of the use of halogenated solvents during synthesis and also during free radical fluoroolefin polymerizations fluorinated free radicals are highly electrophilic, they readily abstract hydrogen atoms from nearly all hydrocarbons thus rendering the synthesis of high molecular weight fluoropolymers in most hydrogen-containing solvents.[7, 8] The use of CFCs circumvents these problems; however, CFCs have fallen under strict regulation due to environmental concerns and as a result, are no longer viable to be used as a reaction media. Fluoromonomers can be polymerized by controlled radical polymerization (CRP) methods in bulk or in solution, which are often involved with specific fluorinated solvents. Although CRP allowed for the development of advanced well-defined copolymers with various architecture (block, star, dendritic, alternating or graft) having predictable molecular weights and low molecular weight distributions. Recent research involving the three main CRP techniques, namely atom transfer radical polymerization (ATRP),[9-14] nitroxide-mediated radical polymerization (NMP),[15, 16] and reversible addition-fragmentation chain-transfer (RAFT),[17-19] have furnished various fluorinated materials and architecture. However, these approaches are focused on achieving desired FPs by detailed synthetic efforts utilizing fluorinated and chlorinated solvents and have limitations such as for NMP, this method works best for styrenes and acrylates. For ATRP catalyst is left in the system and certain functional groups such as carboxylic acids and ionic groups react with catalyst and limited monomer types. Only a few RAFT agents are available commercially and new efforts are welcome to synthesize new agents. Another disadvantage of RAFT is that the products contain the thiocarbonylthio-moiety giving different colored polymers, which for some applications are unacceptable.[20] Table I-1

lists the polymerization process utilized for FPs synthesis, type of monomers that is utilized, reaction conditions, advantages, and limitations.

Other than detailed synthetic efforts and limitations leading to free radical bulk and solution polymerization process one of the main disadvantage is the use of CFCs during synthesis and elaborate synthetic and processing procedures. The use and production of fluoro and chloro-containing polymers was identified as one of the causes for diminishing of the ozone layer due to emission of CFCs.[21] The primary problems associated with the production and applications of fluoro and chloro polymers are their insolubility in common organic solvents, thus requiring the use of CFCs during their polymerization.[5, 6]

Other synthetic approaches utilized in FPs synthesis are suspension and emulsion polymerization. Suspension polymerization occurs when monomer droplets are suspended in a continuous aqueous or organic medium. Organic-soluble initiators are used to induce polymerization inside the monomer droplets. Surfactants can be added as stabilizing agents at concentrations typically too low to form micellar structures. Therefore, polymer particles are unable to remain suspended in the continuous phase without adequate agitation. Typically, bulk polymerization kinetics govern suspension polymerization reactions.[3]

An alternative method for producing FPs is emulsion polymerization[22] which is a free-radically initiated process where monomers are polymerized in the presence of an aqueous solution containing surfactant molecules. The product is a dispersion of solid colloidal particles of polymer in an aqueous medium, which are synthesized via a multi-component process involving monomers, initiators, surfactants, and water as a

continuous phase.[22] However, several factors affect various stages of synthesis to result in stable dispersions. Colloidal dispersion synthesis may be initiated when the surfactant concentration surpasses the critical micelle concentration (CMC) in water. Above the CMC, the concentration of singly dispersed surfactant molecules remains virtually constant due to the formation of micelles which are formed as a result of hydrophobic segments of amphiphilic molecules minimizing their exposure to the aqueous media. As illustrated in Figure I-2, A, these thermodynamically stable entities are capable of compartmentalizing monomer molecules that diffuse through the continuous phase from the monomer droplet. At the same time, a water-soluble initiator is cleaved thermally or photo-chemically (B), which initiates polymerization in the hydrophobic core of the micelle (B). As monomer continues to diffuse from the droplets and polymerize within micelles, surfactant molecules may be adsorbed from other micelles, solution, and monomer droplets.[23] Upon exhaustion of the monomer droplets, the reaction ceases, thus forming solid colloidal particles dispersed in the aqueous phase (C). The number of polymer particles that may be stabilized during synthesis depends on the total surface area created by surfactant molecules and the relationship[24] that governs this process is described as follows in Equation 2.

$$N = k(\rho/\mu)^{(1-z)}(a_s S)^z \qquad (2)$$

Where: N is the particle number, k is a constant with $0.37<k<0.53$, and depends on the efficiency of radical capture by micelles, ρ is the rate of radical generation, μ is the rate of volume increase of a polymer particle, a_s is the interfacial surface area occupied by a surfactant molecule, S is the total amount of surfactant in the micelles, and z, a chain transfer constant ($0.6<z<1.0$) depends on the chain transfer and water solubility of the

monomer.[23] A low value of N indicates a larger particle diameter whereas high numbers represent smaller particle sizes with a greater colloidal viscosity and surface area. As a result, altering the concentration of surface stabilizing species has a dramatic effect on the number of stable colloidal particles formed during synthesis which, when considering polymerization kinetics, may be described in three simplified stages shown in Figure I-3.

As seen in Stage I, the rate of polymerization (R_p) increases as a function of time. During this period, monomers are free-radically initiated within micelles, and as propagation continues, monomers diffuse from droplets to micelles, replenishing those which have reacted. At the same time, surfactant molecules are depleted from the continuous phase and micelles not containing initiated monomer. At the end of Stage I, R_p reach a steady value as a finite number of polymer particles are polymerizing as shown in Figure I-3.

During Stage II, R_p remain constant as monomers diffuse from the monomer droplets to the active polymer particles, and once the droplets have been depleted, Stage III begins. At this point, the remaining monomers are consumed and R_p decreases as the particles cease polymerization (Figure I-3). N increases linearly with increasing Rp in Stage I, and becomes constant after that in stage II and III.

Utilizing fundamental aspects of emulsion polymerization wide range of fluoromonomers can be polymerized via emulsion process. One of the most commonly utilized FPs is PTFE, which is typically prepared by utilizing potassium persulfate as an initiator at 70-120 °C under pressurized suspension or emulsion polymerization conditions.[25] Elevated pressures (10 bar) are required for gaseous monomer (TFE) to be

forced into an aqueous phase. When suspension polymerization is employed, a coagulated PTFE resin is produced by vigorous agitation with virtually no dispersing agents.[25] In emulsion polymerization, a semi-batch reactor with a continuous TFE flow is utilized,[6] thus sharing characteristics of a typical emulsion process, but surfactant concentration levels are typically below CMC.[25,1] In an effort to avoid coagulation of particles, hydrocarbon waxes are employed.

Derivatives of PTFE, such as poly (vinylidene fluoride) (PVDF) and poly (vinyl fluoride) (PVF) can be also prepared by suspension or emulsion polymerization methods under pressurized conditions.[8] Although both synthesis are driven by a free radical polymerization process, there are often a number of complexities during synthesis such as formation of branched chains, removal of the resulting unstable acid fluorides end groups which arises from initiators. [8] This is particularly important if pre-polymers have reactive groups serving as precursors for further crosslinking reactions. Also, one of the important factors to the polymerization is monomer storage and handling, for example, TFE is flammable when mixed with air and has a high propensity for explosion during expansion to a gas from its liquid phase under pressure. Further, TFE is highly explosive as a gas at elevated temperatures. In the presence of oxygen it will undergo auto-polymerization, a process sufficiently exothermic to ignite explosion.

Carbon dioxide (CO_2) has recently been employed as an inert medium for a variety of free-radical polymerization reactions.[26, 27] CO_2 has even proved inert to the highly electrophilic fluorocarbon radicals based on TFE. Thus CO_2 is rapidly becoming alternative to liquid solvents for polymerization process, since it is an environmentally

benign medium which has the potential to eliminate the production of organic wastes and product obtained is usually in powder form after the evaporation of CO_2. Solubility of fluoro monomers in CO_2 gives an opportunity to polymerize under supercritical CO_2 ($ScCO_2$). [28-30] Polymerization in CO_2 phase results in spherical colloidal particles using CO_2-soluble amphiphiles. Figure I-4 shows scanning electron micrographs (SEMs) of colloidal particles of PTFE prepared using a hybrid CO_2/aqueous system with added surfactant (A), and using conventional TFE dispersion polymerization methods (B).[27] As seen spherical particles were produced as by the conventional TFE dispersion polymerization in aqueous medium. Thus successful development of $ScCO_2$ process,[28-30] provides an attractive alternative for a wide variety of chemical and industrial processes that involve pressurized polymerization conditions.[28, 29, 31-33] While these efforts have led to new technologies, one of the limiting factors is attributed to the use of fluoro dispersing agents, pressurized polymerization conditions, and further processing step for coating applications after synthesis.

Although $ScCO_2$ provides approach without the use of CFCs during synthesis of FPs, but one would like to design and synthesize FPs under aqueous system and without the use of fluoro-surfactants; such that the product can be directly applied as coating material. Although TFE and its derivatives are most studied in the literature, Acrylate polymers containing perfluoroalkyl side chains have advantages such as fluorinated acrylates have not been studied in detail and utilized their full potential. Some of the advantages of fluorinated acrylates are good reactivity with fluorine free acrylates, the low intermolecular force between perfluoroalkyl side chains and the air lowers the surface free energy of polymers, and the acrylic main chains ensure that polymers can

adhere to matrices. The $-CF_3$ terminal group on the pendent perfluoroalkyl chain provides much lower surface free energies than $-CF_2-$ moiety in the polymer back-bone of PTFE like materials.[2, 34] Synthetic approaches to utilize fluoro acrylates have been investigated. For example Chen et al,[35, 36] polymerized fluoroacrylates with hydrogenated monomers, but only up to 4 wt% fluoromonomers were copolymerized under emulsion polymerization conditions. Many synthetic manipulations, such as the use of high agitation and cosolvents, have been employed in an effort to produce F-containing colloidal dispersions through classical emulsion polymerization process. Previous studies[37] showed the successful polymerization of perfluorooctylethyl acrylate and perfluoroctylethyl methacrylate with nBA through batch emulsion polymerization, but the resulting solids content (~20-24% w/w) was substantially low and the mechanical stability of the films was questionable. To overcome low F-content, substantial concentration levels of acetone were utilized to facilitate diffusion of the F-containing monomers through the aqueous phase. Acetone addition as high as 10 to 15% (w/w) was necessary to produce stable colloidal particles with minimum coagulation, and although successful copolymerization of F-containing monomers with n-butylacrylate (nBA) was achieved, the removal of acetone was necessary.

Another concern is the choice of surfactant which should be compatible with the fluoropolymer and typically fluorinated dispersing species. However, the use of even small amounts of fluorosurfactants to stabilize colloidal dispersions, which are often mobile after coalescence,[38] still represents environmental concerns. In the case of good surface packing long-chain hydrophobic surfactants such as cetyltrimethylammonium bromide can be utilized,[37] which are very sensitive toward changes. Challenging aspect

during emulsion polymerization is that fluoromonomers are highly hydrophobic or fluorophilic, thus the polymerization with high FPs leads to coagulations in aqueous medium leading to unstable colloidal dispersions. Although several attempts have been made to prepare fluorinated colloidal dispersions, elaborate synthetic procedures and the use of co-solvents along with relatively low solids, high surfactant amount, stability of colloids, and fluorine contents represent significant challenges.[37, 39-44] Another promising studies [45, 46] involved cyclodextrin complexes which were utilized to copolymerize fluorinated styrenes in order to obtain copolymerization of fluorostyrene in an aqueous system. This was achieved by utilizing host/guest relationship of cyclodextrin complexes with fluoromonomers and was shown that effective transport of fluorostyrene was achieved via aqueous medium. Main concerns are the separation of cyclodextrin molecules after polymerization process.

Miniemulsion polymerization process has been also widely used to polymerize highly hydrophobic monomers.[44, 47] Diffusion limitations are avoided by polymerizing inside monomer droplets and to ensure droplet nucleation, small monomer droplets (50–500 nm) are formed and protected from diffusional degradation, and droplet coagulation by using a water-insoluble compound and an efficient surfactant. Water-insoluble compounds employed in miniemulsion include hydrophobic, low molecular weight molecules such as hexadecane, cetyl alcohol, perfluoromethyldecalin, and perfluorohexane,[43, 44, 48] pigments,[49] oligomers, or polymers[50, 51] and are referred to as cosurfactant or hydrophobes. The low water solubility of the hydrophobes prevents them from diffusing through the water phase, and keeps all other comonomers inside the droplet, thus minimizing the system's free energy. Since most hydrophobes are not

covalently bonded to the polymer, they are prone to leaching from the coating or phase separation, prompting research efforts directed at developing reactive hydrophobes.[52-54] Attempts to copolymerize fluorinated monomers were made and yielded only 1.4 % fluorinated polymer, even though initial levels of fluoro-monomers was 25%.[43] Successful synthesis of fluorinated homopolymer and copolymerization with hydrogenated monomers such as styrene, methyl methacrylate and acrylic acid was also reported.[44] Yet another shortcoming of miniemulsion is the requirement of energetic homogenization systems such as rotor-stators, sonifiers, or high pressure homogenizers to create small droplets.[55] Another drawback is that there is a limited control over the initial particle size which often results in a broad particle distribution.

Fluorinated acrylic monomers offer a number of potential synthetic avenues for the production of colloidal particles due to their increased reactivities with non-fluorinated monomers as well as the enhanced ability to diffuse through aqueous medium as compared to their non-acrylic F-containing counterparts. Recent studies utilizing semi-continuous emulsion polymerization and combination of simultaneous presence of the dual tail anionic fluorosurfactant phosphoric acid bis(tridecafluoro-octyl) ester ammonium salt (FSP) and sodium dodecylsulfate (SDS) surfactants facilitate a suitable environment for the aqueous polymerization of methylmethacrylate/n-butyl acrylate/ heptadecafluorodecylmethacrylate (p-MMA/nBA/FMA) colloidal particles. Polymerization was achieved with low-sheer monomer starved emulsion process in which the FSP/SDS surfactant mixture reduces the surface tension of the aqueous phase, thus facilitating mobility and subsequent polymerization of FMA along with MMA and nBA monomers.[56] Using this approach

up to 8.5% w/w of FMA was incorporated in the colloidal dispersions leading to stable non-spherical p-MMA/nBA/FMA colloidal dispersions in which p-FMA phase exists on the p-MMA/nBA core in one step synthetic process, morphologies of particles with increasing FMA content is shown in transmission electron micrographs (TEM) in Figure I-5. As seen the high electron density component due to p-FMA phase increases as the amount of FMA is increased from 0 to 8.5 % w/w. Similar synthetic approach was utilized on heptafluorobutylmethacrylate (FBMA), heptafluorobutylacrylate (FBA), heptadeca fluorodecylacrylate (FA), and heptadecafluoro-1-decene (FD) monomers and stable colloidal dispersions with upto 8.5 % w/w of fluoromonomer was achieved under aqueous system.[57] In all the copolymerization phase separated non-spherical particles were obtained in the presence of FSP/SDS dispersing agent. As stated previously, although very less amount of fluorosurfactants are utilized during synthesis, still these low molecular weight fluorinated compounds once leach out of the films provides environmental threats. Thus there is a need to replace fluorosurfactants with more environmental friendly dispersing agents.

Dispersing Agents

Surfactants play a significant role not only in the synthesis of colloidal particles, but also provide stability as well as alter surface properties of colloidal films. Although fluorosurfactants are quite efficient in lowering the surface-interfacial tension of aqueous system for polymerization of FPs , environmental issues created concerns. In recent studies a new class of dispersing agents, phospholipids (PLs) for colloidal synthesis was utilized as an efficient ability in colloidal synthesis. PLs are the main constituent of cell membrane, where they serve as selective barriers for various bio-

entities as well as provide support for membrane proteins as shown in Figure I-6.[58-60] Phospholipid phosphatidylcholine (PC) is one of the most abundant PLs detected in the cell membrane. PLs are fat derivatives whereby one fatty ester moiety is displaced by a phosphate ester group and as alkyl ammonium cation. Every structural feature of PL performs certain functions, and as illustrated in Figure I-6, each portion of this molecule imparts specific properties. Typically, the hydrophilic head group consists of PO_4^- and NH_3^+ groups separated by CH_2 spacers. The ionic phosphate and amino groups impart hydrophilicity to the molecule. The hydrocarbon chains may vary in length and act as hydrophobic entities of the biological surfactant. Often PLs contain two hydrophobic tails which may possess unsaturated double or triple bonds. These unique structural features result in an amphiphilic molecule having well defined hydrophilic/lipophilic balance (HLB). Subsequently, depending upon structural features, each PL will behave differently in aqueous medium.[58] For example, dual tails PLs organize themselves into bi-layers when placed in water or PLs with diacytylene group in the hydrophobic zone may rearrange themselves to form tubule structures, while single tail phospholipids form micelles with a hydrophilic exterior and hydrophobic interior as shown in Figure I-7. Through this preparation, liposomes and tubules are fairly stable and can be isolated from the solvent in which they were formulated by dialysis, gel filtration chromatography, or centrifugation,[61, 62] and have high potential as models for biological membranes[63-66] and drug delivery vehicles.[65, 67-70]

CMC in PLs depends on the chemical identity of the amphiphile and solution conditions. For amphiphiles with short single tails, for example sodium dodecyl sulfate ($CH_3 (CH_2)_{11}OSO_3^-Na^+$), the CMC is 1mM.[3] Most biological lipids have two long

hydrophobic tails (C_{18}) which lowers the CMC to less than 10^{-6} M. Unique features of PLs is that upon agitation or sonication they rearrange to form self sealing, water filled, bilayer vesicles called liposomes with a uniform diameter of several hundred nm.[58]

As stated above, PLs are capable of forming micelle-like structures, which may open a number of avenues for their utilization as surfactants in emulsion polymerization processes. However, there are limited studies involving the combination of polymeric dispersion synthesis and naturally derived PL. For example, previous studies[71, 72] utilized polymerizable and non-polymerizable PL with dual alkyl chains along with their single tail analogues as emulsifiers in the emulsion polymerization of styrene (Sty). Using acid hydrolysis and X-ray photocorrelation spectroscopy (XPS), it was determined that the PL remains primarily on the particle surfaces with non-polymerizable species being physically adsorbed and the polymerizable species chemically bound. While this study provides important chemical information regarding interfaces of colloidal particles synthesized in the presence of PL, data concerning PL behaviors during particle coalescence and ultimately film formation are recently studied by Urban et al.[59, 73-82] Morphology of colloidal particles and film properties significantly depend on the type of Pl utilized during synthesis and also the type of co-surfactant used. For example, when MMA and nBA monomers were copolymerized in the presence of hydrogenated soybean phosphatidylcholine (HSPC) phospholipid,[83] this species served to stabilize colloidal particles which, upon coalescence, diffused to form organized structures at the F-A interface. However, when HSPC and SDOSS were employed during synthesis, two distinct particle sizes were achieved and the presence of HSPC inhibited the mobility of SDOSS molecules during coalescence. In another

approach, when single tail PL 1-myristoyl-2-hydroxy-sn-glycero-phosphocholine (MHPC) and dual tail PL 1,2-dilauroyl-phosphocholine (DLPC) was used as dispersing agent along with SDOSS gives unimodal distribution of particles. Thus depending upon the type of PLs colloidal synthesis can be tailored.

Unique morphologies such as cocklebur-shape particles and hollow particles can be prepared by utilizing PLs. Upon extrusion and heating at 75° C MMA/nBA colloidal particles containing tubules pointing outward were obtained as a result of 1,2-bis(10,12-tricosadiynoyl)-sn-glycero-3-phosphocholine (DCPC) PLs present at the particle surface.[77] Figure I-8, A illustrates TEM of cocklebur particles and the same cocklebur structures of smaller size (160 nm) can be obtained via classical emulsion polymerization process without a nano-extruder. Another example is the use of nano- and micro-extrusion which provides a simple synthetic procedure of preparing hollow monodispersed colloidal particles of polystyrene dispersed in an aqueous phase, such as that shown in Figure I-8 B.[76]

In summary, PLs offer numerous opportunities for incorporating these bio-active dispersing species in colloidal dispersions which may exhibit stimuli responsive behaviors in the presence of external stimuli. Although only p-MMA/nBA and p-Sty colloidal particles have been synthesized using Pl dispersing agents, their further potential in stabilizing F-containing colloids is yet to be explored.

Heterogeneity of Film Formation

The primary driving force for preparing colloidal dispersions is to utilize them in polymeric films and to understand the mechanism of film formation. Although it is well-known that film formation is accomplished via a process in which initially

dispersed polymer colloids are deposited on a substrate followed by water evaporation[84-100] a detailed molecular level understanding interactions manifested during particle coalescence is limited. Typically, the film formation process has been described by three stages. In Stage 1, as water evaporates, the polymer particles come into close contact with each other which initiates particle coalescence. In Stage 2, as coalescence proceeds, particles deform to fill the voids or interstitial spaces, which give rise to the onset of a continuous film. At this point, a weak film is generated, and evaporation of water trapped between the particles continues. In Stage 3, polymer chain interdiffusion occurs, resulting in a continuous film. During this stage, the mechanical strength increases, and the water permeability of the film decreases.[101]

Various theories have been proposed in the literature to explain the coalescence of colloidal particles. It has been proposed by Brown et al.[102] that as particles approach each other, inter-particle voids produce capillary forces that remove water and cause particle-particle contact.[94, 103, 104] While Kendall and Padget[105] suggested that the major driving force for coalescence is surface energy reduction, surface area of all latex particles is much greater than the surface area of coalesced film, thus the driving force resulting from reduction in surface area is large.

One of the important factors governing the film formation of colloidal dispersions is the glass transition temperature (T_g). Capillary and surface energy forces alone cannot cause coalescence unless the polymer molecules in the latex particles are free to diffuse into neighboring particles which allows for the disappearance of individual particles into the coalesced film. Thus, for coalescence to occur, the T_g of the copolymer must be below the so-called minimum film formation temperature

(MFFT). During coalescence surfactant molecules which are on the surface of colloidal particles also get displaced during film formation. They may be trapped in the bulk of the material or can migrate to film-air (F-A) or film-substrate (F-S) interface in order to minimize surface free energy at the interface.

Previous studies[106] indicated that the distribution of surfactants play a significant role in the film formation process, and that film formation is significantly affected by colloidal particle morphologies as well as compatibility of individual components. Therefore, when considering the film formation process, the three stage model is greatly oversimplified because interactions present between low molecular weight species and the surfaces of colloidal particles depend upon particle morphology as well as the size and type of the surface stabilizing species. Numerous studies[95-100, 107-120] have shown that upon coalescence , the distribution of surfactant molecules in colloidal films exists and it can be greatly affected by external and internal stimuli such as temperature, pH, nature of substrate, ionic concentration and presence of external sources such as enzymes.[75, 81, 92, 121-127] Due to the ability to serve as polymerization medium for numerous monomers during emulsion polymerization sodium dodecyl sulfate (SDS) and SDOSS have been of interest for a number of years,[128-131] and their distribution after film formation is greatly affected by the presence of alternate copolymer microstructures as well as external stimuli. For example for SDOSS in p-sty/nBA colloidal blends (50:50), migration of SDOSS at F-A interface was enhanced at 90 and 120°C.[131] Furthermore, for p-ethyl acrylate/methacrylics acid (p-EA/MAA) colloidal particles, migration of SDOSS to F-A or F-S interfaces can be controlled depending on the type of substrate utilized for coalescence, such as for low surface tension substrate

(PTFE) increased migration to the F-S interface was observed compare to high surface energy (glass) substrate.[128] On the same lines, SDOSS and SDS migration increases to F-A interface by changing copolymer structure from p-EA/MAA to p-MMA/nBA copolymer structure. It was shown that MAA and acrylic acid (AA) limits the migration due to interactions between SDS and the acid functionalities in the copolymer matrix.[95, 96]

While the above polymer/surfactant interactions afford a controlled release of surfactant within a polymer matrix to the F-A interface of coalesced films, another area of particle interest is the preferential orientation of molecular segments. For example, orientation of SDOSS and SDS in p-Sty/nBA/MAA colloidal films is such that hydrophobic chains are preferentially perpendicular to the surface, and hydrophilic ends ($-SO_3^-Na^+$) associated with H_2O and –COOH entities, tend to align parallel to the film surface. Furthermore, once localized at the F-A interface, S-O bonds of $-SO_3^-Na^+$ groups of SDOSS or SDS may take either out-of-plane or in-plane conformations, depending on their environments.[107]

Along with polymer composition and ionic strength, localized interactions between surface stabilizing species as well as solution pH play an important role in surfactant exudations. Such as in recent studies where PLs are utilized as stabilizing agent for p-MMA/nBA colloidal dispersions along with SDSOSS, preferential migration and self-assembly at F-A and F-S interface was observed depending on the type of PL utilized, and stimuli provided.[75, 80-82] Such as for SDOSS and DLPC dispersing agents,[75] Figure I-9 summarizes the responses of SDOSS and DLPC to temperature, pH, ionic strength, and enzyme changes, and illustrates the direction of

migration for these stimuli. As seen, dispersing agents may form lipid rafts called surface localized ionic clusters (SLICs) of DLPC at F-A interface which are stable up to 120°C, at low ionic solutions concentrations, and at low enzymatic concentration levels. However, coalescence may release stabilizing species to the F-S interface with elevated temperature and low ionic strength stimuli. [75] It was observed by spectroscopic techniques and Ab-initio calculations that molecular orientation and interactions of self-organized crystalline structures or SLICs of DLPC molecules have specific interactions, and occurs between C=O of p-MMA/nBA copolymers of diester groups and C-NH_3 groups as H-bonding and electrostatic interactions.[74] These SLICs formed by PLs may serve potential in numerous biological applications ranging from cellular signaling, to transport across cell membranes, and others.[132-134] Thus the responsiveness of PLs can serve in various potential applications in near future.

Migration of surfactants to the interfaces is driven by surface energy minimization at the interface. Similarly, when considering fluoropolymers, significant decrease in surface energy gives rise to an increase in the driving force for migration to the film-air (F-A) interface to elevate excess of the surface free energy. Although an increased surface coverage of fluoropolymers is desirable in coating applications, the processes governing this migration through the colloidal film is not well understood.

Previous studies[43] attempting to address these features generated low surface energy coatings by synthesizing fluorine–containing acrylic latex blends and utilized surface segregation, phase separation, and particle size asymmetry as means of producing fluorinated surfaces. As shown in Figure I- 10, A1, surface segregation occurs when there is a surface free energy difference between two materials in the same

polymer matrix. As a result, surface tension differentials will facilitate the flow of low free energy components to the surface without distinct formation of aggregates. In contrast, phase separation is driven by the incompatibility of components in a mixture having the tendency to form aggregates. Upon coalescence, lower surface tension components diffuse to the surface resulting in stratification, as shown in Figure I-10, A2. Particle size asymmetry (Figure I-10, B1 and B2) utilizes colloidal blends of different particle sizes, and film surface properties are governed by the mobility of these particles. As shown in Figure I-10, B1, when the particle size is comparable, distribution of individual components will be more or less uniform. In contrast, when small particles are present (Figure I-10, B2), they will occupy voids between larger particles, thus increasing the surface concentration. Therefore, surface properties will vary with the size and concentration levels of the particles. Although these studies successfully produced fluorinated surfaces, many questions remain to be unanswered. For example, it should be pointed out that conclusions of these studies are based entirely on surface morphological features of coalesced films which were conducted using atomic force microscopy (AFM). Therefore, the question as to what effects low surface tension component distribution across film thickness will have on the actual film formation needs to be addressed.

Recently stable non-spherical F-containing colloidal dispersions were synthesized with up to 8.5% w/w fluoro acrylates and methacrylates containing both short chain ($-(CF_2)_3-CF_3$) and long chain ($-(CF_2)_7-CF_3$) fluorinated groups.[56, 57] It was observed that the blocky phase of FPs migrate to the F-A Interface after film formation due to low surface energy of fluorinated phase. It was observed that short chain FPs

have lower surface coverage with fluorinated segments compare to longer FPs. Figure I-11 shows coalescence process for short and long chain fluoromonomers of these particles in which phase separation at particle level leads to the segregation and preferential migration to the F-A Interface, forming islands of FPs on the surface.

With this in mind and as stated previously, the exceptionally attractive properties of fluoropolymers offer unique features when utilized in colloidal dispersions that would coalesce under ambient conditions. Despite the importance of the fluorine-containing emulsions, only a few investigations addressed the correlation between emulsion polymerization, particle composition, and film formation of fluorinated colloidal dispersions. Thus there is a need to further explore fluorine containing colloids in which advancement at both synthetic level such as green synthesis in which no use of organic solvents or fluorosurfactants are required, yet higher levels of FPs can be incorporated. Although stratification of low molecular weight entities such as surfactants have been addressed and known in the literature, their exists very limited knowledge on phase-separation of fluoropolymer and their migration to interfaces in copolymer structure after coalescence. Thus further understanding of coalescence mechanism of F-containing colloids is required and will be addressed in this research thesis.

Table I-1. Polymerizations Utilized in FPs Synthesis, Types of Monomers, Reaction Conditions, Advantages, and Limitations.

Polymerization Process	Monomers	Reaction Conditions	Advantages	Limitations
Solution	Fluoroacrylates, fluoromethacrylates, fluorostyrene, fluoroamides	Chlorofluorocarbons (CFCs) solvents utilized, elaborate synthetic procedures	Simple synthetic approach	Poor control over side reactions, MW MWD, CFCs solvents utilized, not environmental friendly process
Controlled Radical				
NMP	Fluoroacrylates, fluoromethacrylates, fluorostyrene, fluoroamides, fluoro 1,3 dienes	Use of CFCs solvents for solubility, TEMPO-tyoe nitroxides for controlling MW and MWD	Narrow MWD, controlled architecture, copolymerization with hydrogenated components	Limited range of monomers specially methacrylates cannot be polymerized, Use of TEMPO-type nitroxides, elaborate synthetic process
ATRP	Fluoroacrylates, fluoromethacrylates, fluorostyrene, fluoroacrylamides, fluoroalkenes, and fluoroacrylomides	Catalysts, Initiator with Halogen groups, ligands, solvents	Low MWD, Controlled architecture, polymer brushes on surface can be synthesized, aqueous based emulsion and miniemulsion can be achieved	Functional groups react with catalyst, presence of undesired metal catalyst –ligand after reaction, number of functional groups such as carboxylic acid cannot be tolerated by catalyst
RAFT	Fluoroacrylates, fluoromethacrylates, fluoroamides and fluoroimides	Utilize CTA agent, solvents for synthesis	Low MWD, Controlled architecture, can polymerize a wide range of monomers	Elaborate synthetic steps, presence of thio-meities after synthesis, additional step for obtaining films, use of solvents during synthesis
Suspension	Tetrafluoroethylene, vinylidene fluoride, vinyl fluoride	Water insoluble initiator, low concentration off surfactants, adequate agitation, pressurized conditions for gaseous monomers	Simple synthesis, no use of CFCs process	Poor polymerization kinetics, coagulation of FPs, poor control over properties such as particle size, stability and MW
Microemulsion	-	-	-	-
Emulsion	Fluoroacrylates, fluoromethacrylates, fluorostyrenes, tetrafluoroethylene, vinylidene fluoride, vinyl fluoride	Water soluble initator, surfactant, aqueous medium, adequate agitation, pressurized conditions for gaseous monomers	Stable fluorocolloids with various amount of fluoromonomers can be achieved, Unimodal particle size distribution, stable colloids can be directly applied to form films, no processing step, environmentally benign	Amount of F-monomer, stability of colloids, presence of F-surfactant after synthesis
Supercritical CO_2	TFE, PVDF, PVF, fluoroacrylates and fluoromethacrylates	Pressurized conditions, surfactants	Inert medium for highly flammable and explosive fluoromonomer gas, good solubility of fluoromonomer in Supercritical CO_2, no solvents required	Pressurized conditions, colloids obtained are solid particles-further processing step required for application method
Miniemulsion	Fluoromethacrylates	High amounts of surfactants, hydrophobes, high agitation	Stable colloids of very low particle size (few nm) can be obtained	Hydrophobes are prone to leach out, low fluoromonomers amount incorporated, limited control over the particle size

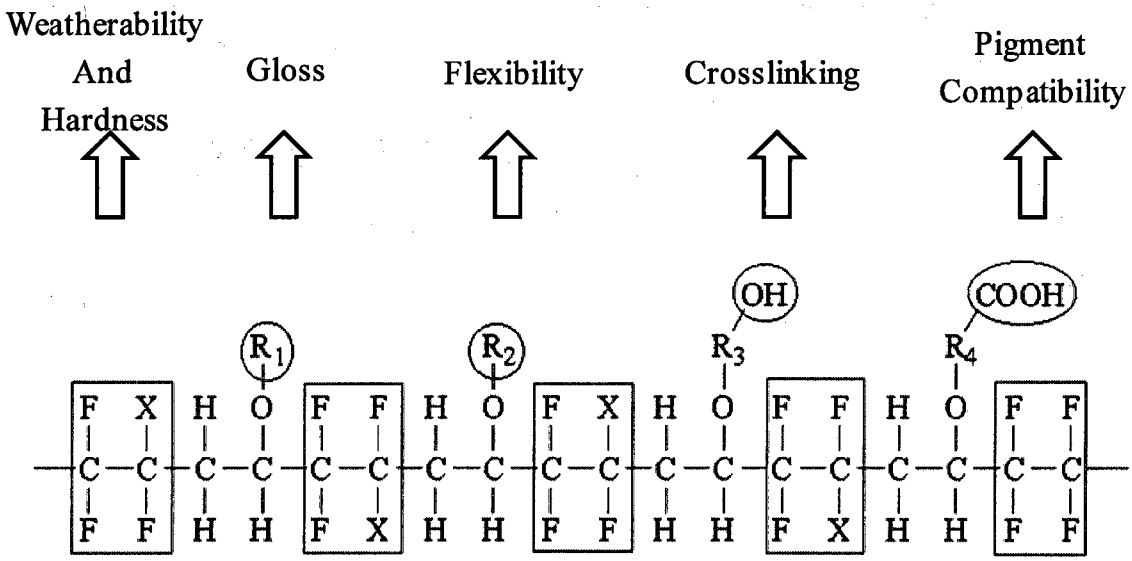

Figure I-1. Structural features of Lumiflon® Polymer where X = F or Cl, R_1 and R_2 = alkyl or cyclcoalkyl group, and R_3 and R_4 = alkene or cycloalkene.[25]

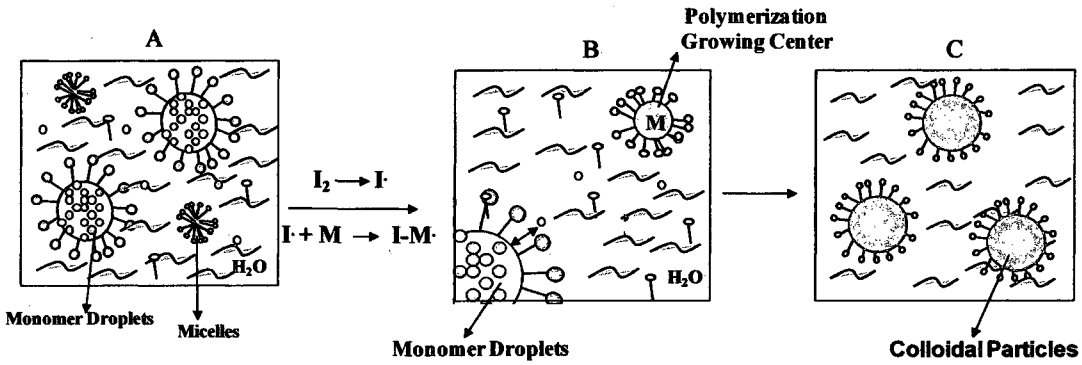

Figure I-2. Schematic diagram depicting the emulsion polymerization process.

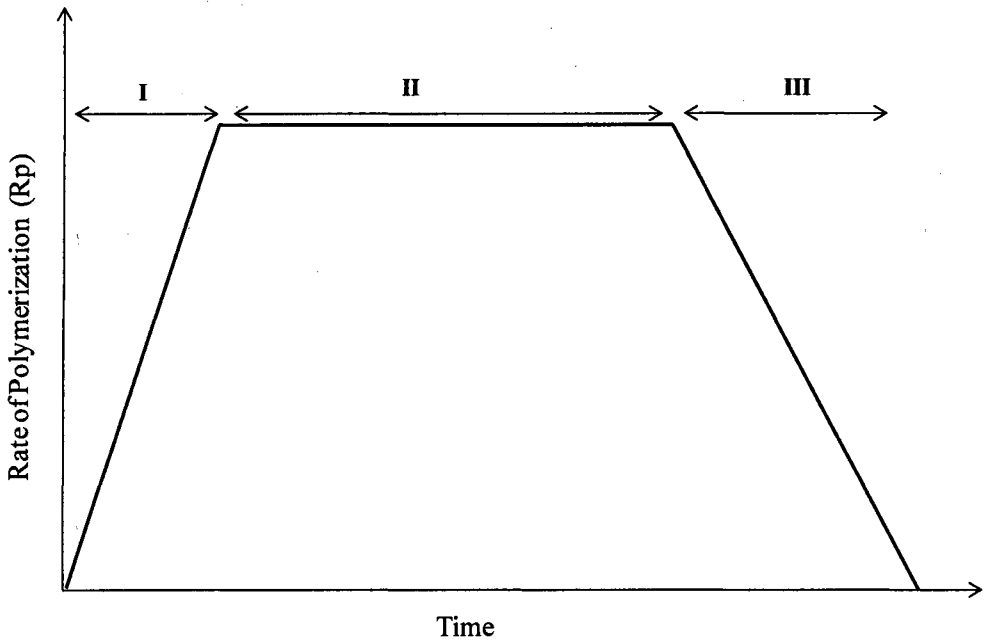

Figure I-3. Relationship between the rate of polymerization (R_p) during the three stages of colloidal dispersion synthesis.

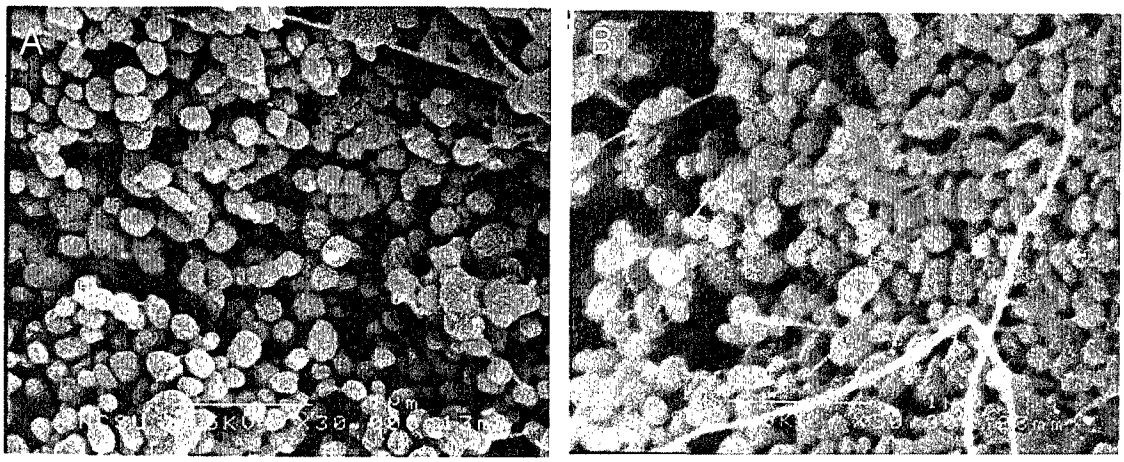

Figure I-4. Scanning electron micrographs of poly(tetrafluoroethylene) prepared using a hybrid CO_2/aqueous system with added surfactant (A), and using conventional TFE dispersion polymerization methods (B).[27]

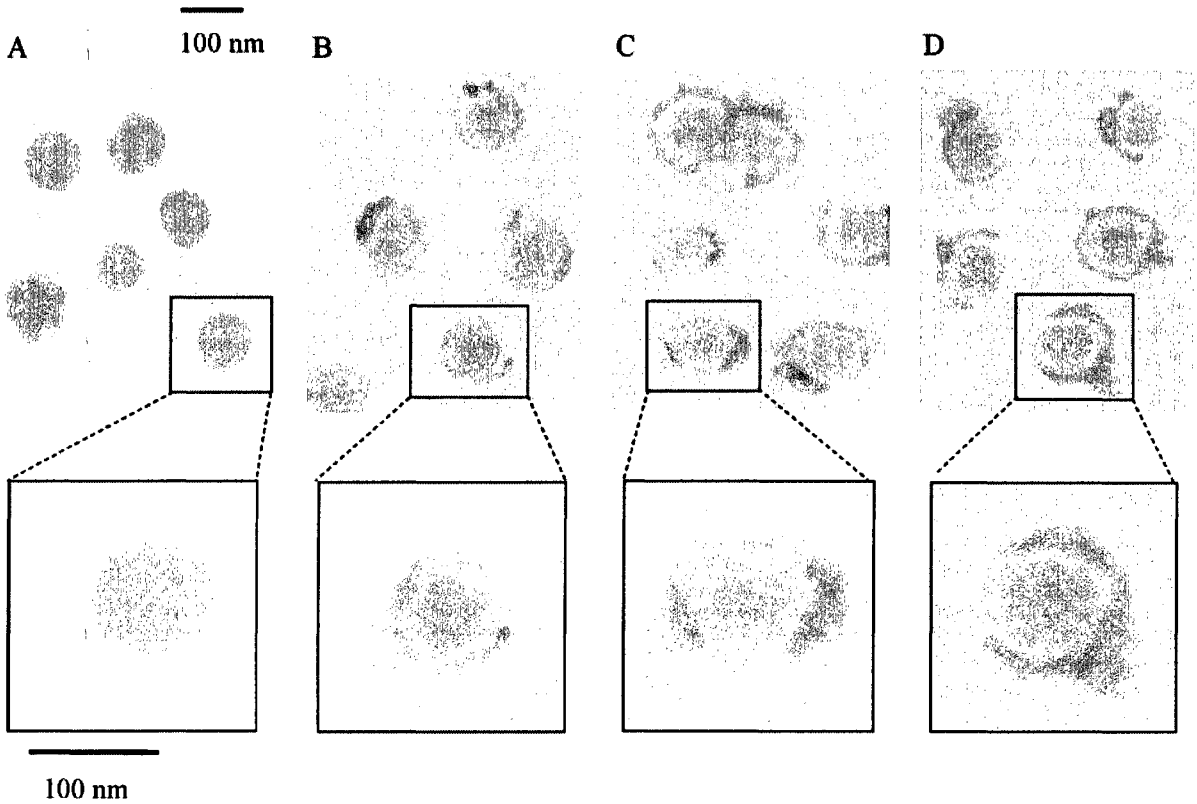

Figure I-5. Transmission electron micrographs: (A) MMA/nBA; (B) MMA/nBA/FMA (3.3% w/w FMA); (C) MMA/nBA/FMA (5% w/w FMA); (D) MMA/nBA/FMA (8.5% w/w FMA).[56]

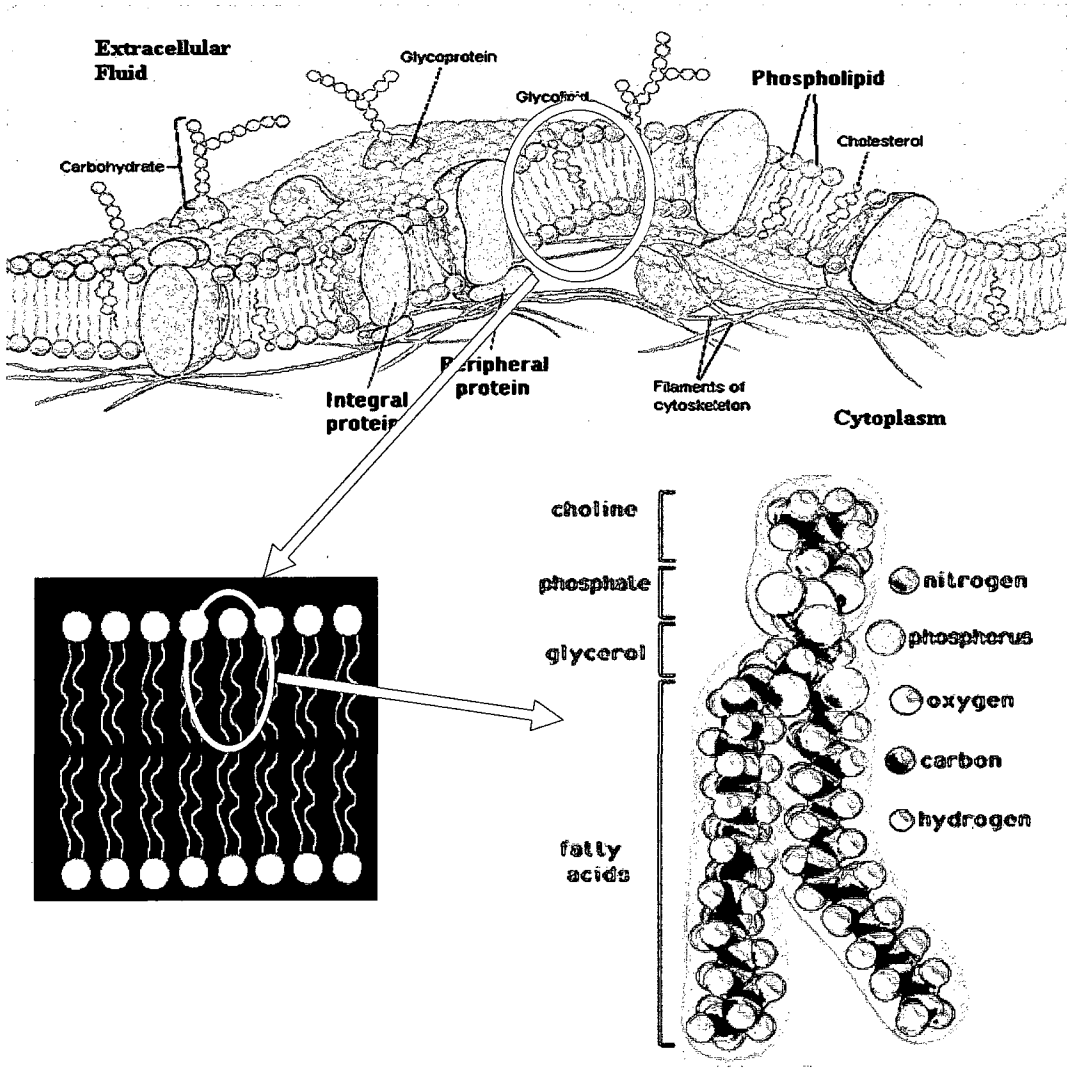

Figure I-6. Cell membrane structure showing PL structural features.[58]

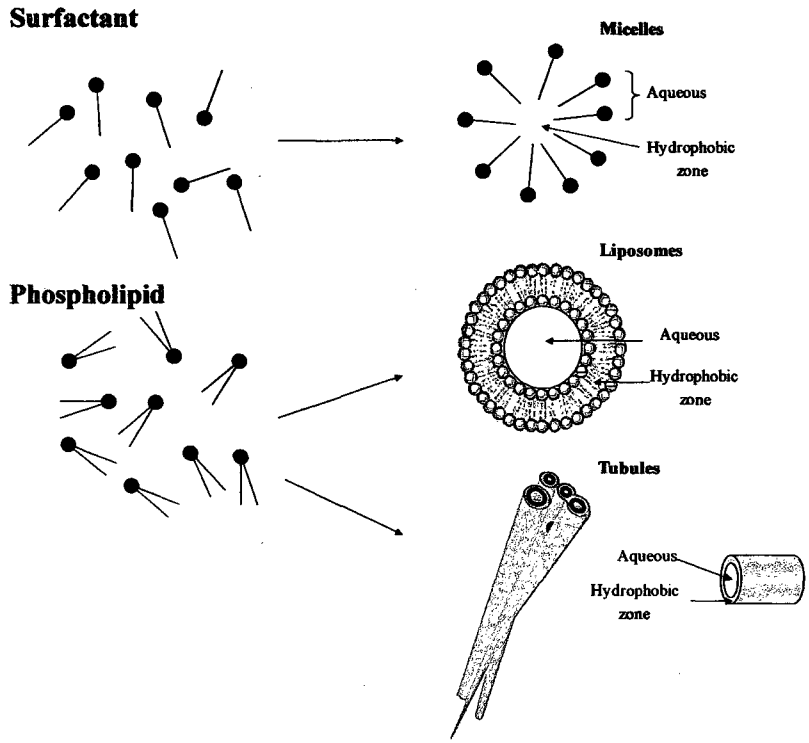

Figure I-7. Surfactant and phospholipid molecular self-assembly of micelles and liposomes.[73]

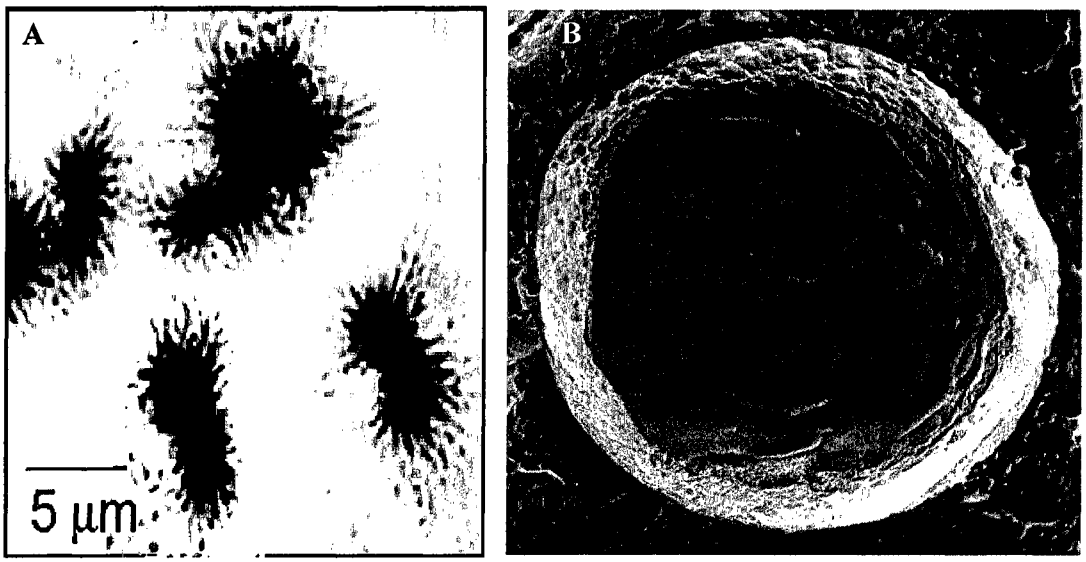

Figure I-8. (A) TEM micrograph p-MMA/nBA copolymer particles stabilized by a SDOSS/DCPC mixture and (B) TEM micrograph of 5 µm hollow p-Sty particle.[76, 77]

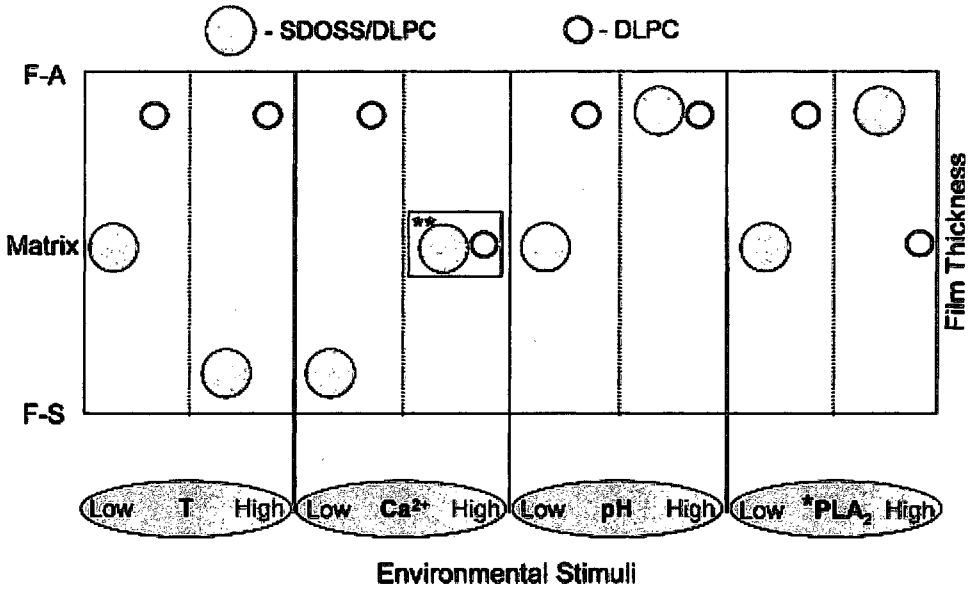

Figure I-9. A schematic diagram illustrating the mobility of SDOSS/DLPC and DLPC surface stabilizing species to the F-A interface, F-S interface, and matrix in response to changes in temperature, ionic strength, pH, PLA_2. Open and closed circles illustrate preferential location of DLPC and SDOSS/DLPC respectfully.[75]

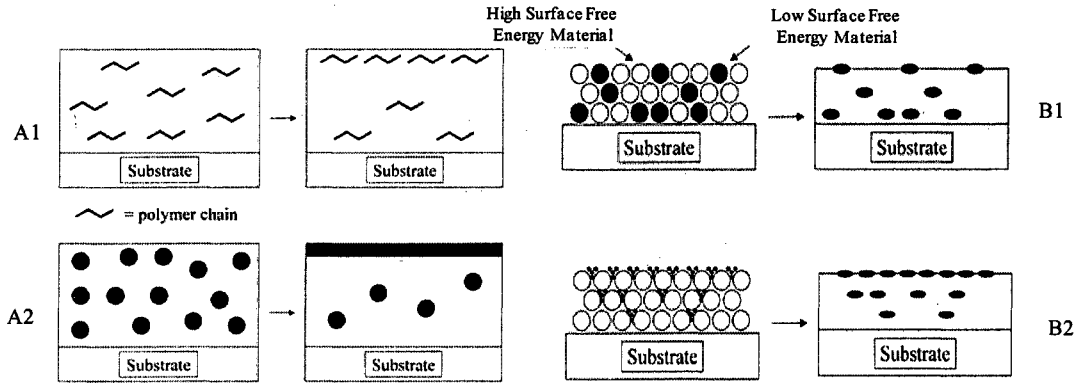

Figure I-10. Proposed mechanisms leading to low surface tension surfaces: surface segregation (A1), phase separation (A2), and the particle size asymmetry (B1 and B2).[43]

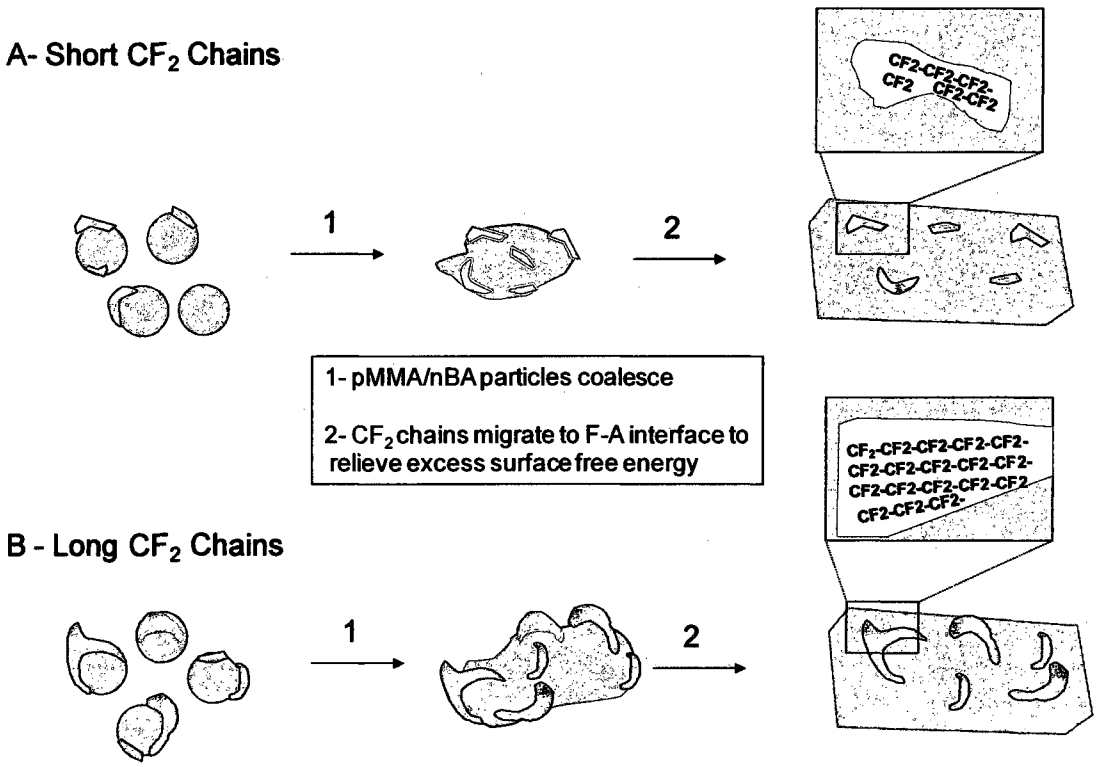

Figure I-11. Pictorial representation of the processes leading to surface phase-separated domains at the F-A interface of F-containing colloidal particles with (A) short CF_2 chains fluoropolymer and (B) long chain CF_2 fluoropolymer.[57]

References

1. Hiyama, T., *Organofluorine Compounds*. Springer: New York, 2000.

2. Wu, S., *Polymer Interface and Adhesion*. Marcel Dekker: New York, 1982.

3. Odian, G., *Principles of Polymerization*. John Wiley & Sons: New York, 2004.

4. Malshe, V. C.; Sangaj, N. S. *Prog. Org. Coat.* **2005,** *53*, 207.

5. Krupers, M.; Slangen, P.-J.; Moller, M. *Macromolecules* **1998,** *31*, 2552.

6. Bucholz, T. L.; Loo, Y.-L. *Macromolecules* **2006,** *39*, 6075.

7. Shi, Z. Q.; Holdcroft, S. *Macromolecules* **2004,** *37*, 2084.

8. Avila, D. V.; Ingold, K. U.; Lusztyk, J.; Dolbier, W. R.; Pan, H. Q.; Muir, M. J. *J. Am. Chem. Soc.* **1994,** *116*, 99.

9. Granville, A. M.; Boyes, S. G.; Akgun, B.; Foster, M. D.; Brittain, W. J. *Macromolecules* **2004,** *37*, 2790.

10. Granville, A. M.; Boyes, S. G.; Akgun, B.; Foster, M. D.; Brittain, W. J. *Macromolecules* **2005,** *38*, 3263.

11. Gan, D.; Mueller, A.; Wooley, K. L. *Journal of Polymer Science, Part A: Polymer Chemistry* **2003,** *41*, 3531.

12. Gudipati, C. S.; Finlay, J. A.; Callow, J. A.; Callow, M. E.; Wooley, K. L. *Langmuir* **2005,** *21*, 3044.

13. Gudipati, C. S.; Greenlief, C. M.; Johnson, J. A.; Prayongpan, P.; Wooley, K. L. *Journal of Polymer Science, Part A: Polymer Chemistry* **2004,** *42*, 6193.

14. Zhang, Z. B.; Ying, S. K.; Shi, Z. Q. *Polymer* **1999,** *40,* 5439.

15. Lacroix-Desmazes, P.; Andre, P.; DeSimone, J. M.; Ruzette, A. V.; Boutevin, B. *J Polym Sci Part A: Polym Chem* **2004,** *42*, 3537.

16. Roche, V.; Vacandio, F.; Bertin, D.; Massiani, Y. *J Electroceram* **2006,** *16*, 41.

17. Ma, Z.; Lacroix-Desmazes, P. *J Polym Sci Part A: Polym Chem* **2004,** *42*, 2405.

18. Eberhardt, M.; Theato, P. *Macromol. Rapid Commun.* **2005,** *26*, 1488.

19. Inoue, Y.; Watanabe, J.; Takai, M.; Yusa, S.; Ishihara, K. *J Polym Sci Part A: Polym Chem* **2005,** *43*, 6073.

20. Hansen, N. M.; Jankova, K.; Hvilsted, S. *European Polymer Journal* **2007,** *43*, 255.

21. Solomon, S.; Garcia, R. R.; Sherwood, F.; Wuebbles, D. J. *Nature* **1986,** *321*, 755.

22. Lovell, P. A.; El-Aasser, M. S., *Emulsion Polymerization and Emulsion Polymers*. John Wiley and Sons: New York, 1997.

23. Flory, P., *Principle of Polymer Chemistry*. Cornell University Press: Ithaca, 1953.

24. Smith, W. V.; Ewart, R. H. *J. Chem. Phys.* **1948,** *16*, 592.

25. Banks, R. E.; Tatlow, J. C.; Smart, B. E., *Organofluorine Chemistry: Principles and Commercial Applications*. Plenum: New York, 1994.

26. Fukui, K. 1970.

27. Romack, T. J.; Kipp, B. E.; DeSimone, J. M. *Macromolecules* **1995,** *28*, 8432.

28. DeSimone, J. M.; Guan, Z.; Elsbernd, C. S. *Science* **1992,** *257*, 945.

29. DeSimone, J. M.; Maury, E. E.; Menceloglu, Y. Z.; McClain, J. B.; Romack, T. J.; Combes, J. R. *Science* **1994,** *265*, 356.

30. McClain, J. B.; Betts, D. E.; Canelas, D. A.; Samulski, E. T.; DeSimone, J. M.; Londono, J. D.; Cochran, H. D.; Wignall, G. D.; Chillura-Martino, D.; Triolo, R. *Science* **1996,** *274*, 2049.

31. Romack, T. J.; DeSimone, J. M.; Treat, T. A. *Macromolecules* **1995,** *28*, 8429.

32. Michel, U.; Resnick, P.; Kipp, B.; DeSimone, J. M. *Macromolecules* **2003,** *36*, 7107.

33. Hyatt, J. A. *J. Org. Chem.* **1984,** *49*, 5097.

34. Johnson, R. E.; Dettre, R. H., *Wetting Ability*. Marcel Dekker: New York, 1993.

35. Cheng, S.; Chen, Y.; Wang, K. *Acta Polym Sinica* **2002,** *5*, 560.

36. Chen, Y.; Zhang, C.; Wang, Y.; Cheng, S.; Chen, P. *J. Appl. Polym. Sci.* **2003,** *90*, 3609.

37. Linemann, R. F.; Malner, T. E.; Brandsch, R.; Bar, G.; Ritter, W.; Mulhaupt, R. *Macromolecules* **1999,** *32*, 1715.

38. Dreher, W. R.; Urban, M. W. *Langmuir* **2004,** *20*, 10455.

39. Chen, Y.; Ying, L.; Yu, W. J.; Kang, E.; Neoh, K. *Macromolecules* **2003,** *36*, 9451.

40. Koendrick, G. H.; Sacanna, S.; Pathmamanoharan, C.; Rasa, M.; Philipse, A. P. *Langmuir* **2001,** *17*, 6086.

41. Sacanna, S.; Koenderink, G. H.; Philipse, A. P. *Langmuir* **2004,** *20*, 8398.

42. Ha, J.; Park, I.; Lee, S.; Kim, D. *Macromolecules* **2002,** *35*, 6811.

43. Thomas, R. R.; Lloyd, K. G.; Stika, L. M.; Stephens, L. E.; Megallanes, G. S.; Dimonie, V. L.; Sudol, E. D.; El-Aasser, M. S. *Macromolecules* **2000,** 33, 8828.

44. Landfester, K.; Rothe, R.; Antonietti, M. *Macromolecules* **2002,** *35*, 1658.

45. Storsberg, J.; Ritter, H. *Macromol. Chem. Phys.* **2002,** *203*, 812.

46. Cinar, H.; Kretschmann, O.; Ritter, H. *Macromolecules* **2005,** *38*, 5078.

47. Marion, P.; Beinert, G.; Juhue, D.; Lang, J. *J. Appl. Polym. Sci.* **1997,** *64*, 2409.

48. Tiars, F.; Landfester, K.; Antonietti, M. *Langmuir* **2001,** *17*, 908.

49. Lelu, S.; Novat, C.; Graillat, C.; Guyot, A.; Bourgeat-Lami, E. *Polym. Int.* **2003,** *52*, 542.

50. Baskar, G.; Landfester, K.; Antonietti, M. *macromolecules* **2000,** *33*, 9228.

51. Miller, C. M.; Sudos, E. D.; Silebi, C. A. *Macromolecules* **1995,** *28*, 2772.

52. Chern, C. S.; Chen, T. J. *Colloid Polym. Sci.* **1997,** *275*, 546.

53. Chern, C. S.; Chen, T. J. *Colloid Polym. Sci.* **1998,** *138*, 65.

54. Alducin, J. A.; Forcada, J.; Asua, J. M. *Macromolecules* **1994,** 27, 2256.

55. Asua, J. M. *Prog. Polym. Sci* **2002,** *27*, 1283.

56. Dreher, W. R.; Jarrett, W. L.; Urban, M. W. *Macromolecules* **2005,** *38*, 2205.

57. Dreher, W. R.; Singh, A.; Urban, M. W. *Macromolecules* **2005,** *38*, 4666.

58. Peter, R.; Johnson, G. B., *Biology*. 5th Ed. ed.; McGraw-Hill Co.: 1999.

59. Yacoub, A.; Urban, M. W. *Biomacromolecules* **2003,** *4*, 52.

60. Hofmann-Berling, H. *Biochim. Biophys. Acta.* **1958,** *27*, 247.

61. Oliger, P.; Schmutz, M.; Hebrant, M.; Grison, C.; Coutrot, P.; Tondre, C. *Langmuir* **2001,** *17*, 3893.

62. Oliger, P.; Hebrant, M.; Grison, C.; Coutrot, P.; Tondre, C. *Langmuir* **2001,** *17*, 6426.

63. Fendler, J. H. *J. Phys. Chem.* **1980,** *84*, 1485.

64. Fendler, J. H. *Acc. Chem. Res.* **1980,** *13*, 7.

65. Gregoriadis, G., *Liposomes as Drug Carriers: Recent Trends and Progress*. John Wiley and Sons: New York, 1988.

66. Tristram-Nagle, S.; Nagle, J. F. *Chem. and Phys. of Lipids* **2004,** *127*, 3.

67. Cornelus, C.; Giulieri, F.; Krafft, M.-P.; Riess, J. G. *Coll. and Surf. A:Physicochem. and Eng. Aspects* **1993,** *70*, 233.

68. Carpentier, Y. A.; Simoens, C.; Siderova, V.; El Nakadi, I.; Vanweyenberg, V.; Eggerickx, D.; Deckelbaum, R. *Nutrition* **1997,** *13*, 9.

69. Gregoriadis, G. *New Eng. J. Med.* **1976,** *295*, 704.

70. Westesen, K.; Bunjes, H.; Hammer, G.; Siekmann, B. *PDA J. Pharm. Sci. and Techn.* **2001,** *55*, 240.

71. Yamaguchi, K.; Watanabe, S.; Nakahama, S. *Makromol. Chem.* **1989,** *190*, 1195.

72. Watanabe, S.; Ozaki, H.; Mitsuhashi, K.; Nakahama, S.; Yamaguchi, K. *Makromol. Chem.* **1992,** *193*, 2781.

73. Urban M.W.; Lestage D. J. *J. Macromol. Sci., Part C: Polymer Review* **2006,** *46*, 1.

74. Yu, M.; Urban, M. W.; Sheng, Y.; Leszczynski, J. *Langmuir* **2008,** *24*, 10382.

75. Lestage, D. J.; Yu, M.; Urban, M. W. *Biomacromolecules* **2005,** *6*, 1561.

76. Lestage, D. J.; Urban, M. W. *Langmuir* **2005,** *21*, 4266.

77. Lestage, D. J.; Urban, M. W. *Langmuir* **2005,** *21*, 10253.

78. Lestage, D. J.; Urban, M. W. *Langmuir* **2005,** *21*, 6753.

79. Lestage, D. J.; Urban, M. W. *Langmuir* **2005,** *21*, 2150.

80. Lestage, D. J.; Urban, M. W. *Langmuir* **2004,** *20*, 6443.

81. Lestage, D. J.; Schleis, D. J.; Urban, M. W. *Langmuir* **2004,** *20*, 7027.

82. Lestage, D. J.; Marek, M. W. *Langmuir* **2005,** *21*, 6753.

83. Yacoub, A.; Urban, M. W. *Biomacromolecules* **2003,** *4*, 52.

84. Winnik, M. A.; Wang, Y.; Haley, F. *J. Coat. Techn.* **1992,** *64*, 51.

85. Dillon, R. E.; Bradford, E. B.; Andrews, R. D. *Ind. Eng. Chem.* **1953,** 45, 728.

86. Voyutskii, S. S. *J. Polym. Sci.* **1958,** *32*, 528.

87. Boczar, E. M.; Dionne, B. C.; Fu, Z.; Kirk, A. B.; Lesko, P. M.; Koller, A. D. *Macromolecules* **1993,** *26*, 5772.

88. Keddie, J. L.; Meredith, P.; Jones, R. A.; Donald, A. M. *Macromolecules* **1995,** *28*, 2673.

89. Protzman, T. F.; Brown, G. L. *J. Appl. Polym. Sci.* **1960,** *4*, 81.

90. van Tent, A.; te Nijenhuis, K. *Prog. Org. Coat.* **1992,** *20*, 459.

91. Eckersley, S. T.; Rudin, A. *J. Coat. Techn.* **1990,** *62*, 89.

92. Holl, Y. *Macrom. Symp.* **2000,** *151*, 473.

93. Winnik, M. A.; Feng, J. *J. Coat. Techn.* **1996,** *68*, 39.

94. Vanderhoff, J. W.; Tarkowski, H. L.; Jenkins, M. C.; Bradford, E. B. *J. Macrom. Chem.* **1966,** *1*, 131.

95. Evanson, W.; Thorstenson, T. A.; Urban, M. W. *J. Appl. Polym. Sci.* **1991,** *42*, 2297.

96. Evanson, W.; Urban, M. W. *J. Appl. Polym. Sci.* **1991,** *42*, 2287.

97. Kunkel, J.; Urban, M. W. *J. Appl. Polym. Sci.* **1993,** *50*, 1217.

98. Thorstenson, T. A.; Tebelius, L. K.; Urban, M. W. *J. Appl. Polym. Sci.* **1993,** *50*, 1207.

99. Thorstenson, T. A.; Urban, M. W. *J. Appl. Polym. Sci.* **1993,** 47, 1381.

100. Thorstenson, T. A.; Tebelius, L. K.; Urban, M. W. *J. Appl. Polym. Sci.* **1993,** *49*, 103.

101. Provder, T.; Winnik, M. A.; Marek, M. W., *Film Formation in Waterborne Coating; ACS Symposium Series*. 1996.

102. Brown, G. L. *J. Polym. Sci.* **1956,** 22, 423.

103. Sheetz, D. P. *J. Appl. Polym. Sci.* **2001,** *9*, 3759.

104. Vanderhoff, J. W.; Tarkowski, H. L.; Jenkins, M. C.; Bradford, E. B. *J. Macromol. Chem.* **1966,** *1*, 361.

105. Kendall, K.; Padget, J. C. *Int. J. Adhesive* **1982,** *2*, 149.

106. Zhao, Y.; Urban, M. W. *Langmuir* **2001,** *17*, 6961.

107. Zhao, Y.; Urban, M. W. *Langmuir* **2000,** *16*, 9439.

108. Zhao, Y.; Urban, M. W. *Polym. Mater. Sci. and Eng.* **1999,** *80*, 571.

109. Zhao, Y.; Urban, M. W. *Macromolecules* **2000,** *33*, 2184.

110. Zhao, Y.; Urban, M. W. *Macromolecules* **2000,** *33*, 7573.

111. Zhao, Y.; Urban, M. W. *Macromolecules* **2000,** *33*, 8426.

112. Niu, B. J.; Urban, M. W. *J. Appl. Polym. Sci.* **1996,** *62*, 1903.

113. Niu, B. J.; Urban, M. W. *J. Appl. Polym. Sci.* **1996,** *60*, 371.

114. Niu, B. J.; Urban, M. W. *J. Appl. Polym. Sci.* **1996,** *60*, 379.

115. Niu, B. J.; Urban, M. W. *J. Appl. Polym. Sci.* **1998,** *70*, 1321.

116. Keddie, J. L. *Mater. Sci. and Eng.* **1997,** *21*, 101.

117. Beltran, C. M.; Guillot, S.; Langevin, D. *Macromolecules* **2003,** *36*, 8506.

118. Sethumadhavan, G. N.; Nikolov, A.; Wasan, D. *Langmuir* **2001,** *17*, 2059.

119. Shin, J. S.; Lee, D. Y.; Ho, C. C.; Kim, J. H. *Langmuir* **2000,** *16*, 1882.

120. Tebelius, L. K.; Urban, M. W. *J. Appl. Polym. Sci.* **1995,** *56*, 387.

121. Zhao, C. L.; Holl, Y.; Pith, T.; Lambla, M. *Coll. Polym. Sci.* **1987,** *265*, 823.

122. Reiter, G.; Khanna, R.; Sharma, A. *J. Phys.: Cons. Matt.* **2003,** *15*, S331.

123. Mallegol, J.; Gorce, J.; Dupont, O.; Jeynes, C.; McDonald, P.; Keddie, J. *Langmuir* **2002,** *18*, 4478.

124. Aydogan, N.; Abbott, M. *Langmuir* **2001,** *18*, 5703.

125. Keitz, E.; Holl, Y. *Colloids and Surfaces A: Physiochemical and Engineering Aspects* **1993,** *78*, 255.

126. Lam, S.; Hellgren, A.; Sjoberg, M.; Holmberg, K.; Schoonbrood, H.; Unzue, M.; Asua, J.; Tauer, K.; Sherrington, D.; Montoya Goni, A. *J. Appl. Polym. Sci.* **1997,** *66*, 187.

127. Amalvy, J.; Soria, D. *Prog. in Org. Coat.* **1996,** *28*, 279.

128. Evanson, K. W.; Thortenson, T. A.; Urban, M. W. *J. Appl. Polym. Sci.* **1991,** *42*, 2309.

129. Zhao, Y.; Urban, M. W. *Langmuir* **2000,** *16*, 9439.

130. Zhao, Y.; Urban, M. W. *Langmuir* **2001,** *17*, 6961.

131. Zhao, Y.; Urban, M. W. *Macromolecules* **2000,** *33*, 7573.

132. Pike, L. J. *Biochem. J.* **2004,** *378*, 281.

133. Simons, K.; van Meer, G. *Biochemistry* **1988,** *27*, 6197.

134. Simons, K.; Ikonen, E. *Nature* **1997,** *387*, 569.

CHAPTER II

PHOSPHOLIPID-ASSISTED SYNTHESIS OF FLUORINE CONTAINING COLLOIDAL PARTICLES AND THEIR FILM FORMATION

Abstract

Polymerization of fluorine-containing monomers into aqueous colloidal particles has been of interest for a long time, but often impossible to overcome synthetic and film formation challenges of incorporating low surface tension species into an aqueous phase only recently resulted in the development of co-polymerized fluorinated and non-fluorinated acrylate monomers using standard emulsion polymerization process. However, the main limiting factor was that up to 8.5% w/w of heptadecafluorodecyl methacrylate (FMA) could be incorporated into p-methyl methacrylate/n-butyl acrylate/FMA (p-MMA/nBA/FMA) copolymer to form stable dispersions. These studies illustrate for the first time the synthesis of p-MMA/nBA/FMA colloidal dispersions containing up to 15 % w/w of FMA which is accomplished by utilization of biologically active phospholipids (PLs) and ionic surfactants. Using monomer starved conditions during emulsion polymerization and utilization of 1,2-dilauroyl-sn-glycero-3-phosphocholine (DLPC), sodium dodecyl sulfate (SDS) and phosphoric acid bis(tridecafluoro-octyl) ester ammonium salt (FSP) as surfactants which function as transfer and dispersing agents, facilitates a suitable environment for polymerization of p-MMA/nBA/FMA colloidal dispersions that exhibit non-spherical particle morphologies. Such non-spherical particles upon coalescence form phase-separated films with unique surface properties.

Introduction

Recently, a simple methodology of incorporating heptadecafluorodecyl methacrylate (FMA) monomers into methyl methacrylate/n-butyl acrylate (MMA/n-BA) particles in the presence of ionic and F-containing dispersing agents is reported.[1, 2] Although stable, non-spherical water-dispersible p-MMA/n-BA/FMA colloidal particles were produced containing up to 8.5 % w/w of FMA, attempts to incorporate higher FMA quantities lead to unstable dispersions. Typically, the incorporation of fluorinated monomers has been an elaborate process where miniemulsion polymerization was utilized.[3, 4] These efforts, however, require the presence of organic solvents as well as more elaborate methodologies ranging from sonication to passing the pre-emulsion through a microfluidizer. Furthermore, two-step processes were also utilized that were achieved by using homogenizers and organic solvents, such as acetone or ethanol.[5] Although these approaches have may have lead to colloidal dispersions, the main drawbacks are elaborative synthetic procedures and, more importantly, low % solids ranging from 0.2 to 20%, which become unstable leading to coagulation as the F-monomer content increases.[6, 7]

In response to these drawbacks and realizing that dispersing agents play a crucial role in the transport of highly hydrophobic fluoromonomers into a reaction site, we present for the first time a simple synthetic procedure for the incorporation of F-monomers utilizing biologically active phospholipids. As shown in the previous studies, up to 8.5% w/w of FMA can be incorporated into p-MMA/n-BA particles when phosphoric acid bis(tridecafluoro-octyl) ester ammonium salt (FSP) is utilized, and other dispersing agents may also produce stable dispersions with smaller FMA

contents.[2, 8] It appears that lower critical micelle concentration (CMC) values are responsible for facilitating environments allowing p-MMA/nBA/FMA to copolymerize into one particle.[1, 2, 9] Using this as a rule of thumb, we utilized biologically active phospholipids (PLs), which recently have been shown to function as useful dispersing agents for colloidal particles.[10-12] In the presence of sodium dodecyl sulfate (SDS) and FSP; PLs facilitate environments suitable for the synthesis of stable p-MMA/nBA/FMA colloidal particles containing as much as 15% w/w of FMA. While experimental details are provided later, the following section discusses the resulting non-spherical particle morphologies and their film formation.

Experimental

The following materials, MMA, nBA, FMA, potassium persulfate (KPS), FSP, and SDS were purchased from Aldrich Chemical Co. DLPC phospholipid was purchased form Avanti Polar Lipids, Inc. p-MMA/nBA/FMA emulsions were synthesized using a semicontinuous process outlined elsewehere,[1] and adapted for small-scale polymerization. The reaction flask was placed in a water bath set at 78°C and purged using N_2 gas. The reaction flask was charged with 20 ml of DDI water and while purging for 1hr, the content was stirred at 300 rpm. At this point all monomers and surfactants were dissolved in water and stirred under high agitation to produce a semi-stable pre-emulsion. After which, 10% (w/w) of the pre-emulsion and 18% (w/w) of the initiator solution was injected into the reaction kettle thus facilitating the seeding of the emulsion polymerization. The remaining pre-emulsion was fed continuously over 4 hr while the initiator solution was fed over 4.5hr. Upon the completion of initiator feed, polymerization was allowed to continue for another 4 hr. The amount of F-monomer incorporated into colloidal particles was determined from the initial feed composition of the initiator monomer mixture combined with the analysis of the solid content after the synthesis. Particle size measurements were obtained using a Microtrac UPA 250, and Table II-1 lists the resulting particle sizes, % solids (% w/w) based on both the initial feed as well as solid content analysis after polymerization, and concentration levels of individual components for p-MMA/nBA (A), p-MMA/nBA/FMA (8.5% w/w FMA) (B), and p-MMA/nBA/FMA (15% w/w FMA) (C). It should be noted that Table II-1 lists the w/w% of each composition utilized in the synthesis, and the % w/w of FMA listed above represents the FMA content with respect to MMA and nBA monomers. Such prepared

colloidal dispersions were cast on a poly(vinyl chloride) (PVC) substrate and allowed to coalescence at 50% relative humidity (RH) for 3 days at 23 °C to form approximately 20 μm thick films.

Colloidal particles were analyzed using a Zeiss EM 109-transmission electron microscope (TEM) in which colloidal dispersions were diluted to a 10,000:1 vol. ratio (DDI H_2O: dispersions) and deposited on formvar coated copper TEM grids (Ted Pella, Inc.). IRIRI measurements[13] were performed using a Bio-Rad FTS 6000 Stingray focal plane array detector using the procedure described earlier. The spectra and image analysis was performed using the ENVI software package (Research Systems, Inc.).

Results and Discussion

As indicated above,[1, 2] up to 8.5 % w/w of FMA can be incorporated into MMA/nBA/FMA colloidal particles when SDS/FSP dispersing agents are utilized under monomer starved conditions. This combination of ionic species reduces the surface tension, thus facilitating transport through an aqueous phase, allowing FMA polymerization at the surface of MMA/nBA particles. However when SDS/FSP/DLPC surfactant mixture is utilized, which facilitates further reduction of the surface tension, thus increasing the ability of fluorine containing monomers to diffuse into micelles, higher amounts of FMA can be incorporated into MMA/nBA particles. Figure II-1, A, B, and C illustrates transmission electron microscopy (TEM) micrographs of a series of p-MMA/nBA, p-MMA/nBA/FMA (FMA 8.5 % w/w) and p-MMA/nBA/FMA (FMA 15 % w/w) colloidal particles, respectively. As seen, p-MMA/nBA particles are spherical, whereas p-MMA/nBA/FMA exhibit more complex morphologies. As shown in Figure II-1, B, p-MMA/nBA/FMA particles (8.5 % w/w FMA) are non-spherical with the high electron density areas due to p-FMA phase forming non-uniform shell around the p-MMA/nBA core. As the FMA content increases to 15% w/w, and DLPC phospholipid was utilized, the size of p-FMA phase attached to the exterior of the particles increases, giving multi-lobe morphologies. This is illustrated in Figure II-1, C. Again, these results are in agreement with the previous studies,[1, 2] which also showed the phase separation between p-MMA/nBA and p-FMA phases, but in the presence of PLs suitable stability during and after polymerization is achieved, thus allowing incorporation up to 15 % w/w of FMA. Further increase of FMA during polymerization leads to unstable dispersions and coagulation.

The choice of DLPC was dictated by the fact that combining this PL with SDS/FSP surfactants results in the reduction of the overall surface tension of the aqueous phase from 72 mN/m to about 1-5 mN/m.[14, 15] These conditions appear to be essential during polymerization of F-containing colloidal particles because lower surface tension facilitates not only efficient monomer transport to the polymerization loci, but also provides stability of colloidal particles after synthesis. As shown earlier,[16] DLPC in the presence of sodium dioctyl sulfosuccinate (SDOSS) forms unimodal micelles and consequently monodispersed particles are polymerized. In contrast Hydrogenated soybean phosphatidylcholine (HSPC) phospholipid in the presence of SDOSS forms bimodal distribution of particles. Thus, the choice of PL is crucial. [11] As shown in Table II-1, monodispersed particles are produced when DLPC and SDS/FSP surfactants are utilized. We believe that this is attributed to similarities of head groups of DLPC and FSP and hydrophobic tails of SDS and DLPC. When monomers diffuse through an aqueous phase to the nucleation site, the reduced surface tension and monomer starvation conditions facilitate transport of higher quantities and polymerization of FMA into p-MMA/nBA particles. This is schematically illustrated in Figure II-2. As MMA and nBA monomers initially migrate to the polymerization site, and upon initiation polymerize at the reactive site, monomer starvation conditions force FMA to migrate to the reactive site and diffuse to p-MMA/nBA copolymer site, which is facilitated by the presence of PL which lowers the surface tension such that colloidal particles containing hydrophobic-lipophobic entities of p-FMA are stable and thus do not coagulate. Particle size measurements during polymerization which are shown in Figure II-3, indicate that the increase of the particle size is significant at the initial stages, whereas at later stages is

much slower. This is attributed to relative fast MMA/nBA polymerization at the early stages, followed by slower polymerization, which requires migration of FMA to the reactive site.

While one objective of these studies was to polymerize stable p-MMA/nBA/FMA particles, another goal was to examine potential stratification processes during coalescence. Since p-FMA phase by itself exhibit T_g of 172°C, it is not capable of coalescence under ambient conditions. Although copolymers prepared in these studies contain up to 15 % w/w of FMA, colloidal particles coalesce under ambient conditions forming continuous films. In an effort to illustrate the progression of film formation we monitored the morphology development during film formation using TEM. As shown in Figure II-4, A, B, C, and D, the particles coalesce, but the p-FMA phase forms its own network, which is initiated by the formation of p-FMA aggregates, most likely induced by coalescence of p-MMA/nBA phase (Figure II-4, B). As more particles coalesce (Figure II-4, C), p-FMA phase forces a separate network and eventually two distinct phases are detected: p-MMA/nBA and p-FMA (Figure II-4 D).

In an effort to verify the chemical compositions of each phase observed using TEM Figure II-5, a, illustrate internal reflection infrared images (IRIRI) of the 1203 cm^{-1} band due to p-FMA phase. As seen, there are regions which are primarily due to pMMA/nBA phase (area 1) and due to p-FMA phases (area 2) and the corresponding IR spectra recorded from area 1 and 2 are shown in Figure II-5, b, Traces, B, and C, provides evidence for the presence of these species. For reference purposes, Traces A and D are IR spectra of FMA polymer and p-MMA/nBA copolymer. As seen, area 1 primarily consists of p-MMA/nBA copolymer, whereas area 2 is mainly p-FMA. it should be noted

that the observed phase separation phenomenon is in agreement with previous studies on grafted fluorinated copolymers,[17, 18] lattices with core-shell structures,[5, 19, 20] and blends of hydrogenated and fluorinated polymers,[7] which also have shown that homogeneous networks cannot be obtained.

Conclusions

In summary, FMA, being most hydrophobic among the three monomers MMA, nBA, and FMA, exhibits the lowest surface tension and poor water solubility, and as previous studies indicated, its incorporation into MMA/n-BA particles results from monomer-starved conditions utilized in the later stages of polymerization. As shown in Figure II-3, the particle growth is steady and monomodal during polymerization, thus ruling out the possibility of FMA polymerization as a separate phase. Furthermore, p-FMA bonding to the p-MMA/n-BA particles seems to be physical because during film formation there is clear phase separation between the p-FMA and p-MMA/n-BA phases, as illustrated in Figures II-4 and II-5. Thus, the mechanism depicted in Figure II-2 seems to be the most probable during which first MMA and nBA monomers migrate from the monomer droplets to the reactive site to form colloidal particles, and because of lower FMA solubility, these species migrate to the polymerizing site under starvation conditions and polymerize onto MMA/nBA colloidal particles.

Table II-1. Composition and Particle Size Analysis of Colloidal Dispersions Prepared for the Purpose of These Studies.

	(A) MMA/nBA	(B) MMA/nBA/FMA(8.5%)	(C) MMA/nBA/FMA(15%)
FMA (%w/w)	0	3.3	5.8
nBA (%w/w)	18.9	17.33	16.1
MMA (%w/w)	19.7	18.04	16.73
SDS (%w/w)	0.91	0.91	0.91
FSP (%w/w)	0.58	0.58	0.58
DLPC (%w/w)	0.05	0.05	0.19
KPS (%w/w)	0.23	0.23	0.23
DDI (% w/w)	59.5	59.5	59.5
Particle Size (nm)	110	124	150
% Solids	40.5	40.5	40.5

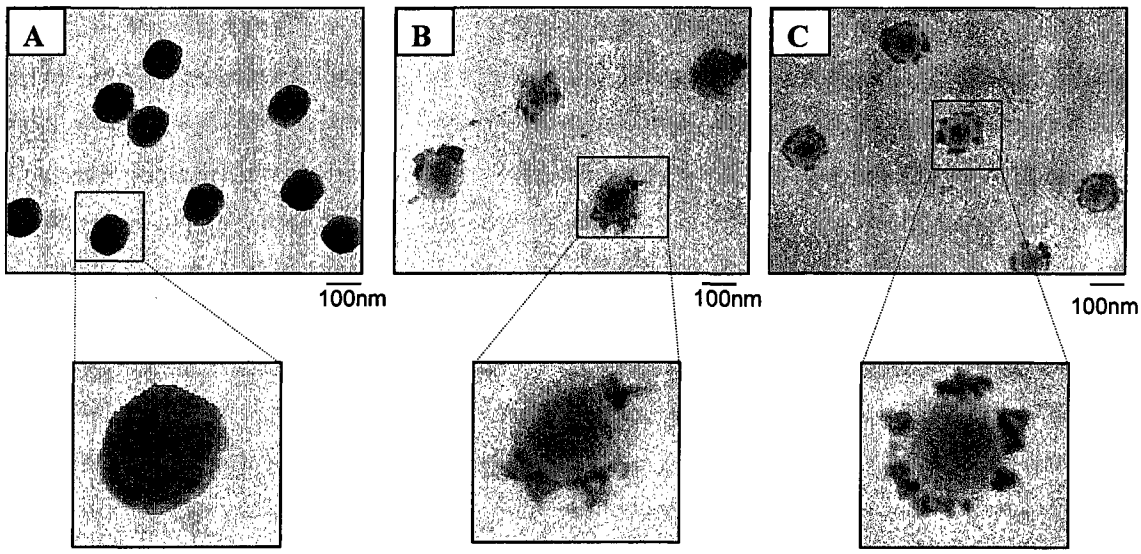

Figure II-1. Transmission electron micrographs of (A) MMA/nBA, (B) MMA/nBA/FMA (8.5% w/w of FMA), and (C) MMA/nBA/FMA (15% w/w of FMA).

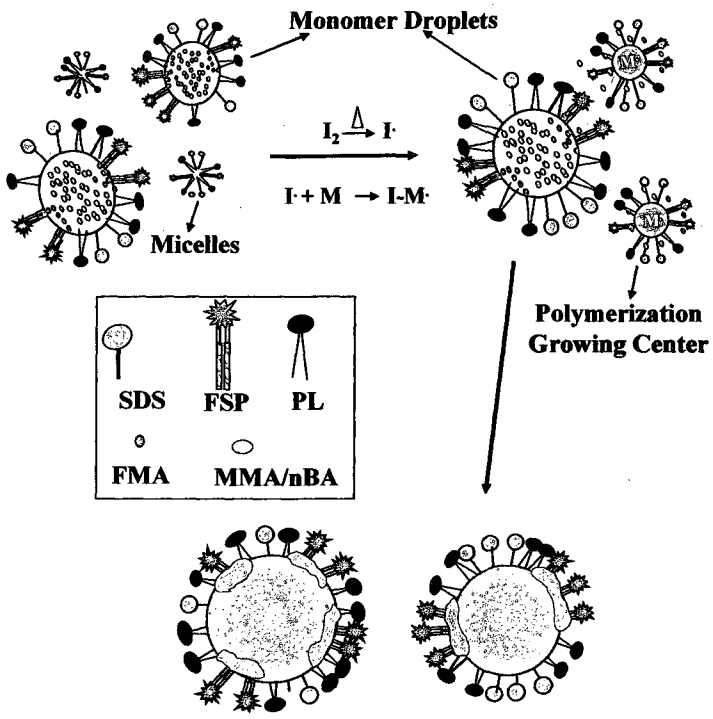

Figure II-2. Schematic diagram illustrating the formation of mixed micelles and polymerization of non-spherical p-MMA/nBA/FMA colloidal particles.

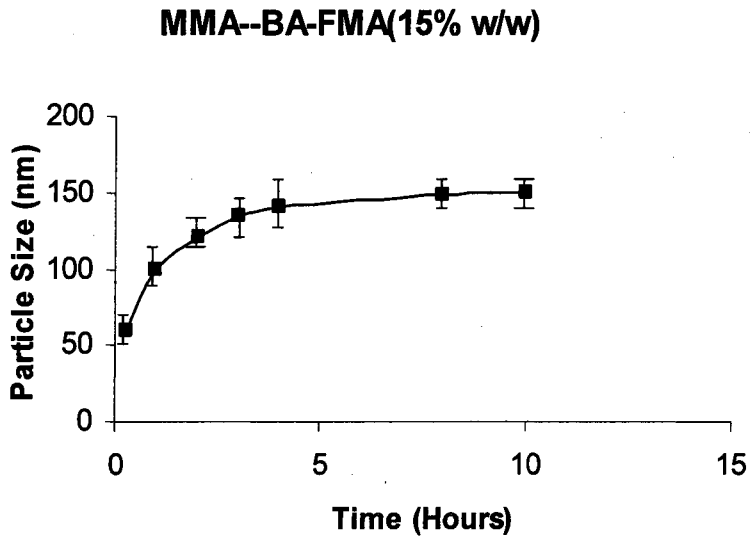

Figure II-3. Particle size plotted as a function of time during polymerization of p-MMA/nBA/FMA colloidal dispersions.

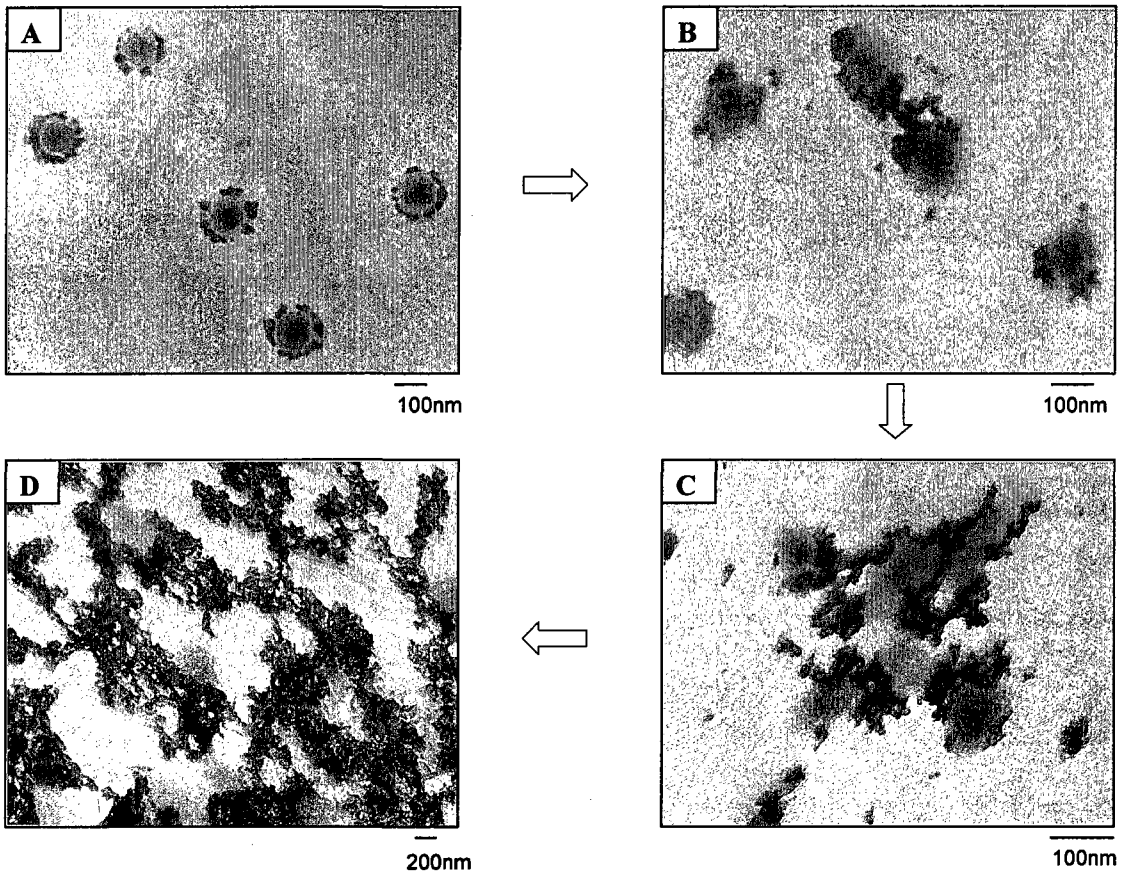

Figure II-4. Transmission electron micrographs of p-MMA/nBA/FMA colloidal particles recorded at various stages of coalescence: (A) isolated particles prior to coalescence; (B) initial stages of coalescence illustrating particles colliding with each other; (C) final stages of coalescence and initiation of phase separation; (D) network formation and phase separation of p-FMA and p-MMA/BA.

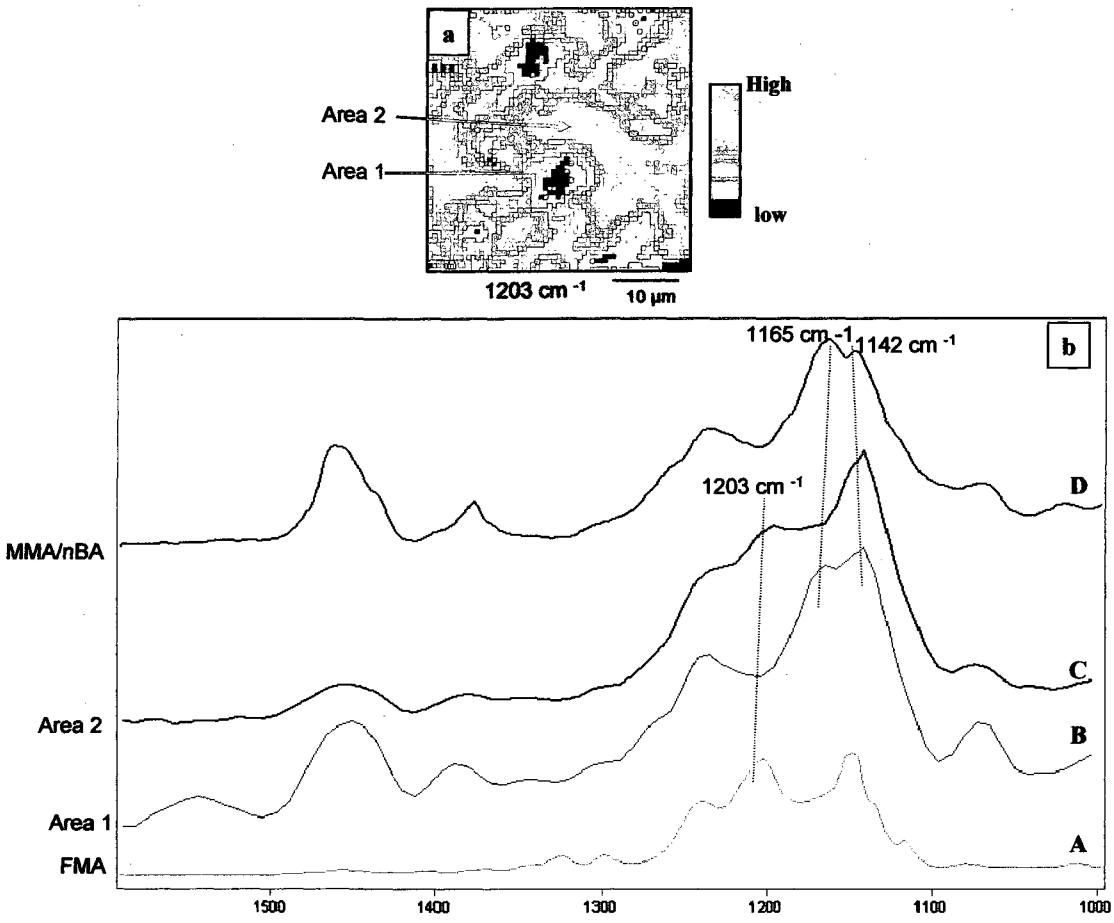

Figure II-5. (a) IRIR image of the 1203 cm^{-1} band due to C-F vibrations, (b) IR spectra of (A) FMA monomer; (B) IR spectra recorded from area labeled 1 in the image A; (C) IR spectra recorded from area labeled 2 in the image A; (D) IR spectra of p-MMA/nBA.

References

1. Dreher, W. R.; Jarrett, W. L.; Urban, M. W. *Macromolecules* **2005,** 38, 2205.

2. Dreher, W. R.; Singh, A.; Urban, M. W. *Macromolecules* **2005,** 38, 4666.

3. Thomas, R. R.; Lloyd, K. G.; Stika, L. M.; Stephens, L. E.; Megallanes, G. S.; Dimonie, V. L.; Sudol, E. D.; El-Aasser, M. S. *Macromolecules* **2000,** 33, 8828.

4. Landfester, K.; Rothe, R.; Antonietti, M. *Macromolecules* **2002,** 35, 1658.

5. Ha, J.; Park, I.; Lee, S.; Kim, D. *Macromolecules* **2002,** 35, 6811.

6. Koendrick, G. H.; Sacanna, S.; Pathmamanoharan, C.; Rasa, M.; Philipse, A. P. *Langmuir* **2001,** 17, 6086.

7. Linemann, R. F.; Malner, T. E.; Brandsch, R.; Bar, G.; Ritter, W.; Mulhaupt, R. *Macromolecules* **1999,** 32, 1715.

8. Dreher, W. R.; Jarrett, W. L.; Urban, M. W. *Macromolecules* **2005,** 38, 2205.

9. Mele, S.; Murgaia, S.; Monduzzi, M. *Journal of Fluorine Chemistry* **2004,** 125, 261.

10. Yacoub, A.; Urban, M. W. *Biomacromolecules* **2003,** 4, 52.

11. Lestage, D. J.; Schleis, D. J.; Urban, M. W. *Langmuir* **2004,** 20, 7027.

12. Lestage, D. J.; Urban, M. W. *Langmuir* **2005,** 21, 2150.

13. Otts, D.; Zhang, P.; Urban, M. W. *Langmuir* **2002,** 18, 6473.

14. Nii, T.; Ishii, F. *Colloids Surf. B: Biointerfaces* **2004,** 39, 57.

15. Pinazo, A.; Wen, X.; Liao, Y. C.; Prosser, A. J.; Franses, E. I. *Langmuir* **2002,** 18, 8888.

16. Lestage, D. J.; Yu, M.; Urban, M. W. *Biomacromolecules* **2005,** 6, 1561.

17. Mawson, S.; Johnston, K. P.; Betts, D. E.; MaClain, J. B.; Desimone, J. M. *Macromolecules* **1997,** 30, 71.

18. Park, I.; Lee, S. b.; Choi, C. K. *Macromolecules* **1998,** 31, 75553.

19. Marion, P. B.; Juhue, D.; Lang, J. *Macromolecules* **1997,** 30, 123.

20. Chen, Y.; Ying, L.; Yu, W. J.; Kang, E.; Neoh, K. *Macromolecules* **2003,** 36, 9451.

CHAPTER III

FLUOROMETHACRYLATE-CONTAINING COLLOIDAL DISPERSIONS: ORIGIN OF NON-SPHERICAL PARTICLE MORPHOLOGY AND TEMPERATURE-RESPONSIVE STRATIFICATION

Abstract

Due to unique properties of fluoropolymers, F-containing water dispersible colloidal dispersions continue to be of great interest and represent significant scientific challenges. These studies focus on the development and understanding of morphologies of F-containing colloidal particles synthesized in an aqueous phase in the presence of bio-active dispersing agents. When methyl methacrylate (MMA), n-butyl acrylate (n-BA), and heptadecafluorodecylmethacrylate (FMA) monomers are copolymerized in an aqueous phase, in the presence of phospholipids (PL), non-spherical particle morphologies are obtained. Their morphologies depend upon MMA/nBA ratios and lead to significantly different coalescence mechanisms and consequently surface properties. For higher MMA content, the particles are spherical, but at higher nBA contents, non-spherical morphologies are produced. This behavior is attributed to monomer starved conditions and the differences in reactivity ratios which forces copolymerization of FMA on the surface of p-MMA/n-BA particles, giving rise to non-spherical morphologies in the presence of biologically active PLs. Such prepared aqueous dispersions upon coalescence form films that exhibit ultra-low static and kinetic coefficients of frictions which are attributed to internal phase stratification during coalescence.

Introduction

The attractiveness of fluoropolymers originates from their unique thermal, chemical, and mechanical stability, and low surface energies. While these attributes make fluoropolymers particularly suitable candidates in biotechnology,[1] microelectronics, and other applications, processing temperatures and particularly film formation may be troublesome.[2-4] Further complexity arises from limited or no solubility of fluoromonomers in an aqueous phase. One approach to overcome these obstacles is to utilize colloidal copolymerization of fluoro-monomers with other monomeric species to form stable colloidal particles capable of coalescence. Although several attempts have been made to prepare fluorinated colloidal dispersions, elaborate synthetic procedures and the use of co-solvents along with relatively low solids and fluorine contents represent significant challenges.[4-9] Another approach is to utilize a combination of dispersing agents during aqueous copolymerization of flouro and acrylate families of monomers.[10-12] As recently shown,[10] the use of bioactive dispersing agents provides an opportunity for the synthesis of stable colloidal dispersions containing up to 15% w/w copolymerized F-monomers and, under monomer starvation conditions, p-methylmethacrylate/n-butylacrylate/heptadeca fluorodecyl methacrylate (p-MMA/nBA/FMA) stable colloidal dispersions with unique non-spherical morphologies were obtained. It should be noted that without the use of bioactive dispersants only 8.5 % w/w of a fluoropolymer was incorporated into pMMA/nBA. During the course of these studies, which primarily focused on synthetic aspects, it became quite apparent that understanding the mechanisms of the formation of non-spherical particle morphologies is essential to control particle morphologies and

subsequently their film formation.[10] With this in mind, and considering the inherent complexity of F-containing colloidal dispersion synthesis, initial observations indicated that by varying MMA/nBA ratios while maintaining the same fluoro-acrylate (FMA) content composition, significant variations in particle morphologies were detected.

In view of these observations, one objective of these studies is to elucidate the origin of morphological changes in p-MMA/nBA/FMA particles, and to further advance limited knowledge of their coalescence. These issues are particularly relevant because previous studies showed that during film formation, phase separation between fluorinated and non-fluorinated components is observed for grafted fluorinated copolymers,[13, 14] lattices with core-shell structures,[10-12, 15, 16] and blends of hydrogenated and fluorinated polymers.[4] Furthermore, F-containing components preferentially stratify near the film-air (F-A) interface which results from unfavorable enthalpic interactions between fluoro and hydrocarbon polymer phases, leading to the reduction of the free energy driven by stratification of individual components.[17-20] Thus, stratification during coalescence is of particular interest which may be responsive to temperature changes and one example of fluoropolymer surfaces which exhibit temperature responses are fluoropolymer brushes.[21, 22] Thus, another objective of this study is to determine how p-MMA/nBA/FMA particle morphologies affect thermo-responsive behavior during and after film formation.

Experimental

MMA, nBA, FMA, potassium persulfate (KPS), phosphoric acid bis(tridecafluoro-octyl) ester ammonium salt (FSP), and sodium dodecyl sulfate (SDS) were purchased from Aldrich Chemical Co. 1,2-dilauroyl-sn-glycero-3-phosphocholine (DLPC) phospholipid was purchased from Avanti Polar Lipids, Inc. p-MMA/nBA/FMA dispersions were synthesized using a semicontinuous process outlined elsewehere,[12, 23] and adapted for small-scale polymerization. The reaction flask was placed in a water bath set at 78°C, purged with N_2 gas, charged with 20 ml of DDI water under continuous stirring at 300 rpm. SDS, FSP, and DLPC surfactants were utilized and Table III- 1 provides ratio of all dispersions prepared for the purpose of these studies. Surfactants were dissolved in water under continuous stirring at 600 rpm, followed by the addition of monomers to produce a semi-stable pre-emulsion. It should be noted that pre-dispersions are monomer droplets dispersed in water which require continuous stirring in order to avoid monomer-water phase separation. For seeded dispersion process, 10% (w/w) of the pre-emulsion and 18% (w/w) of the initiator solution were initially injected into the reaction kettle, thus facilitating the seed formation. The remaining pre-dispersion was fed continuously without stirring over period of 4 hrs while the initiator solution was added for 4.5 hrs. Upon completion of the initiator feed, polymerization was allowed to continue for another 5 hrs. This process resulted in 40.5% w/w solids which was determined from the initial feed composition of the initiator monomer mixture and the analysis of the solid content after the synthesis. As listed in Table III- 1, the following compositions of colloidal particles containing 15% w/w of FMA were prepared: (A) MMA/nBA (100:0), (B) MMA/nBA (90:10), (C)

MMA/nBA (75:25), (D) MMA/nBA (50:50), (E) MMA/nBA (25:75), (F) MMA/nBA (10:90), (G) MMA/nBA (0:100).

Table III-1 lists the particle size analysis with the accuracy of ± 5 nm obtained using a Microtrac UPA 250 instrument. Monomodal dispersions were obtained for all compositions listed in Table III-1. Morphologies of colloidal particles were determined using a Zeiss EM 109-transmission electron microscope (TEM) in which colloidal dispersions were diluted to a 10,000:1 vol. ratio (DDI H_2O: dispersions) and deposited on a formvar coated copper TEM grid (Ted Pella, Inc.).

Colloidal particle solutions were allowed to coalesce for 72 hrs in a controlled environment at 23 °C temperature and 60% relative humidity (RH) to form approximately 10μm thick films. The films were obtained by draw down on the polyvinyl chloride substrates (PVC). For contact angle measurements as well as atomic force microscopy (AFM) experiments colloidal solutions were coalesced on a glass slide using a draw bar to give an approximate film thickness of 10μm. For thermoresponsive investigation, selected films were annealed at 60, 90, 120 and 150 °C for 2h.

Solid-state ^{13}C NMR measurements were performed on a Varian ^{UNITY} INOVA 400 spectrometer using a standard Chemagnetics 7.5 mm PENCIL-style probe. Samples were loaded into zirconia rotor sleeves, sealed with Teflon caps, and spun at a rate of 4.5 kHz. The standard cross polarization magic angle spinning (CP/MAS) technique was used with high-power proton decoupling implemented during data acquisition. The acquisition parameters were as follows: The ^{1}H 90° pulse width was 4.0 μs, the cross-polarization contact time was 1 ms, the dead time delay was 6.4 μs, and the acquisition

time was 45 ms.[24] A recycle delay of 3 s between scans was utilized. Experiments requiring simultaneous ^{1}H and ^{19}F decoupling were performed using a 3.2 mm HFXY probe. The ^{1}H and ^{19}F 90° pulse widths were 4.0 *is*, the acquisition time was 26 ms, and the 19F-13C cross-polarization contact time was 10 ms. A recycle delay of 2 s and a samples spinning rate of 5 kHz were used.

Internal reflection infrared (IRIR) images were obtained using a Bio-Rad FTS 6000 Stingray system with a Ge internal reflection element (IRE). This system consists of a Bio-Rad FTS 6000 spectrometer, a UMA 500 microscope, an Image IR focal plane array (FPA) image detector, and a semispherical germanium IRE. IRIR images were collected using the following spectral acquisition parameters: under sampling ratio 4, step-scan speed 2.5 Hz, number of spectrometer steps 1777, number of images per step 64, and spectral resolution 8 cm^{-1}. the use of a Ge crystal in contact with the analyzed surface allows spatial resolution in the range of 1 μm.[25] In a typical experiment, spectral data set acquisition time was 17 minutes and image processing was performed using ENVI software (The Environment for Visualizing Images, Research Systems, Inc.) version 3.5.

Atomic force microscopy (AFM) measurements were conducted on a Nanoscope III Dimension 3000 scanning probe microscope, Digital Instruments. A silicon probe with 125μm long silicon cantilever, nominal force constant of 40 N/m and resonance frequency of 275 KHz were used in a tapping mode, allowing estimation of surface topography and roughness. Surface topography was determined on a 10 μm x 10 μm area with an image resolution of 256 x 256 pixels at a scan rate of 1Hz. Surface roughness analysis was performed using Nanoscope version 5.30 r2 image analysis

software. Surface tension measurements were obtained using a FTA200 dynamic contact angle analyzer, and a Qualitest 1055 friction tester was utilized to determine coefficients of friction.[26]

Results and Discussion

One of the objectives of these studies is to elucidate the origin of the formation of non-spherical morphologies obtained during the synthesis of p-MMA/nBA/FMA colloidal particles. During the first step, different nBA/MMA ratios containing the same amount of FMA (15% w/w) were synthesized and Table III-1 provides their compositions along with the particle size analysis. The particle size data indicate that for exactly the same polymerization conditions and % w/w solids, particle sizes varies from 95 to 160 nm. This increase parallels an increase of the nBA/MMA ratio. This behavior is attributed to lower density of p-nBA and the increased free volume of the p-nBA phase (Tg= -46°C)[27] which, for the same molar amount of the monomer, result in the increased particle size. TEM images shown in Figure III-1 A-G illustrate morphologies of synthesized particles in the order of the increasing nBA/MMA ratio. As seen in Figure III-1 A, spherical morphologies of p-MMA/FMA colloidal dispersions with no differences in electron density are observed. Similarly, for 90:10 and 75:25 MMA/nBA ratios, uniform morphologies are observed, as illustrated in Figure III-1 B and C, respectively. However, for 50:50 nBA/MMA ratio, non-spherical morphologies are produced and Figure III-1 D illustrates TEM image of these particles. Similarly, as the nBA/MMA ratio increases (while maintaining the same FMA content), non-spherical morphologies prevail. This is illustrated in Figure III-1, Images E, F, and G, respectively.

Although TEM images shown in Figure III-1 provide evidence that p-MMA/nBA/FMA particles exhibit non-spherical core-shell morphologies, in an effort to determine particle composition, solid state NMR spectroscopy was utilized and films

containing p-nBA/MMA/FMA (nBA/MMA ratio = 50:50) and p-MMA/FMA (ratio = 85:15) were analyzed. Figure III-2, Trace A, illustrates ^{13}C NMR spectrum of p-MMA/FMA and the presence of perfluoroalkyl side chain of FMA is detected at 115 ppm due to CF_2 groups of p-FMA.[12] In order to enhance selectivity of NMR analysis, we utilized cross-polarization of ^{19}F and ^{13}C along with the decoupling of ^{1}H and ^{19}F nuclei.[12] This technique facilitates through-space conditions, and the resulting spectrum provides information about functional groups in close proximity of the perfluoroalkyl side chains. For the purpose of these studies, experiments with the increasing cross polarization contact times ranging from 2 to 10ms were conducted. As shown in Figure III-2, Trace B, upon increasing cross polarization contact time to 10ms, only CF_2 and CF_3 groups are detected at 115 and 118 ppm, respectively. However, in p-MMA/FMA spectrum shown in Figure III-2, Trace B', the CH_2 and C=O resonances at 50 and 180 ppm due to MMA are detected along with the 115 and 118 ppm peaks due to CF_2 groups.[28] Since this is through space and not bond-to-bond experiment, these data show that MMA units are in a close proximity to FMA, thus indicating the formation of p-MMA/FMA random copolymer particles.

These experiments show that, under the same polymerization conditions, for higher MMA content, colloidal dispersions containing 15% FMA spherical morphologies are obtained. Also, p-MMA/FMA forms random copolymer under monomer starved conditions when both monomers are fed at the same time. However, the access of nBA (> 50% w/w with respect to MMA) leads to the formation of non-spherical particles. If one considers the hydrophobicity of the employed monomers, it appears that nBA being more hydrophobic with respect to MMA,[27] should generate

homogeneous particles in the presence of FMA. This is, however, not the case. FMA exhibits significantly higher hydrophobicity and oleophobicity with respect to nBA and MMA, and phase separates at higher nBA contents during polymerization. This behavior is attributed to the fact that during polymerization, MMA migrates to reactive sites and compositional drift in the growing particles occurs only when nBA/MMA ratios are equal or greater than 50:50. This behavior is attributed to higher reactivity ratios of MMA with respect to FMA (39), as compared to nBA, which is significantly smaller toward FMA (23).[29,*] As a result, when MMA and FMA are polymerized, random copolymers are obtained, whereas copolymerization of nBA/FMA results in block copolymers in which the p-FMA phase is present on the exterior of the particles, resulting in non-spherical morphologies.

The next question is what is the driving force for the growth of p-FMA phase on the surface of p-MMA/nBA seeds and what are the limiting factors that allow us to obtain stable dispersions containing up to 15% FMA solids. Due to higher and comparable reactivity ratios of MMA and FMA, spherical morphologies with no phase separation are produced, which is schematically shown in Scheme III-1 (A). For (B) p-nBA/FMA copolymer, p-FMA is locally polymerized on the p-nBA core, thus producing non-spherical morphologies. This was illustrated in Figure III-1, Images, D-G. Furthermore, when MMA/nBA/FMA monomers are copolymerized, there is competition between nBA and FMA monomers for copolymerization with MMA and since FMA exhibits low aqueous solubility, it slowly migrates to reactive sites which is facilitated by the presence of PLs, thus allowing MMA-nBA to polymerize first,

* Since no Q and e values for FMA are available in the literature, the reactivity ratios were estimated utilizing Q and e values for MMA, nBA, and tetrafluoroethylene (TFE).

followed by FMA reactions on the existing p-MMA/nBA core. As a consequence, non-spherical core-shell are obtained for the nBA higher content. It should be noted that the particle size measurements during polymerization revealed monomodal particle size distribution at all stages, thus showing that pFMA phase does not polymerize as a separate entity.

Although one may argue that Q and e values of TFE should not be used to access the reactivity of FMA, which is a valid point, there is no literature data available on fluoroacrylates. However, taking into account the solubility of each monomer in an aqueous phase in the presence of other monomers, and considering the order of reactivity being MMA>nBA>>FMA and polarity of each monomer, the following scenario may be considered: FMA is more miscible in more polar MMA, but less miscible within nBA, and therefore spherical particles are formed for pMMA/FMA, whereas non-spherical particles are obtained for p-nBA/FMA polymerizations. Although solubility and polarity indeed contribute to the sequence of events leading to the formation of non-spherical particles, the reactivity of each monomer and the lowering of the surface tension facilitated by PL dominate the polymerization process.

The limiting factor for FMA incorporation into colloidal dispersions is the stability of colloidal particles. In these studies we utilized bio-active PLs which form random mixed micellar structures with SDS and FSP surfactants. PLs being the main constituents of the cell membranes serve as selective barriers for bio active species as well as provide support for membrane protein transport.[30] When PLs along with SDS and FSP form mixed micellar structures, the p-FMA phase growth on the p-MMA/nBA colloidal particles is facilitated due to the reduction of the overall surface tension of the

aqueous phase from 72 to about 1-5 mN/m.[31, 32] This is the reason for choosing DLPC as one of the dispersing agents during synthesis in order to form p-MMA/nBA seeds, followed by creating monomer starvation conditions which forces FMA monomers to migrate to reactive sites. Although exact mechanism of PL's needs further examination, one can envision that DLPC may form bilayered structures with hydrophobic interior and hydrophilic exterior, thus facilitating transport of FMA monomers to already formed p-MMA/nBA seeds. In essence, PLs exhibit dual functions: (1) they facilitate transport of FMA to the p-MMA/nBA core and (2) stabilize the growing particles. A schematic diagram illustrating formation of p-MMA/FMA (A), nBA/FMA (B), and p-MMA/nBA/FMA (C) colloidal dispersions with different particle morphologies are illustrated in Scheme III-1.

Another objective of this study is to create polymeric films which coalesce under ambient condition and exhibit fluoropolymer properties. In the context of the formation of non-spherical particle morphologies, the next question is how the presence of the FMA phase on p-MMA/nBA particles will affect coalescence. For that reason colloidal dispersions of p-nBA/FMA and p-MMA/FMA were allowed to coalesce and their surfaces were analyzed using IRIRI which allows us to spatially resolve chemical surface heterogeneities with 1 μm spatial resolution. Analysis of the C-O-C stretching modes due to p-MMA and p-nBA at 1165 and 1145 cm^{-1} as well as C-F stretching bands at 1203 cm^{-1} due to FMA are of particular interest because these bands allow us to follow the mobility of fluorinated species within the film. The choice of the C-F stretching mode at 1203 cm^{-1} for monitoring pFMA distribution on the surface over the C-O-C stretching at 1145 cm^{-1} was dictated by the C-O-C overlap with the same C-O-C

vibrations in pMMA. Figure III-3 illustrates an IRIR image of the films obtained from p-nBA/FMA colloidal particles which was obtained by tuning into the 1203 cm^{-1} band due to FMA. Analysis of the image shown in Figure III-3 A indicates that the distribution of the p-FMA phase is heterogeneous. The corresponding IR spectra recorded from areas 1 and 2 show that the 1203 cm^{-1} band is absent in area 1 (Figure III-3, B, Trace B), but detected in the area 2 (Figure III- 3B, spectrum C), thus showing the presence of p-FMA in the red region (area 2) of Image A. For reference purposes, Trace A illustrate IR spectrum of FMA monomer. These data show that during coalescence of p-FMA component, which is present on the exterior of the colloidal particles, the p-FMA phase separates out from p-nBA, thus leading to vertically stratified films. Previous studies have shown that for the films coalesced from p-MMA/nBA/FMA (15% w/w FMA) dispersions two distinct phases of p-FMA and p-MMA/nBA are formed.[10]

Similar analysis of the films containing p-MMA/FMA was conducted by tuning into the 1203 cm^{-1} band due to FMA and the 1145 cm^{-1} band due to MMA. This is illustrated in Figure III- 4 A and B. In contrast to p-nBA/FMA, no compositional variations exist and no phase separation occurs, as indicated by the corresponding IR spectrum recorded from areas 1 and 2. These data are in agreement with the results of TEM and NMR analysis. It is apparent that the heterogeneity during film formation is influenced by acrylate components of colloidal dispersions and their mobility during and after coalescence. In the case of p-nBA/FMA, due to low T_g of p-nBA phase (-46 ^0C),[27] the minimum film formation temperature (MFFT) is significantly lower which facilitates mobility during film formation, and thus ability of the p-FMA phase to

diffuse to the F-A interface driven by its low surface energy. In contrast, for p-MMA/FMA with the T_g of p-MMA and p-FMA of 100°C and 175 °C, respectively, film formation is inhibited.

In order to facilitate coalescence under ambient conditions,[12, 27] p-MMA/FMA and p-nBA/FMA dispersions were mixed in equal amounts and allowed to coalesce, followed by measurements of the static and kinetic coefficients of friction. The values of 0.145 and 0.042, respectively, were obtained, which are significantly smaller than for p-MMA/nBA films (0.78 and 0.38). Although only 15% w/w of fluoropolymer with respect to MMA/nBA ratio was incorporated, the changes of surface properties are drastic. This is attributed to stratification of the p-FMA phase to the F-A interface, leading to surface enrichment resulting from stratification of low surface energy p-FMA phase. As shown by the previous studies,[10] p-FMA forms network structure during coalescence and due to low surface energy, migrates to the F-A interface.

It is well established that temperature significantly affects phase separation in polymeric films. In order to determine the effect of temperature on the degree of stratification of the p-FMA phase in p-MMA/FMA and p-nBA/FMA mixture, films containing 15% w/w FMA were annealed at 60, 90, 120, and 150 °C and AFM measurements were conducted. The results are shown in Figure III-5, where AFM images A-D illustrate a series of phase and height images recorded from the F-A interface of the films coalesced at 23°C (A/A'), annealed at 60 (B/B'), 120 (C/C'), and 150°C (D/D'). The root mean square roughness (RMS) of height deviations taken from the mean data plane is shown in Figure III-5, Image A, and illustrates two phase components attributed to fluorinated (brighter regions) and non-fluorinated phases

(darker regions). Upon annealing at 60 ^{0}C, small domains begin to appear, and at 120 and 150 ^{0}C, phase separation becomes prominent, where the increase of the domain size is observed. This is also reflected in the RMS roughness values which increase as a function of temperature.

In order to confirm that indeed upon annealing the fluoropolymer is responsible for the formation of surface domains IRIRI measurements were conducted. While Figure III-6 A illustrates an AFM phase image of the film annealed at 150 ^{0}C, Figure III-6 B represents IRIR image of the 1203 cm^{-1} band due to C-F stretching vibrations of p-FMA. As seen, distribution of the p-FMA phase is heterogeneous with red areas corresponding to elevated p-FMA phase. Furthermore, analysis of areas 1 and 2 indicate that area 1 exhibits enhanced intensities of the 1203 cm^{-1} band, thus signifying the presence of the p-FMA rich domains, and reduced intensities in area 2. These changes correspond to the phase image data shown in Figure III-6 A. Furthermore, these features are also responsible for the increase of the contact angle. As illustrated in Figure III-7, static, advancing, and receding water contact angle measurements show that static and advancing contact angle increase to 118^0 and 124^0, respectively, upon annealing at 150°C. In summary, temperature has a significant effect on stratification not only of low molecular weight species, but also on high molecular weight polymers such as p-FMA phase in p-MMA/nBA/FMA system. Scheme III-2 illustrates a schematic diagram depicting the effect of temperature on surface roughness.

Conclusions

Colloidal dispersions p-MMA/nBA/FMA containing 15% w/w FMA and various nBA/MMA ratios were synthesized using a combination of SDS/FSP/DLPC dispersing agents under monomer starved conditions. The formation of stable F-containing particles is attributed to the presence of bio-active DLPC phospholipids and monomer starvation conditions during polymerization. These studies also showed that when nBA/MMA ratio is greater than 1:1, FMA polymerizes on the surface of p-MMA/nBA, and non-spherical particles of p-MMA/nBA/FMA are formed. In order to facilitate film formation p-MMA/FMA particles and p-nBA/FMA phases were mixed which upon coalescence forms stratified films and the degree of p-FMA stratification towards the F-A interface depends on temperature. As a result, a number of surface properties such as surface roughness and contact angle or surface energy can be altered.

Table III- 1. Composition and Particle Size Analysis of Colloidal Dispersions Containing 15%W/W of FMA with Different Ratios of MMA/nBA: A- MMA/nBA(100:0); B- MMA/nBA (90:10); C- MMA/nBA (75:25); D- MMA/nBA (50:50); E- MMA/nBA (25:75); F- MMA/nBA (10:90); G- MMA/nBA (0:100).

Composition	MMA/FMA	MMA/nBA/FMA	MMA/nBA/FMA	MMA/nBA/FMA	MMA/nBA/FMA	MMA/nBA/FMA	MMA/nBA/FMA
MMA/nBA Ratio	100:0	90:10	75:25	50:50	25:75	10:90	0:100
Individual Components (w/w%)	(A)	(B)	(C)	(D)	(E)	(F)	(G)
DDI	59.5	59.5	59.5	59.5	59.5	59.5	59.5
Methyl methacrylate	33.17	29.85	24.88	16.59	8.29	3.32	0
N-butylacrylate	0	3.32	8.29	16.58	24.88	29.85	33.17
FMA	5.8	5.8	5.8	5.8	5.8	5.8	5.8
SDS	0.91	0.91	0.91	0.91	0.91	0.91	0.91
FSP	0.58	0.58	0.58	0.58	0.58	0.58	0.58
DLPC	0.05	0.05	0.05	0.05	0.05	0.05	0.05
$K_2S_2O_8$	0.23	0.23	0.23	0.23	0.23	0.23	0.23
Solids %	40.5	40.5	40.5	40.5	40.5	40.5	40.5
Particle Size (nm)	95	106	120	140	146	150	160

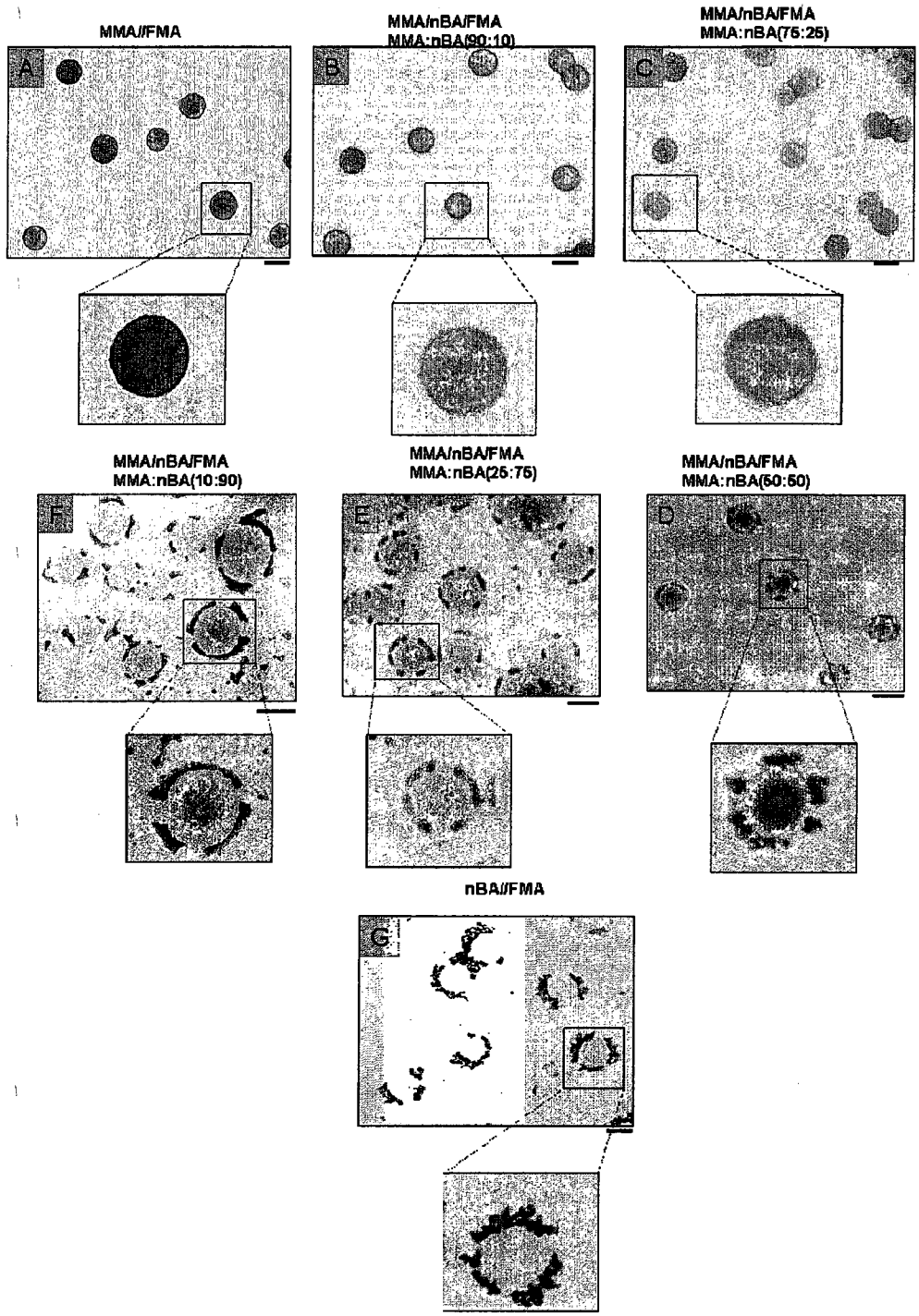

Figure III- 1. Transmission electron micrographs of colloidal particles containing 15%w/w of FMA with different MMA/nBA ratios: A- MMA/nBA (100:0); B- MMA/nBA (90:10); C- MMA/nBA (75:25); D- MMA/nBA (50:50); E- MMA/nBA (25:75); F- MMA/nBA (10:90); G- MMA/nBA (0:100) (FMA to MMA/nBA ratio was maintained constant at 15:85 ratio).

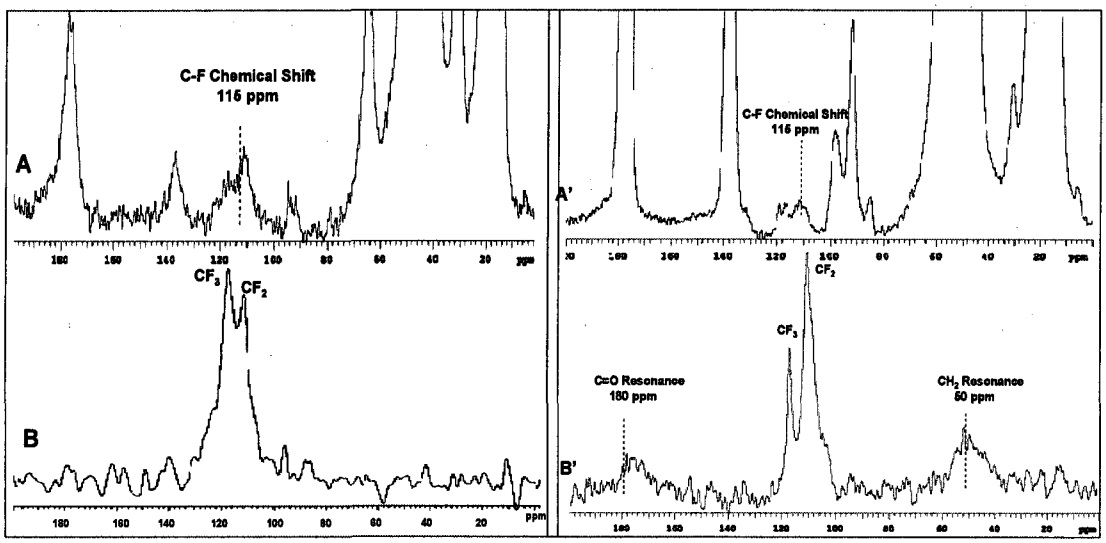

Figure III- 2. Solid state NMR spectra of p-MMA/nBA/FMA copolymer films: A - ^{13}C NMR spectrum; B - ^{19}F and ^{13}C cross-polarization experiments with ^{1}H and ^{19}F decoupling; A' - ^{13}C NMR spectrum; B' - ^{19}F and ^{13}C cross-polarization spectrum obtained using ^{1}H and ^{19}F decoupling.

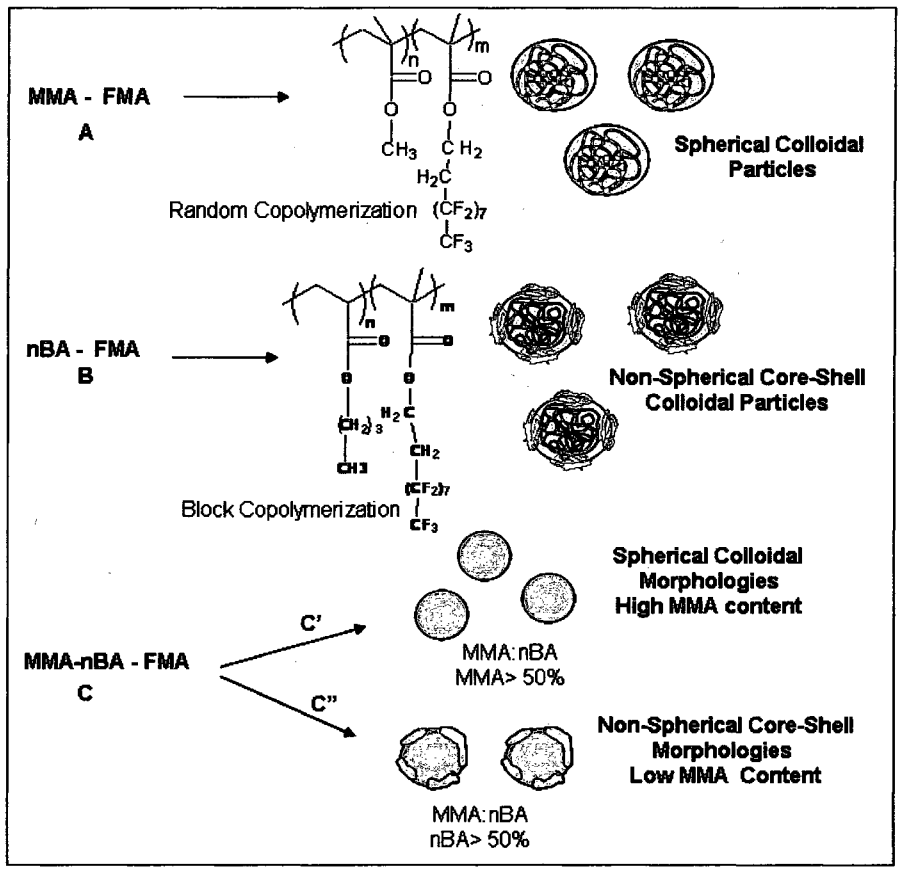

Scheme III-1. Schematic diagram illustrating the effect of monomer copolymerization on particle surface morphology.

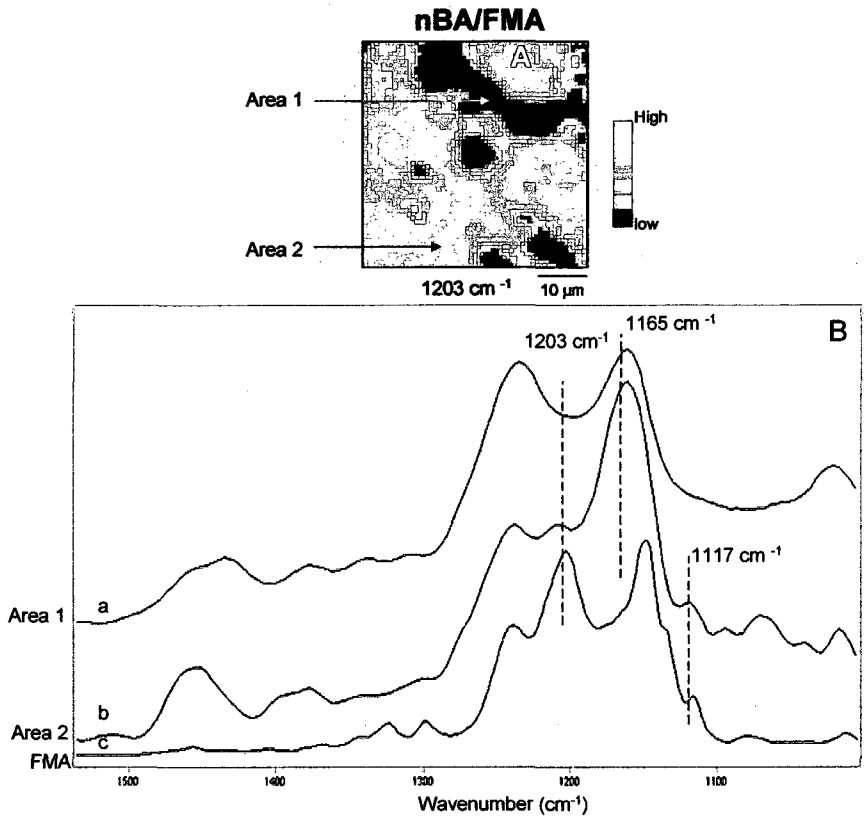

Figure III- 3. IRIR images recorded from the F-A interface of coalesced films obtained from p-nBA/FMA colloidal dispersions: A - image obtained by tuning into 1203 cm^{-1}; B - IR spectra recorded from areas labeled 1 and 2 in image A; a - IR spectrum of area 1; b - IR spectrum of area 2; c - IR spectrum of FMA.

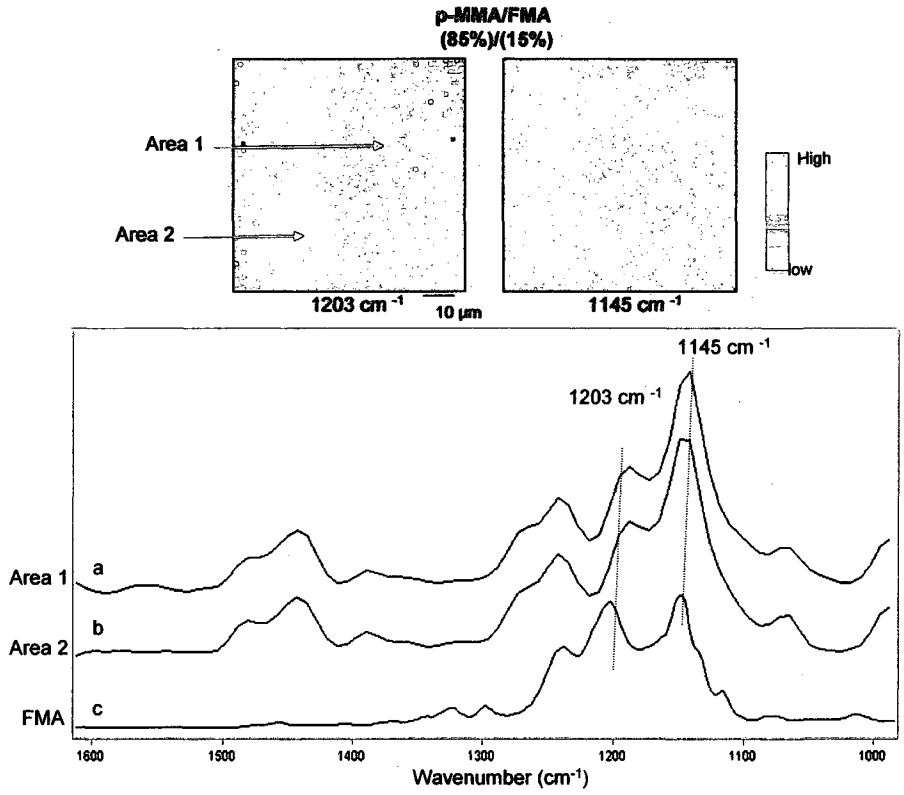

Figure III- 4. IRIR images recorded from the F-A interface of coalesced films obtained from p-MMA/FMA colloidal dispersions: A - image obtained by tuning into 1203 cm^{-1}; B - image obtained by tuning into 1145 cm^{-1}, C - IR spectra recorded from areas labeled 1 and 2 in image A.; a - IR spectrum of area 1; b - IR spectrum of area 2; c - IR spectrum of FMA.

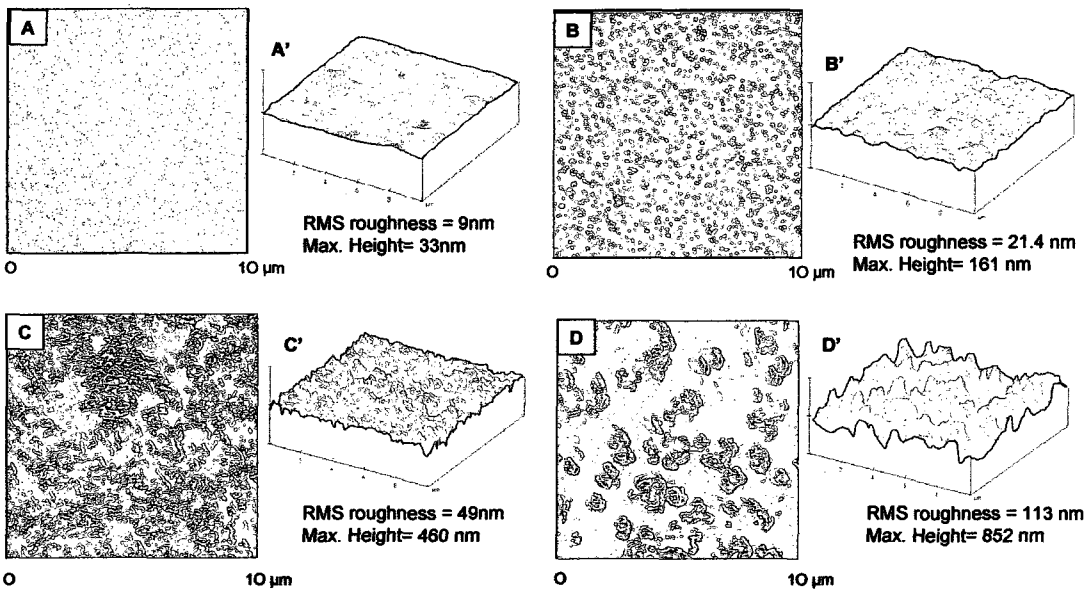

Figure III- 5. AFM phase (A) and AFM 3-D (A') images of polymeric films coalesced from p-MMA/FMA and p-nBA/FMA 50:50 colloidal mixture coalesced at 23 °C. Images B/B', C/C', and D/D' were obtained from the same films annealed at 60, 120, and 150 °C, respectively.

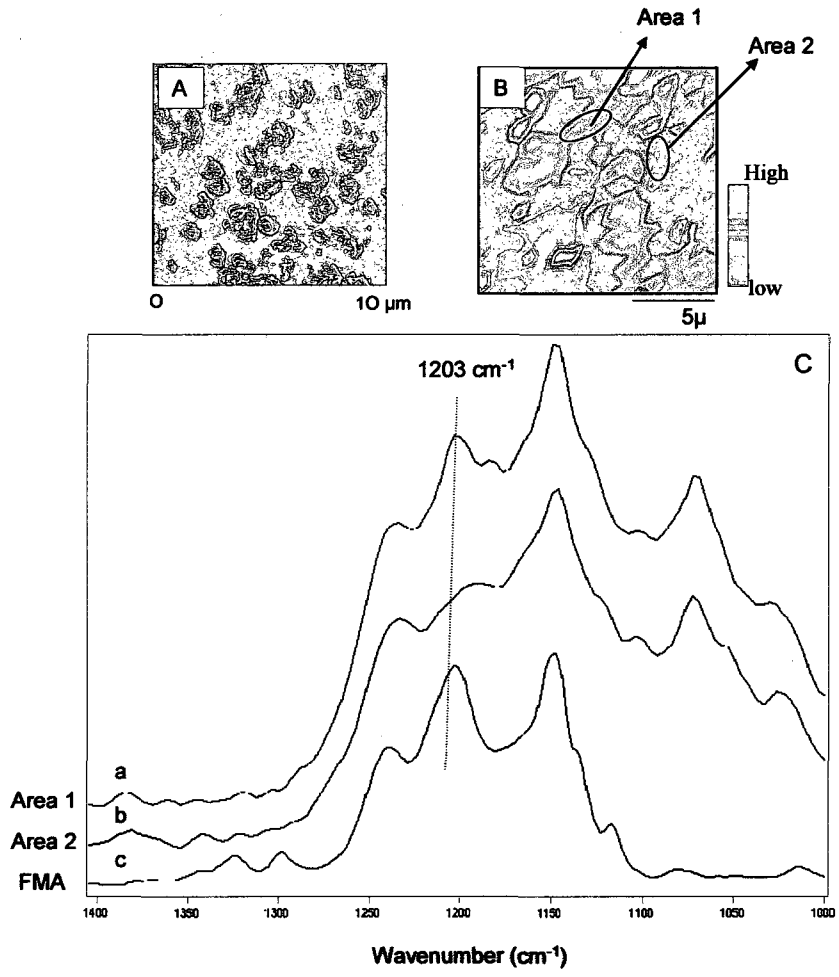

Figure III- 6. IRIR images recorded from the F-A interface of coalesced films obtained from p-MMA/FMA and p-nBA/FMA colloidal dispersion mixture (50:50) after annealing at 150 ^{0}C: A - AFM phase image; B - image obtained by tuning into 1203 cm $^{-1}$ band; C- IR spectra recorded from areas labeled 1 and 2 in image B.; a- IR spectrum of area 1; b – IR spectrum of area 2; c- IR spectrum of FMA.

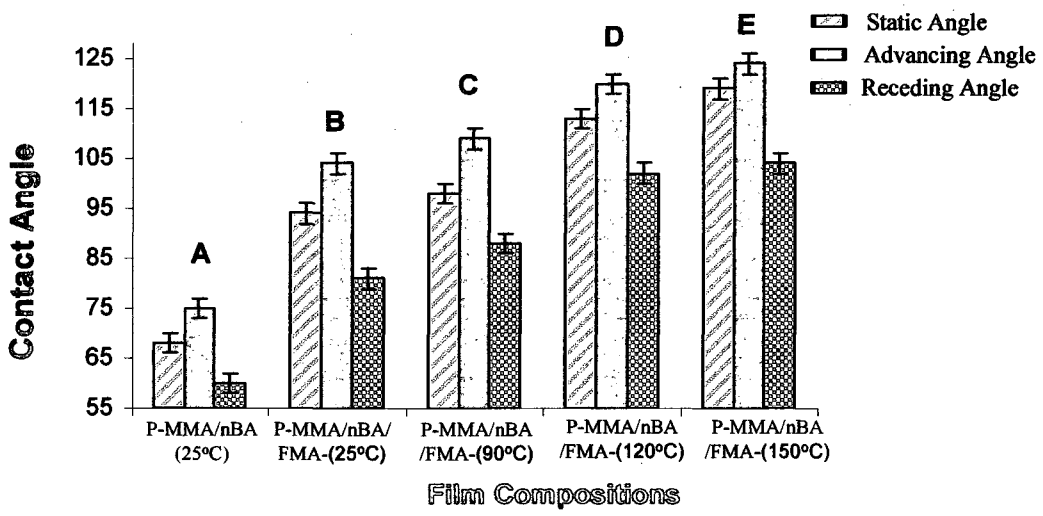

Figure IIII- 7. Contact angle measurements (water) for A - p-MMA/nBA (25°C); B - p-MMA/nBA/FMA (15% w/w) (25° C); and p-MMA/nBA/FMA films annealed at C- 90 °C; D- 120°C; and E- 150°C.

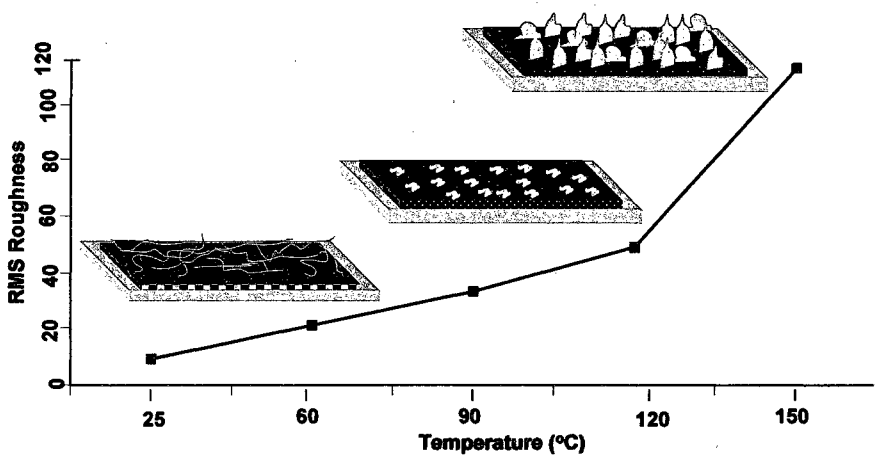

Scheme III-2. Schematic diagram illustrating the effect of temperature on surface roughness.

References

1. Wang, J.; Mao, G.; Ober, C. K.; Kramer, E. J., *Macromolecules* **1997,** *30*, 1906.

2. Milner, S. T., *Science* **1991,** *251*, 905.

3. Lednev, I. K.; Karnoup, A. S.; Sparrow, M. C.; Asher, S. A., *J. Am. Chem. Soc.* **1998,** *120*, 6518.

4. Linemann, R. F.; Malner, T. E.; Brandsch, R.; Bar, G.; Ritter, W.; Mulhaupt, R., *Macromolecules* **1999,** *32*, 1715.

5. Koendrick, G. H.; Sacanna, S.; Pathmamanoharan, C.; Rasa, M.; Philipse, A. P., *Langmuir* **2001,** *17*, 6086.

6. Sacanna, S.; Koenderink, G. H.; Philipse, A. P., *Langmuir* **2004,** *20*, 8398.

7. Ha, J.; Park, I.; Lee, S.; Kim, D., *Macromolecules* **2002,** *35*, 6811.

8. Thomas, R. R.; Lloyd, K. G.; Stika, L. M.; Stephens, L. E.; Megallanes, G. S.; Dimonie, V. L.; Sudol, E. D.; El-Aasser, M. S., *Macromolecules* **2000,** *33*, 8828.

9. Landfester, K.; Rothe, R.; Antonietti, M., *Macromolecules* **2002,** *35*, 1658.

10. Singh, A.; Dreher, W. R.; Urban, M. W., *Langmuir* **2006,** *22*, 524.

11. Dreher, W. R.; Singh, A.; Urban, M. W., *Macromolecules* **2005,** *38*, 4666.

12. Dreher, W. R.; Jarrett, W. L.; Urban, M. W., *Macromolecules* **2005,** *38*, 2205.

13. Mawson, S.; Johnston, K. P.; Betts, D. E.; MaClain, J. B.; Desimone, J. M., *Macromolecules* **1997,** *30*, 71.

14. Park, I.; Lee, S. b.; Choi, C. K., *Macromolecules* **1998,** *31*, 75553.

15. Marion, P. B.; Juhue, D.; Lang, J., *Macromolecules* **1997,** *30*, 123.

16. Chen, Y.; Ying, L.; Yu, W. J.; Kang, E.; Neoh, K., *Macromolecules* **2003,** *36*, 9451.

17. Li, K.; Wu, P.; Han, Z., *Polymer* **2002,** *43*, 4079.

18. Kassis, C. M.; Steehler, J. K.; Betts, D. E.; Guan, Z.; Romack, T. J.; DeSimone, J. M.; Linton, R. W., *Macromolecules* **1996,** *29*, 3247.

19. Krupers, M.; Mo¨ller, M., *Macromol. Chem. Phys.* **1997,** *198*, 2163.

20. McCloskey, C. B.; Yip, C. M.; Santerre, J. P., *Macromolecules* **2002,** *35*, 924.

21. Granville, A. M.; Boyes, S. G.; Akgun, B.; Foster, M. D.; Brittain, W. J., *Macromolecules* **2004,** *37*, 2790.

22. Granville, A. M.; Boyes, S. G.; Akgun, B.; Foster, M. D.; Brittain, W. J., *Macromolecules* **2005,** *38*, 3263.

23. Davis, S. D.; Hadgraft, J.; Palin, K. J., *Encyclopedia of Emulsion Technology*. Marcel Dekker: New York, 1985; Vol. 2.

24. Schaefer, J.; Stejskal, E. O.; Buchdahl, R., *Macromolecules* **1977,** *10*, 384.

25. Otts, D.; Zhang, P.; Urban, M. W., *Langmuir* **2002,** *18*, 6473.

26. *ASTM Standard Test D 1894-01.*

27. Lestage, D. J.; Urban, M. W., *Langmuir* **2004,** *20*, 6443.

28. Liu, S. F.; Schmidt-Rohr, K., *Macromolecules* **2001,** *34*, 8416.

29. Odian, G., *Principles of Polymerization*. John Wiley & Sons: New York, 2004.

30. Voet, D.; Voet, J. G., *Biochemistry*. 1st Ed. ed.; Wiley & Sons, Inc.: 1995.

31. Nii, T.; Ishii, F., *Colloids Surf.* **2004,** *39*, 57.

32. Pinazo, A.; Wen, X.; Liao, Y. C.; Prosser, A. J.; Franses, E. I., *Langmuir* **2002,** *18*, 8888.

CHAPTER IV

GREEN SYNTHESIS OF FLUORINE CONTAINING P-MMA/nBA COLLOIDAL DISPERSIONS: EFFECT OF PERFLUOROALKYL SIDE CHAIN LENGTH, MOLECULAR MODELING, AND COALESCENCE

Abstract

While the aqueous phase colloidal synthesis of F-containing dispersions is often restricted by low solubility and surface tension of monomers, the use of bio-active dispersing agents, such as phospholipids, may alleviate these problems. Using 1,2-dilauroyl-sn-glycero-3-phosphocholine (DLPC) we copolymerized heptafluorobutylmethacrylate (FBMA), heptafluorobutylacrylate (FBA), heptadecafluorodecylmethacrylate (FMA), heptadecafluorodecylacrylate (FA) with methyl methacrylate (MMA) and n-butyl acrylate (n-BA) monomers which resulted in the formation of stable non-spherical colloidal dispersions that contain up to 15% (w/w) of the fluoropolymer (FP) phase. These studies report for the first time an aqueous phase FP colloidal dispersion synthesis without the use of fluoro-dispersing agents.

Experimentally determined by transmission electron microscopy (TEM) particle phase-separated morphologies consist of the FP phase that polymerize on the surface of p-MMA/nBA core particles. Thermodynamic molecular modeling simulations show that the co-existence of fluorinated and non-fluorinated segments is energetically favorable and the presence of FP phase decreases the cohesive energy density of macromolecular chains. These predictions are in agreement with the experimental results. Non-spherical FP containing colloidal particles coalesce to form stable films with ultra low static and kinetic coefficients of friction as well as the low surface energy

which result from stratification of the FP phase near the film-air (F-A) interface. As a result, property gradients are achieved, with low friction coefficients near the F-A interface due to the presence of FP phase and lower phase transition temperature (Tg) of p-MMA/nBA phase near the film-substrate (F-S) interface, thus facilitating coalescence.

Introduction

The use and production of fluoro and chloro-containing polymers was identified as one of the causes for diminishing of the ozone layer due to emission of chlorofluorocarbons (CFCs).[1] The primary problems associated with the production and applications of fluoro and chloro polymers are their insolubility in common organic solvents, thus requiring the use of CFCs during their polymerization. Even under these reaction conditions, copolymerization of fluorinated monomers with hydrophilic or lipophilic co-monomers may be troublesome because fluorinated monomers inhibit reactions in aqueous environment without addition of dispersing agents or co-solvents. Attempts to overcome these conditions have led to the successful development of supercritical CO_2 (SCO) process,[2-4] an attractive alternative for a wide variety of chemical and industrial processes that involve pressurized polymerization conditions.[2, 3, 5-7] While these efforts have led to new technologies, one of the limiting factors is the use of F-containing non-polymerizable species during synthesis. Ideally, one would like to design environmentally benign FPs that can be applied to a substrate from an aqueous phase and form polymeric films or coatings with the properties characteristics of FPs, but free of low molecular weights F-containing dispersing agents. Unfortunately, low solubility and low surface tension of F-monomers often restrict traditional synthetic steps and required the use of F-surfactants.

In response to these challenges colloidal copolymerization of F-monomers with other monomeric species to form stable colloidal particles using classical emulsion[8-10] and miniemulsion processes[11] were developed. Although several attempts have been made to prepare fluorinated colloidal dispersions, elaborate synthetic procedures, the

use of complex starting materials such as cyclodextrin[12, 13] or other co-solvents,[14] as well as relatively low % solids and consequently lower FP content, represent significant restrictions.[8-11, 15, 16] One approach that has partially addressed these problems was the utilization of a combination of fluoro-containing dispersing agents during aqueous copolymerization of acrylate families of monomers.[17-20] However, the use of even small amounts of F-surfactants to stabilize colloidal dispersions, which are often mobile after coalescence,[21] still represents environmental concerns.

To entirely eliminate the use of F-surfactants as well as any other potential hazardous components during synthesis, processing, and applications, these studies report for the first time the development of colloidal dispersions without F-surfactants using simple free radical semi-continuous process of the following copolymers: p-methylmethacrylate/n-butylacrylate/heptafluorobutylmethacrylate (p-MMA/nBA/FBMA), p-methylmethacrylate/n-butylacrylate/heptafluorobutylacrylate (p-MMA/nBA/FBA), p-methylmethacrylate/n-butylacrylate/heptadecafluorodecyl methacrylate (p-MMA/nBA/FMA), and p-methylmethacrylate/n-butylacrylate/heptadeca fluorodecylacrylate (p-MMA/nBA/FA). These studies consist of two parts: 1- colloidal particle synthesis and Modeling; 2- coalescence of F-particles, and the Results and Discussions are organized into these two sections.

Experimental

MMA, nBA, FBMA, FBA, FMA, FA, potassium persulfate (KPS), and sodium dodecyl sulfate (SDS) were purchased from Aldrich Chemical Co. 1,2-dilauroyl-sn-glycero-3-phosphocholine (DLPC) phospholipid was purchased from Avanti Polar Lipids, Inc. p-MMA/nBA/FBMA, p-MMA/nBA/FBA, p-MMA/nBA/FMA, and p-MMA/nBA/FA emulsions were synthesized using a semicontinuous process outlined elsewehere,[19, 22] and adapted for a small-scale polymerization. The reaction flask was placed in a water bath set at 78°C, purged with N_2 gas, charged with 20 ml of DDI water under continuous stirring at 300 rpm. SDS and DLPC surfactants were utilized and Table IV- 1 provides ratio of all dispersions prepared for the purpose of these studies. Surfactants were dissolved in water under high agitation followed by addition of monomers to produce a semi-stable pre-emulsion. For seeded emulsion process, 10% (w/w) of the pre-emulsion and 18% (w/w) of the initiator solution were initially injected into the reaction kettle, thus facilitating the seed formation. The remaining pre-emulsion was fed continuously over the period of 4 hrs while the initiator solution was added for 4.5 hrs. Upon completion of the initiator feed, polymerization was allowed to continue for another 5 hrs. This process resulted in 40.5% w/w solids which was determined from the initial feed composition of the initiator monomer mixture and the analysis of the solid content after the synthesis.

The particle size analysis was obtained using a Microtrac UPA 250 instrument. Morphologies of colloidal particles were determined using a Zeiss EM 109-transmission electron microscope (TEM) in which colloidal dispersions were diluted to a 10,000:1 vol. ratio (DDI H_2O: dispersions) and deposited on a formvar coated copper TEM grid

(Ted Pella, Inc.). Table IV- 1 illustrates composition, molecular weight, solid content, and particle sizes of colloidal dispersions of p-MMA/nBA/FBMA, p-MMA/nBA/FBA, p-MMA/nBA/FMA, and p-MMA/nBA/FA.

Colloidal particle solutions were allowed to coalesce for 72 hrs in a controlled environment at 23°C temperature and 60% relative humidity (RH) to form approximately 10μm thick films. The films were obtained by draw down on the polyvinyl chloride substrates. For contact angle measurements colloidal solutions were coalesced on glass slide using a draw bar to give an approximately film thickness of 10 μm. Molecular weight was determined using gel permeation chromatography (GPC) system consists of a Waters Alliance 2695 Separation Module, a Waters 2410 interferometric refractometer, and two PL HFIPgel (Polymer Laboratories Inc.) with GPC columns connected in series. Freshly distilled HFIP serves as the mobile phase with a flow rate of 1.0 mL/min. Sample concentrations were 10-12 mg/mL in freshly distilled HFIP, with an injection volume of 50 micro liters. The detector signals were recorded using Empower 2 Chromatography Data Software (Waters Corporation) and molecular weights were determined relative to narrow molecular weight p-MMA standards.

Internal reflection infrared imaging (IRIRI) experiments were conducted on a Varian Stingray system. This system consists of a Bio-Rad FTS 6000 spectrometer, a UMA 500 microscope, an Image IR focal plane array (FPA) image detector, and a semispherical germanium IRE. IRIR images were collected using the following spectral acquisition parameters: under sampling ratio 2, step-scan speed 5 Hz, and spectral resolution 8 cm^{-1} and the use of a Ge crystal in contact with the analyzed

surface allows spatial resolution in the range of 1 μm.[23] In a typical experiment, spectral data set acquisition time was 2 minutes and image processing was performed using ENVI software (The Environment for Visualizing Images, Research Systems, Inc.) version 3.5. When appropriate, baseline correction algorithms were applied to compensate for baseline deviations which were accomplished by built-in application software supplied by GRAMS/A1 v 7.02 (Galactic Ind.). Contact angle measurements were obtained using a FTA200 dynamic contact angle analyzer using water as solvent, and a Qualitest 1055 friction tester was utilized to determine the coefficients of friction.[24] We analyzed surface components using polarized microscopic attenuated total reflectance fourier transform infrared (ATR FT-IR) spectroscopy by collecting spectra from the F-A interfaces of coalesced films of a 10 μm thick films deposited on a polyvinyl chloride substrate. The spectra were collected using a 2 mm Ge crystal with a 45° angle maintaining constant contact pressure between the crystal and the specimens using a Bio-Rad FTS-6000 FT-IR single beam spectrometer at a 4 cm^{-1} resolution. All spectra were corrected for spectral distortions using the Urban-Huang algorithm.[25] To determine preferential orientation of surface components, transverse electric (TE; 0) and transverse magnetic (TM; 90) polarization ATR FT-IR spectra were collected.

Quantum mechanical semiemperical calculations were conducted using Material Studio software (Accerlrys Inc., version 4.1). Computer modeling simulations were performed using a classical (Newton) molecular dynamics theory combined with the COMPASS force field conditions. In the first step, we created an alternate polymeric unit of MMA and nBA consisting of four monomer units of each, followed by block copolymerization of fluoropolymer (two monomer units). In an effort to determine

thermodynamic response of molecular segments, a 25 x 25 x 25 Å periodic unit cell was constructed at 298 K using eight polymeric chains of block copolymerized fluoropolymers with p-MMA/nBA units. After amorphous cell construction first the control parameter were number, volume, and temperature (NVT) (298 K, 25 ps dynamic time, 25000 number of steps, and frame output at every 1000 steps), and second step was to control number, pressure, temperature (NPT) (298K, 50 ps dynamic time, 50000 number of steps, and frame output at every 5000 steps) to determine the change in volume and total energy required for the cell construction with varying chain length of perfluoroalkyl side chain of fluoromonomers. Cohesive energy density (CED) was determined by using forcite calculations after the NPT cell construction was performed. Binding energies of surfactants and polymer associations were calculated by taking binding energy of the fluoropolymer associated with the surfactant and subtracting it from the binding energy of the polymer and the surfactant.

Results and Discussion

Colloidal Particle Synthesis and Modeling

As stated in the Introduction, the main objective of these studies was the synthesis of p-MMA/nBA/FBMA, p-MMA/nBA/FBA, p-MMA/nBA/FMA, and p-MMA/nBA/FA colloidal particles without the use of F-containing dispersing agents. Such prepared dispersions were synthesized using traditional free radical emulsion polymerization process, and as listed in Table IV- 1, the particle size ranges from 102 to 130 nm. As the perfluoroalkyl side chain length of monomers increases, the particle size also increases. Figure IV-1 illustrates TEM images of individual particle morphologies of p-MMA/nBA (A), p-MMA/nBA/FBMA (B), p-MMA/nBA/FBA (C), p-MMA/nBA/FMA (D), and p-MMA/nBA/FA (E) particles and, as seen in Image A, p-MMA/nBA particles exhibit spherical shape. However, upon copolymerizing FBMA, FBA, FMA, and FA with MMA/nBA monomers, the particle morphology changes. The observed high electron density regions observed in Images B-E of Figure IV-1 exist on the exterior of the p-MMA/nBA core and are due to the FP phase, thus forming intra-particle phase separated non-spherical shapes. These data also show that by increasing the length of the perfluoroalkyl side chain from $(CF_2)_2CF_3$ to $(CF_2)_7CF_3$, when going from FBMA to FMA monomers, not only the size of the particles increases, but the phase-separated FP domains within each particle also increases. The results of these studies are in agreement with the previous findings, in which F-surfactants were utilized in the synthesis of fluorine-containing colloidal dispersions,[18-20] and also resulted in phase separated heterogeneous non-spherical colloidal particles.

Although the origin of the phase separation and non-spherical morphologies of colloidal particles containing FP prepared in the presence of fluorosurfactants have been proposed,[17-19] we are also interested in determining the location of the FP phase on the p-MMA/nBA particle core. While TEM and NMR measurements clearly allowed us to determine phase separation regions and the copolymer type, the formation of FP phase domains within one particle are quite intriguing. Conceptually, one can envision that when polymerization is carried out under monomer starvation conditions, it is expected that the monomer hydrophobicity and solubility differences will facilitate F-monomer migration to the reactive site at the later stages of the polymerization, thus leading to the block copolymerization of the FP phase.[17] Also, if one considers the presence of SDS and DLPC dispersing agents on the surface of the p-MMA/nBA core, another possibility is that the F-monomer polymerizes on the surface areas of the p-MMA/nBA core where there is an access of DLPC creating energetically favorable conditions for copolymerization.

Postponing temporarily further experimental data, we utilized computer modeling experiments where molecular thermodynamics simulations were employed for each p-MMA/nBA, p-MMA/nBA/FBMA, p-MMA/nBA/FBA, p-MMA/nBA/FMA, and p-MMA/nBA/FA copolymer. The unit cells were constructed using packing energy minimized polymer chains under 3D periodic boundary conditions and the details of the computational analysis are provided in the Experimental Section. The visual representation of the results of the analysis is depicted in Figure IV-2, A–E, for p-MMA/nBA (A), p-MMA/nBA/FBMA (B), p-MMA/nBA/FBA (C), p-MMA/nBA/FMA (D), and p-MMA/nBA/FA (E), respectively. As seen, by incorporating F-monomers,

significant conformational changes are observed within the amorphous cell. Comparison of p-MM/nBA (A) with p-MM/nBA/FBMA (B) and p-MM/nBA/FBA (C) clearly shows that the FP phase is less compact and exhibit larger particle size, and more pronounced changes are shown for p-MM/nBA/FMA (D) and p-MM/nBA/FA (E) due to larger perfluoroalkyl side chain length and exhibit surface phase separation. These predictions are in agreement with the TEM images shown in Figure IV-1 and experimental measurements of the particle size data listed in Table IV-1. The total volume changes increase from 12.9 nm^3 for p-MMA/nBA to 15.1 and 14.8 nm^3 for p-MMA/nBA/FBMA and p-MMA/nBA/FBA, respectively, and 19.0 nm^3 for p-MMA/nBA/FMA which is directly related to the perfluoroalkyl side chain lengths of fluoromonomers (FBA being the shortest and FMA the longest).

Total energies (G) required to obtain the copolymer packing of the individual unit cells are listed in Table IV-2. For p-MMA/nBA copolymer, the G value comprised of the potential energy (E_{pot}) and the kinetic energy (E_{kin}) is 3779 kcal/mol. Upon incorporating the p-FBMA phase, the G value decreases by 128 kcal/mol (from 3779 to 3651 kcal/mol). At the same time, the E_{pot} decreases by 199 kcal/mol, but the E_{kin} is increased by 71 kcal/mol. These results show that the incorporation of the FP phase results in thermodynamically, but not kinetically, favorable conditions. Since the E_{pot} changes account for conformational changes, the most energetically favorable conformations for the FP exists when the FP segments are on the exterior of the p-MMA/nBA particle surface. In contrast, the E_{kin} changes account for the ease with which conformational arrangements can be altered. Simple mass considerations indicate that higher molecular weight FP phase has higher E_{kin} compared to p-

MMA/nBA. As the F content increases due to FMA and FA copolymerization, the total energy is reduced due to the reduction of the potential energy in order to attain most stable conformations illustrated in Figure IV- 2. Also, the decrease of the G values upon incorporation of the FP phase is attributed to their lower surface energy, hence the incorporation in copolymer structure leads to the reduction of the total energy, as the system approaches more stable phase-separated configuration.

In order to establish whether block or random copolymerization of MMA, nBA, and fluoromonomers are favorable, similar modeling experiments were conducted on block and random copolymers of p-MMA/nBA/FP. The amorphous cell construction incorporated the formation of random p-MMA/nBA/FP copolymers, followed by NVT and NPT thermodynamic calculations. Although these calculations showed that for the random copolymer the G values vary only ±25 kCal/mol from blocked copolymer, these calculations do not take into account the presence of dispersing agents which as will be seen later, will play a significant role in this two-phase systems.

In order to determine how much energy is required to remove one polymer chain from p-MMA/nBA, p-MMA/nBA/FBMA, p-MMA/nBA/FBA, p-MMA/nBA/FMA, and p-MMA/nBA/FA copolymers, we calculated the cohesive energy density (CED) which represents the amount of energy required to completely remove a polymer chain as a function of composition. Ultimately, the CED changes will provide an estimate of intramolecular forces between polymeric chains. As shown in Table IV- 2, the CED changes determined for different copolymer compositions show that the smaller values are obtained for the FP containing copolymers. In contrast, the CED values for p-MMA/nBA copolymer are the largest, compared to copolymers containing the FP phase.

This is attributed to the fact that the FP is phase-separated and less energy is required to separate individual polymeric chains. Furthermore, the decrease of CED is proportional to the amount of the F-content present in the backbone of the copolymer structure, reaching the value of 192 J/cm^3 for p-MMA/nBA/FA.

Due to useful properties of FPs it is desirable to incorporate as much of the FP phase as possible. However, for p-MMA/nBA/FP colloidal particles the limiting factor is the stability of colloidal dispersions. As indicated in the experimental section, we utilized bio-active PLs which form mixed micellar entities with SDS without the use of F-containing dispersing agents. PLs, being main constituents of the cell membranes, serve as selective barriers for bio-active species as well as provide support for membrane protein transport.[26] As was shown in the literature, PLs along and SDS form miscible micellar structures, the FP phase growth on the p-MMA/nBA colloidal particles is facilitated by the reduction of the overall surface tension of the aqueous phase from 72 to about 1-5 mN/m.[27, 28] This was the primary reason for choosing DLPC as one of the dispersing agents during colloidal synthesis, thus allowing p-MMA/nBA seed formation, followed by employing the monomer starvation conditions, forced F-monomers to migrate to reactive sites. Since PLs exhibit dual functions: (1) they facilitate transport of F-monomers to the p-MMA/nBA core and (2) stabilize the growing particles, thus eliminating the use of F-surfactants.

In view of these considerations it is particularly important to determine the location of SDS and DLPC on the surface of colloidal particles. The hypothesis is that if DLPC facilitates the growth of the FP phase on the surface of p-MMA/nBA, DLPC should exhibit energetically favorable interactions with the FP phase. Since SDS and

DLPC form miscible micellar structures,[20] we determined the binding energy for the association of SDS and DLPC molecules with p-MMA/nBA and FP segments using computer modeling simulations. Figure IV- 3 shows the results of the modeling experiments in which the total energies of p-FMA/SDS and p-FMA/DLPC were calculated (Figure IV- 3, A and B). In a separate experiment, the same calculations were conducted for p-FMA (C), SDS (D), and DLPC (E), while maintaining conformations of p-FMA/SDS and p-FMA/DLPC. These values were subtracted from the total energies of p-FMA/SDS and p-FMA/DLPC, respectively. To obtain energies responsible for p-FP/SDS and p-MMA/nBA interactions, similar calculations were conducted for p-MMA/nBA, p-FBMA, p-FBA, and p-FA. The results are tabulated in Table IV- 3. As seen, more favorable associations (higher negative values) are observed between the polymer and the dispersing agent molecules. Specifically, favorable associations (higher negative values) are observed for p-MMA/nBA, compared to the FP-SDS interactions. However, in contrast to p-MMA/nBA, FP-DLPC pairs exhibit favorable interactions, giving more negative binding energies for the long chain perfluoroalkyl side chain FPs. Thus, based on the binding energy calculations in mixed micellar structures, PL molecules exhibit energetically more favorable associations with the FP phase, whereas SDS prefer binding with the p-MMA/nBA phase.

Coalescence of p-MMA/nBA/PF particles

As shown in the previous studies,[18-20] particle morphologies and dispersing agents play a significant role in particle coalescence. In an effort to identify surface chemical composition of films prepared from p-MMA/nBA/FP and to determine the

distribution of the FP phase at the F-A interface, we utilized IRIR imaging. The results of these experiments are shown in Figure IV- 4, Images A-F. Figure IV- 4, A illustrates IR image of the F-A interface of p-MMA/nBA, which was generated by tuning into the 1165 cm^{-1} band due to C-O-C stretching vibrations of p-nBA at 1 μm level spatial resolution, no compositional variations are detected and highly uniform films with no phase separation are produced, as confirmed in Figure IV- 4, A' by the analysis of the IR spectrum recorded from areas 1 and 2 with no changes of the 1165 and 1145 cm^{-1} bands due to nBA and MMA components, respectively. Figure IV- 4, B illustrates IR image of the F-A interface of p-MMA/nBA/FBMA, which was generated by tuning into the 1122 cm^{-1} band due to C-F stretching vibrations. As seen, the C-F stretching bands of the copolymer matrix are detected and their distribution is heterogeneous, with the regions consisting of the higher concentration levels of the C-F moieties. While the IR image in Figure IV- 4, B provides spatial distributions of the chemical entities near the F-A interface, Figure IV- 4, B' represents averaged IR spectra obtained from the areas labeled 1 and 2 in Figure IV- 4, B. As seen, the area 1 is largely saturated by the C-F groups, as manifested by the higher intensities of the 1122 and 1230 cm^{-1} bands, thus signifying the presence of the FP phase. However, the same band exhibits lower intensity in the area 2, as shown in Trace b. For reference purposes, Trace c is the spectrum of FBMA.

The same analysis was conducted on p-MMA/nBA/FBA, p-MMA/nBA/FMA, and p-MMA/nBA/FA films, and the results of these experiments are displayed in Figure IV- 4, C-E, respectively. Chemical mapping using IRIRI of these surfaces (Images C-E) shows again heterogeneous morphologies, where the FP phase (red color) forms

islands at the F-A interface. IR analysis of the areas 1 and 2 also shows that the area 1 consists of the higher concentration levels of the FP phase, as manifested by the IR spectra shown in Traces a and b. Traces c in Figure IV- 4, B'-E' represent IR spectra of respective F-monomers. These results again illustrate the development of heterogeneous phase-separated surfaces for FP containing films, in which FP phase migrates to the F-A interface during film formation.

To elucidate how stratification affects film interfacial properties, contact angle and coefficient of friction measurements were conducted. Table IV- 4 provides advancing, static, and receding contact angle results for p-MMA/nBA, p-MMA/nBA/FBMA, p-MMA/nBA/FBA, p-MMA/nBA/FMA, and p-MMA/nBA/FA copolymer compositions. For p-MMA/nBA films, the static water contact angle is 65°, which upon incorporation of the FP phase increases to 98° for p-MMA/nBA/FBMA, 94° for p-MMA/nBA/FBA, 105° for p-MMA/nBA/FMA, and 104° for p-MMA/nBA/FA films. This increase appears to be directly related to the perfluoroalkyl side chain length of the fluoromonomers utilized in the synthesis. As anticipated, static and kinetic coefficients of friction also change significantly. As shown in Figure IV- 5, the static coefficient of friction is reduced from 0.78 for p-MMA/nBA to 0.18 for p-MMA/nBA/FMA films. Also, the kinetic coefficient of friction is reduced from 0.38 to 0.02, thus exceeding polytetrafluoroethylene (0.04).[29] The static coefficient of friction is relatively high due to the presence of p-MMA/nBA component which provides significant adhesiveness during the static measurements, but longer perfluoroalkyl chains result in the lowest static and kinetic coefficients of frictions.

We also analyzed surface components using ATR-FTIR spectroscopy and specifically examined mobility and stratification of dispersing agents near the F-A interface. Figure IV- 6 shows a series of polarized ATR-FTIR spectra recorded from the F-A interface of p-MMA/nBA (Traces A), p-MMA/nBA/FBMA (Traces B), p-MMA/nBA/FBA (Traces C), p-MMA/nBA/FMA (Traces D), and p-MMA/nBA/FA (Traces E). Since elevated temperatures significantly impact the mobility of individual components, each film was annealed for 2h at 60, 90, and 120°C. Figure IV- 6, A, Traces a/a' shows the absence of the bands at 1098 cm^{-1} due to P-O-C and the presence of the 1078 cm^{-1} band due to S-O symmetric stretch vibrations in the TE and TM polarizations. As seen, the presence of SDS with preferential perpendicular orientation with respect to the F-A interface for p-MMA/nBA copolymer films is observed.[30-33] Upon the incorporation of fluoropolymers (FPs), the 1098 cm^{-1} band due to P-O-C and the presence of the 1078 cm^{-1} band in TE and TM polarization is detected. Similar bands were observed at 60°C (Figure S-1, B, b-b'). Upon annealing at 90 and 120 °C, the 1098 and 1078 cm^{-1} bands diminish, as shown in Figure IV- 6, A, Trace c-d', indicating that DLPC and SDS migrate to the bulk of the film. Similar observations were recorded for p-MMA/nBA/FBA (Figure IV- 6, C), p-MMA/nBA/FMA (Figure IV- 6, D), and p-MMA/nBA/FA (Figure IV- 6, E). However it should be noted that the DLPC bands exhibit increased intensity for longer perfluoroalkyl side chain polymers of FMA, and FA (Figure S-1, D-E), in contrast to shorter perfluoroalkyl side chain polymers of FBA and FBMA (Figure IV- 6,, B-C). These observations agree with the computational binding energy predictions provided in Table IV- 3. Since the FP phase at the surface of colloidal particles is stabilized by DLPC and SDS, during coalescence,

as the FP phase stratifies near the F-A interface during coalescence, SDS and DLPC associated with the FP phase also migrate to this interface. As shown by the computer modeling experiments, longer perfluoroalkyl side chains exhibit favorable interactions between the FP phase and DLPC, as demonstrated by lower (FP/DLPC) binding energies listed in Table IV- 3.

Conclusions

The utilization of SDS/DLPC dispersing agents facilitates green synthesis of acrylics and methacrylics F-monomers using classical emulsion polymerization process without the use of fluorosurfactants. Computer simulations and experimental results show that the FP phase forms energetically favorable phase-separate entity on the surface of p-MMA/nBA. The presence of the FP phase results in the decrease of the cohesive energy density of macromolecular chains. Polymeric films obtained as a result of the coalescence of p-MMA/nBA/FP self-stratify, where the FP phase is near the F-A interface and forms phase-separated domains of fluorinated and non-fluorinated layers resulting in low coefficients of frictions.

Table IV-1. Composition, Molecular Weight, and Particle Size Analysis of Colloidal Dispersions Containing (A) p-MMA/nBA, (B) p-MMA/nBA/FBMA, (C) p-MMA/nBA/FBA, (D) P-MMA/nBA/FMA, and (E) p-MMA/nBA/FA Copolymers.

	p-MMA/nBA A	p-MMA/nBA/FBMA B	p-MMA/nBA/FBA C	p-MA/nBA/FMA D	p-MMA/nBA/FA E
MMA	19.5	16.5	16.5	16.5	16.5
nBA	19.5	16.5	16.5	16.5	16.5
F-monomer	0	5.9	5.9	5.9	5.9
SDS	1.5	1.5	1.5	1.5	1.5
DLPC	0.26	0.26	0.26	0.26	0.26
DDI	59.2	59.2	59.2	59.2	59.2
KPS	0.23	0.23	0.23	0.23	0.23
Mol. Wt. (gm/mol) x 10^{-5}	0.96	0.93	0.95	1.05	1.15
Solid Content	41	41	41	41	41
Particle Size	100	110	102	130	128

Table IV-2. Volume, Energy, and Cohesive Energy Density Calculations for p-MMA/nBA, p-MMA/nBA/FBMA, p-MMA/nBA/FBA, p-MMA/nBA/FMA, and p-MMA/nBA/FA Copolymers.

Copolymer Composition	Volume (nm^3)	Total Energy (kcal/mol)	Potential Energy (kcal/mol)	Kinetic Energy (kcal/mol)	Cohesive Energy Density (J/cm^3)
p-MMA/nBA	12.9	3779	2652	1127	254
p-MMA/nBA/FBMA	15.1	3651	2453	1198	221
p-MMA/nBA/FBA	14.8	3356	2193	1163	218
p-MMA/nBA/FMA	19.0	3004	1582	1422	203
p-MMA/nBA/FA	18.7	2675	1295	1380	192

Table IV-3. Binding Energy Calculations for p-MMA/nBA, p-FBMA, p-FBA, p-FMA, and p-FA Copolymers with SDS and DLPC Association.

Composition	p-MMA/nBA	p-FBMA	p-FBA	p-FMA	p-FA
Binding Energy with SDS (kcal/mol)	-408	-247	-219	-366	-317
Binding Energy with DLPC(kcal/mol)	-907	-1657	-1472	-2441	-2154

Table IV-4. Advancing, Static, and Receding Contact Angles for p-MMA/nBA, p-MMA/nBA/FBMA, p-MMA/nBA/FBA, p-MMA/nBA/FMA, and p-MMA/nBA/FA Films Obtained from Coalesced Colloidal Particles.

Composition	Advancing contact angle (°)	Static contact angle (°)	Receeding contact angle (°)
p-MMA/BA	75	65	50
p-MMA/BA/FBMA(15%)	102	99	87
p-MMA/BA/FBA(15%)	100	94	85
p-MMA/BA/FMA(15%)	112	104	98
p-MMA/BA/FA(15%)	110	102	97

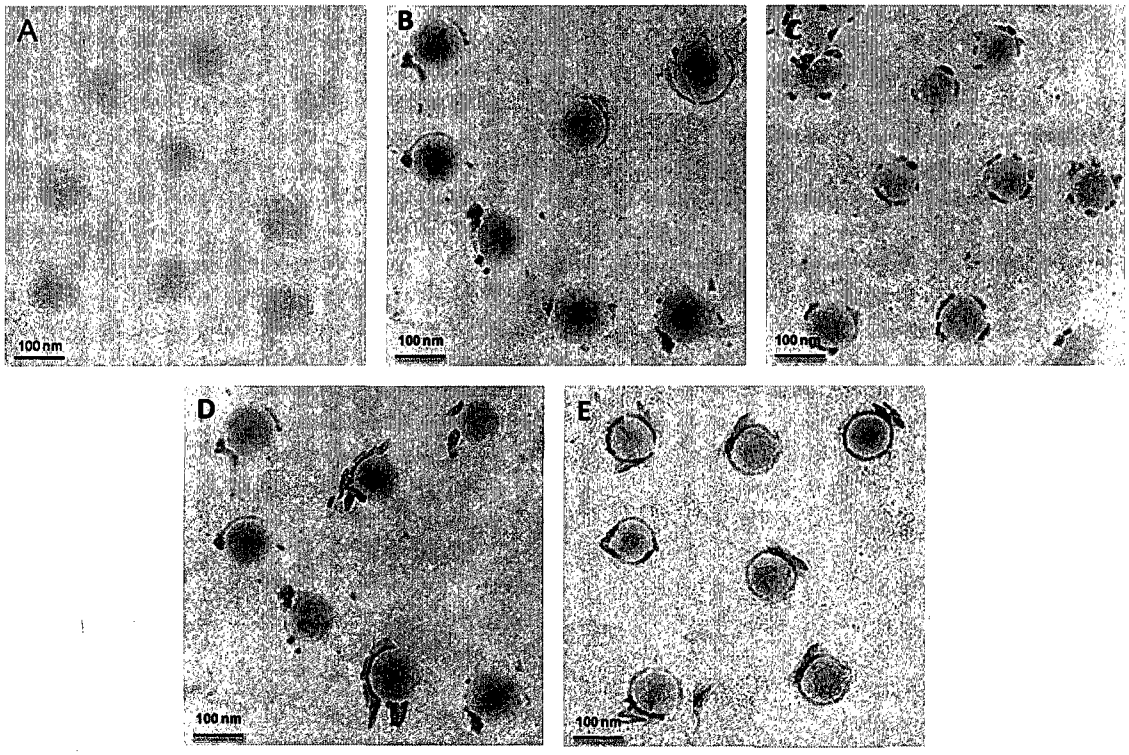

Figure IV-1. Transmission electron micrographs of colloidal particles containing (A) p-MMA/nBA, (B) p-MMA/nBA/FBMA, (C) p-MMA/nBA/FBA, (D) p-MMA/nBA/FMA, and (E) p-MMA/nBA/FA copolymers.

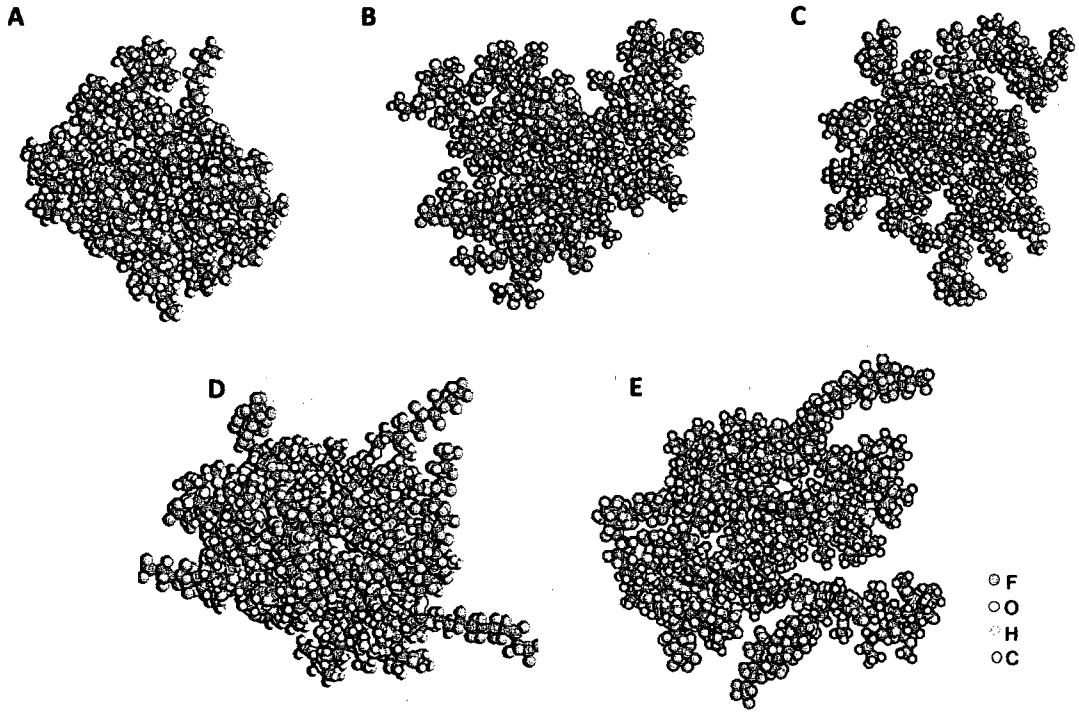

Figure IV-2. Results of computational simulations leading to significant volume and conformational changes for; (A) p-MMA/nBA, (B) p-MMA/nBA/FBMA, (C) p-MMA/nBA/FBA, (D) p-MMA/nBA/FMA, and (E) p-MMA/nBA/FA copolymers.

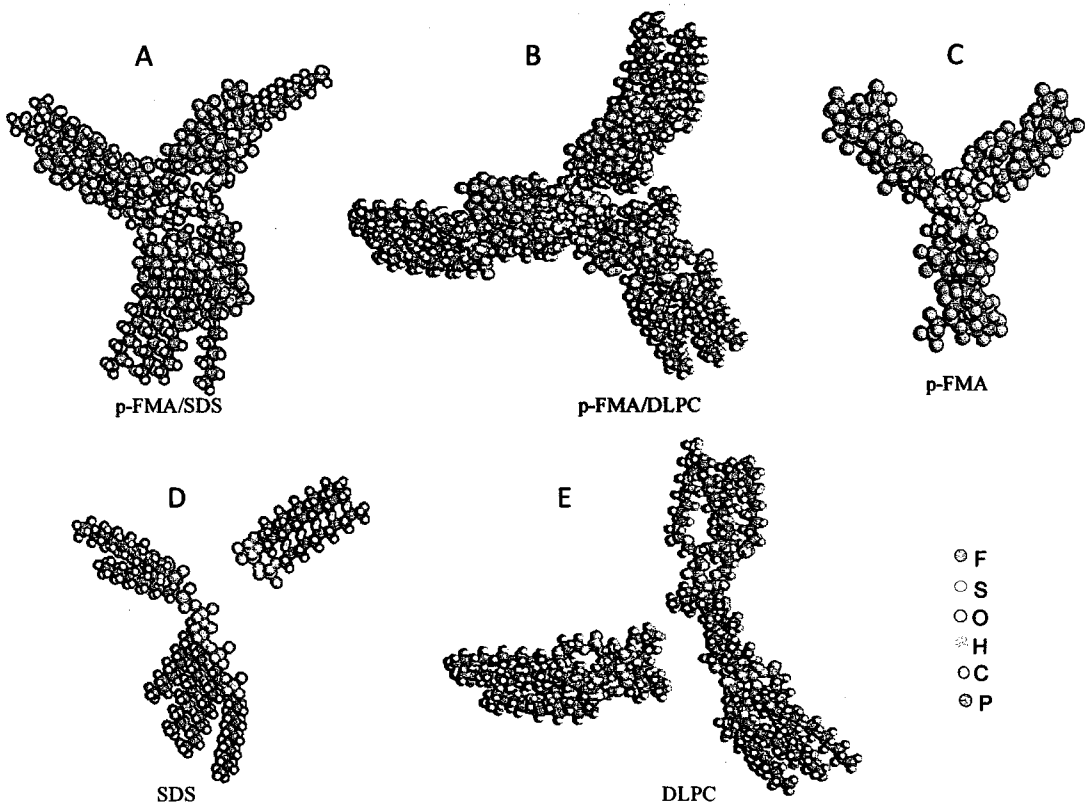

Figure IV-3. Molecular structures of (A) p-FMA association with SDS molecules, (B) p-FMA, (C) SDS, (D) p-FMA association with DLPC molecules, and (E) DLPC arrangement for binding energy computation.

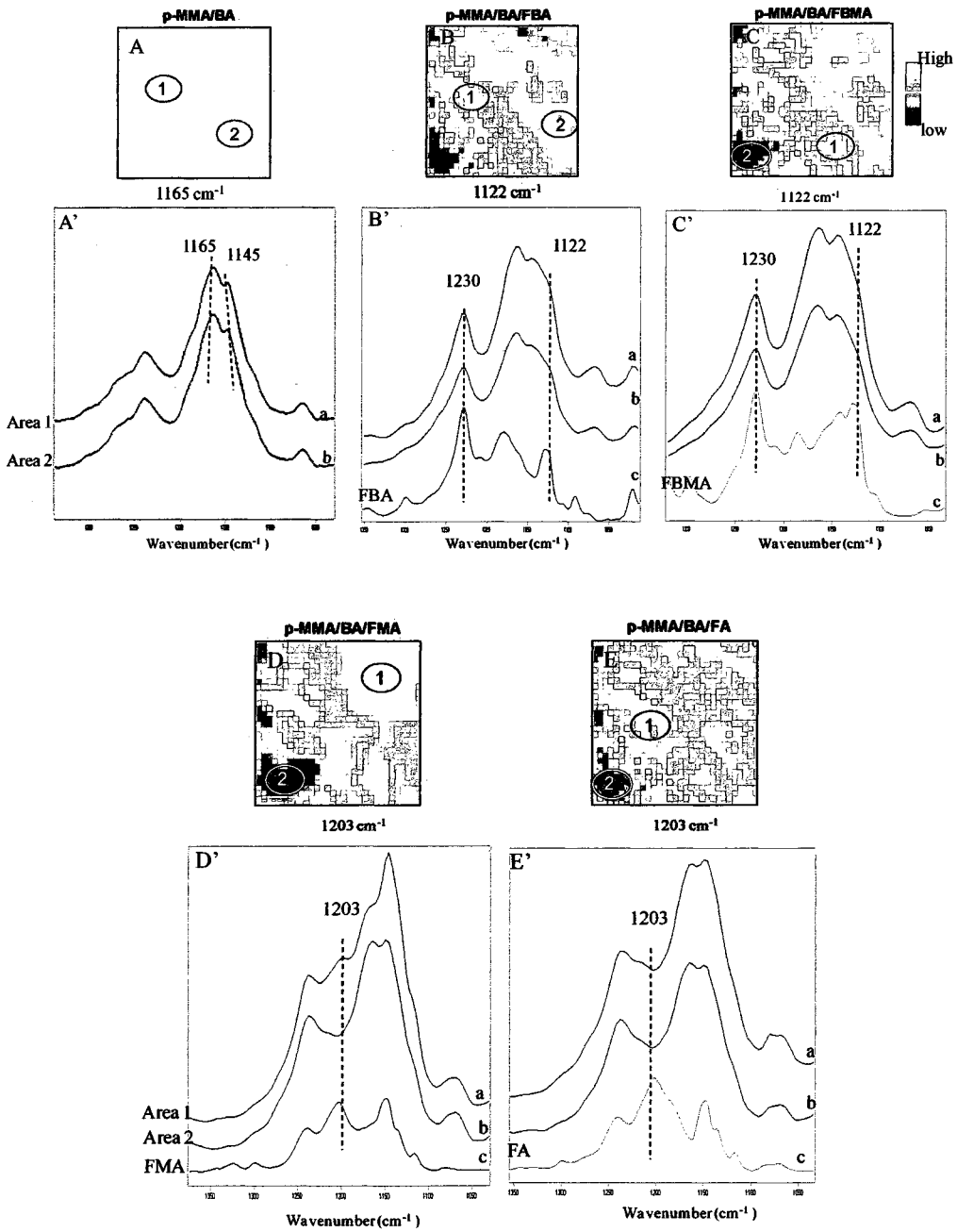

Figure IV-4. IRIR images recorded from the F-A interface of films obtained from (A) p-MMA/nBA colloidal dispersions: A - image obtained by tuning into 1165 cm^{-1}; A' - IR spectra recorded from areas labeled 1 and 2 in image A; a - IR spectrum of area 1; b - IR spectrum of area 2, (B) p-MMA/nBA/FBMA, (c), p-MMA/nBA/FBA, (D), p-MMA/nBA/FMA, and (E) p-MMA/nBA/FA.

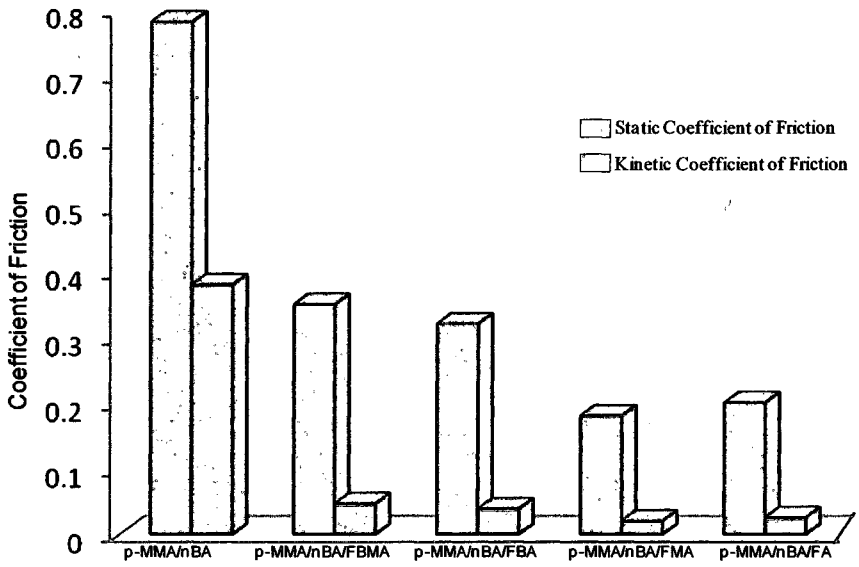

Figure IV-5. Static and kinetic coefficients of friction for p-MMA/nBA, p-MMA/nBA/FBMA, p-MMA/nBA/FBA, p-MMA/nBA/FMA, and p-MMA/nBA/FA films plotted for each copolymer colloidal composition.

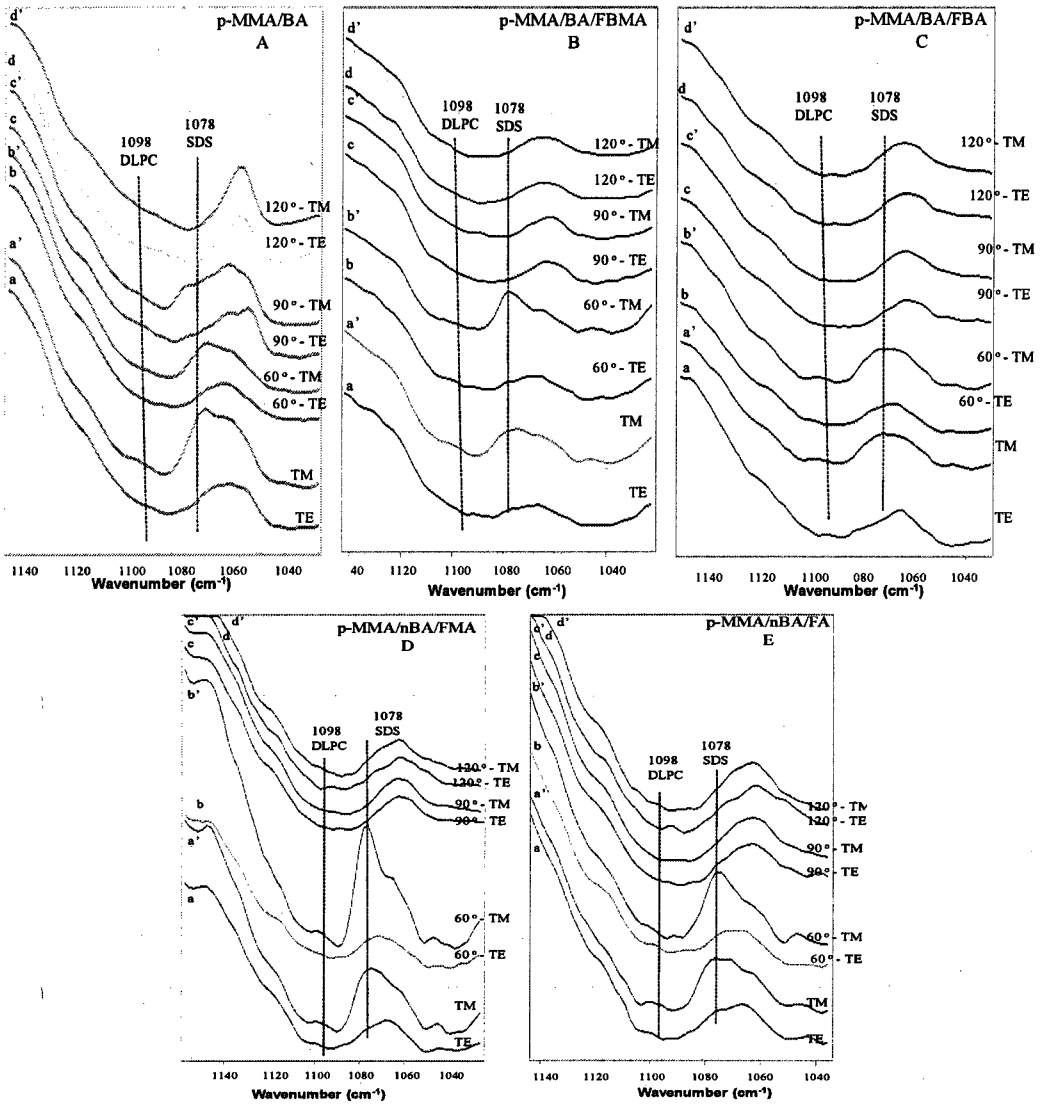

Figure IV- 6. ATR-FTIR spectra recorded from F-A Interface in the spectra region of 1150-1040 cm^{-1} for p-MMA/nBA (A), p-MMA/nBA/FBMA (B), p-MMA/nBA/FBA (C), and p-MMA/nBA/FMA(D), and p-MMA/nBA/FA (E), TE and TM polarization; a and a', TE and TM polarization at 60°C; b and b', TE and TM polarization at 90°C; c and c', and TE and TM polarization at 120°C; d and d'.

References

1. Solomon, S.; Garcia, R. R.; Sherwood, F.; Wuebbles, D. J. *Nature* **1986,** 321, 755.

2. DeSimone, J. M.; Guan, Z.; Elsbernd, C. S. *Science* **1992,** 257, 945.

3. DeSimone, J. M.; Maury, E. E.; Menceloglu, Y. Z.; McClain, J. B.; Romack, T. J.; Combes, J. R. *Science* **1994,** 265, 356.

4. McClain, J. B.; Betts, D. E.; Canelas, D. A.; Samulski, E. T.; DeSimone, J. M.; Londono, J. D.; Cochran, H. D.; Wignall, G. D.; Chillura-Martino, D.; Triolo, R. *Science* **1996,** 274, 2049.

5. Romack, T. J.; DeSimone, J. M.; Treat, T. A. *Macromolecules* **1995,** 28, 8429.

6. Michel, U.; Resnick, P.; Kipp, B.; DeSimone, J. M. *Macromolecules* **2003,** 36, 7107.

7. Hyatt, J. A. *J. Org. Chem.* **1984,** 49, 5097.

8. Koendrick, G. H.; Sacanna, S.; Pathmamanoharan, C.; Rasa, M.; Philipse, A. P. *Langmuir* **2001,** 17, 6086.

9. Ha, J.; Park, I.; Lee, S.; Kim, D. *Macromolecules* **2002,** 35, 6811.

10. Thomas, R. R.; Lloyd, K. G.; Stika, L. M.; Stephens, L. E.; Megallanes, G. S.; Dimonie, V. L.; Sudol, E. D.; El-Aasser, M. S. *Macromolecules* **2000,** 33, 8828.

11. Landfester, K.; Rothe, R.; Antonietti, M. *Macromolecules* **2002,** 35, 1658.

12. Cinar, H.; Kretschmann, O.; Ritter, H. *Macromolecules* **2005,** 38, 5078.

13. Lau, W. *Macromol. Symp.* **2002,** 182, 283.

14. Wood, C. D.; Senoo, K.; Martin, C.; Cuellar, J.; Cooper, A. I. *Macromolecules* **2002,** 35, 6743.

15. Linemann, R. F.; Malner, T. E.; Brandsch, R.; Bar, G.; Ritter, W.; Mulhaupt, R. *Macromolecules* **1999,** 32, 1715.

16. Sacanna, S.; Koenderink, G. H.; Philipse, A. P. *Langmuir* **2004,** 20, 8398.

17. Misra, A.; Jarrett, W. L.; Urban, M. W. *Macromolecules* **2007,** 40, 6190.

18. Dreher, W. R.; Singh, A.; Urban, M. W. *Macromolecules* **2005,** 38, 4666.

19. Dreher, W. R.; Jarrett, W. L.; Urban, M. W. *Macromolecules* **2005,** 38, 2205.

20. Singh, A.; Dreher, W. R.; Urban, M. W. *Langmuir* **2006,** 22, 524.

21. Dreher, W. R.; Urban, M. W. *Langmuir* **2004,** 20, 10455.

22. Davis, S. D.; Hadgraft, J.; Palin, K. J., *Encyclopedia of Emulsion Technology.* Marcel Dekker: New York, 1985; Vol. 2.

23. Otts, D.; Zhang, P.; Urban, M. W. *Langmuir* **2002,** 18, 6473.

24. Evanson, K. W.; Thortenson, T. A.; Urban, M. W. *J. Appl. Polym. Sci.* **1991,** 42, 2309.

25. Urban, M. W., *Attenuated Total Reflectance Spectroscopy of Polymers - Theory and Practise.* 1989; Vol. Vol. 2.

26. Voet, D.; Voet, J. G., *Biochemistry.* 1st Ed. ed.; Wiley & Sons, Inc.: 1995.

27. Nii, T.; Ishii, F. *Colloids Surf.* **2004,** 39, 57.

28. Pinazo, A.; Wen, X.; Liao, Y. C.; Prosser, A. J., *Langmuir* **2002,** 18, 8888.

29. Brandrup, J.; Immergut, E. H., *Polymer Handbook.* 2nd ed.; Johnwiley & Sons: New York, 1966.

30. Silverstein, R. M.; Webster, F. X., *Spectrometeric Indentification of Organic Compounds.* John Wiley and Sons: New York, 1998.

31. Lestage, D. J.; Urban, M. W. *Langmuir* **2005,** 21, 2150.

32. Lestage, D. J.; Yu, M.; Urban, M. W. *Biomacromolecules* **2005,** 6, 1561.

33. Dreher, W. R.; Urban, M. W. *Langmuir* **2003,** 19, 10254.

CHAPTER V

NEW p-METHYLMETHACRYLATE/n-BUTYL ACRYLATE/ PENTAFLUOROSTYRENE/POLYETHYLENE GLYCOL COLLOIDAL DISPERSIONS; SYNTHESIS, FILM FORMATION, AND PROTEIN ADSORPTION

Abstract

A new family of water dispersible colloidal particles composed of p-methyl methacrylate/n-butyl acrylate/pentafluorostyrene/poly (ethylene glycol) dimethacrylate (p-MMA/nBA/PFS/PEG) copolymers which coalesce at room temperature was developed using free radical emulsion polymerization. These stable colloidal dispersions contain up to 30% w/w PEG and 35% w/w PFS, and exhibit core-shell morphologies that consist of the p-MMA/nBA/PFS core and the PEG shell. Solid state 2D NMR, internal reflection infrared imaging (IRIRI), and atomic force microscopy (AFM) analysis showed that after coalescence the surface contains PEG-rich component which, combined with fluorinated domains result in hydrophobic and hydrophilic segments that inhibit protein adsorption. Adsorption of bovine serum albumin (BSA), lipopolysacharide (Lipopoly), and fibrinogen (Fib) on p-MMA/nBA/PFS, and p-MMA/nBA/PFS/PEG (5, 10, 20, and 30 %) film surfaces revealed that the proteins exhibit higher affinity towards p-MMA/nBA/PFS surfaces, but the presence of PEG incorporated into p-MMA/nBA/PFS colloidal particles results in significantly reduced protein adsorption and compositional heterogeneity of the PFS and PEG phases is believed to be responsible for a minimal affinity for the protein adsorption.

Introduction

Controllable adsorption-to or desorption-from polymeric surfaces of biologically active species has been of a considerable interest and numerous studies advanced understanding of interactions governing forces responsible for these processes.[1-3] One quantity that relates the adhesion strength (A) of a fouling organism to the surface energy (γ) and modulus (E) of the surface is expressed as $A= \sqrt{\gamma}E$.[3] Among many promising polymeric materials with low surface energies fluoropolymers (FPs) exhibit relatively low friction,[4-7] but their high modulus often overwrites other useful properties. On the other hand, thermoplastic elastomers, such as styrene-ethylene/butylene-styrene (SEBS) block copolymers, offer desirable mechanical properties, but elevated surface energies result in a high adhesion strength to protein molecules.[8] In contrast, poly(ethylene glycol) (PEG) exhibits low protein adsorption values, low toxicity, acceptable compatibility with biological systems, and its incorporation into other polymeric coatings has been shown to inhibit protein adsorption, thereby reducing the adhesion strength of bioorganisms.[9, 10] The presence of the PEG layer shields the surface by introducing the high activation barrier for proteins to adsorb to surfaces, and the chain length as well as the surface coverage were shown to impart protein resistance.[11-16] Another useful feature of PEG was shown upon its incorporation to polyurethanes which resulted in a distinct phase separation.[17-19] Taking advantage of the PEG properties as well as the low surface energy of FPs, other successful approaches focused on achieving desired physico-chemical properties by controlled synthesis of fluorinated and PEGylated networks using atom transfer radical polymerization.[1, 2, 20-22] Other approaches included patterning of surfaces with

fluorinated and PEG phases,[23] formation of crosslinked networks,[8, 24] and surface grafting of PEG and fluoropolymers to surfaces.[25-27]

In the view of these considerations, the synthesis of environmentally benign colloidal particles containing PEG and Fps that upon coalescence form polymeric films have not been exploited. If successful, this approach will offer a new platform of aqueous colloids that exhibit antifouling characteristics. Particular challenges are to combine low surface tension fluoromonomers which impose severe restrictions on polymerization in aqueous environments with methacrylates and acrylates. The first part of this study describes the synthesis of pentafluorostyrene (PFS), methylmethacrylates (MMA), n-butylacrylate (nBA), and PEG that form colloidal particles. The second part will discuss stratification processes during coalescence of p-MMA/nBA/PFS/PEG particles which result in uniquely stratified films that inhibit protein adsorption.

Experimental

MMA, nBA, PFS, PEG (Mol. Wt. = 750), and sodium dioctylsulfosuccinate (SDOSS) were purchased from Aldrich Chemical Co. Water soluble initiator 2,2'-Azobis[2-(2-imidazolin-2-yl)propane] dihydrochloride (VA-44) was purchased from Wako Pure Chemicals Ind. Ltd.

p-MMA/nBA/PFS/PEG emulsions were synthesized using a semicontinuous process outlined elsewehere,[28, 29] and adapted for small-scale polymerization. The reaction flask was placed in a water bath set at 50°C, purged with N_2 gas, charged with 35 ml of DDI water under continuous stirring at 300 rpm. SDOSS surfactant was utilized and Table V- 1 provides compositional ratios of colloidal dispersions prepared for the purpose of these studies. SDOSS was dissolved in water under high agitation followed by addition of monomers to produce a semi-stable pre-emulsion. The pre-emulsion was fed continuously over the period of 4 hrs while the initiator solution was added for 4.5 hrs. Upon completion of the initiator feed, polymerization was allowed to continue for another 10 hrs. This process resulted in 21 % w/w solids which was determined from the initial feed composition of the initiator monomer mixture and the analysis of the solid content after the synthesis. As listed in Table V- 1, the following compositions of colloidal particles containing (A) p-MMA/nBA/PFS, (B) p-MMA/nBA/PFS/PEG (5% w/w), (C) p-MMA/nBA/PFS/PEG (10% w/w), (D) p-MMA/nBA/PFS/PEG (20% w/w), and (E) p-MMA/nBA/PFS/PEG (30% w/w), were prepared and their particle size was analyzed using a Microtrac UPA 250 instrument. Molecular weight was determined using gel permeation chromatography (GPC) system which consisted of a Waters Alliance 2695 Separation Module, a Waters 2410

interferometric refractometer, and two polymer laboratories hexafluoroisopropanol (PL HFIP) gel (Polymer Laboratories Inc.), with the GPC columns connected in series. Freshly distilled hexafluoro isopropanol (HFIP) serves as the mobile phase with a flow rate of 1.0 mL/min. Sample concentrations were 10-12 mg/mL in freshly distilled HFIP, with an injection volume of 50 micro liters. The detector signals were recorded using Empower 2 Chromatography Data Software (Waters Corporation) and molecular weights were determined relative to narrow molecular weight p-MMA standards. The number average molecular weight of p-MMA/nBA/PFS copolymer was observed to be $1.5*10^5$ gm/mol. Due to crosslinking after PEG incorporation molecular weight for the p-MMA/nBA/PFS/PEG copolymer samples could not be obtained due to their insolubility in HFIP solvent.

Colloidal particle solutions were allowed to coalesce for 72 hrs at 23 °C and 70% relative humidity (RH) to form approximately 10 μm thick films. The films were obtained by a draw down on the polyvinyl chloride (PVC) substrates. For contact angle measurements as well as atomic force microscopy (AFM) experiments colloidal solutions were coalesced on a glass slides using a draw bar to give an approximately film thickness of 10 μm.

Solid-state ^{13}C NMR spectroscopy was performed on solid films using a Varian ^{UNITY}INOVA 400 spectrometer using a standard Chemagnetics 7.5 mm PENCIL^{TM}-style probe in order to determine copolymer composition. Films were loaded into zirconia rotor sleeves, sealed with Teflon™ caps, and spun at rate of 4.0 kHz. The standard cross-polarization/magic angle spinning (CP/MAS) technique was used with high-power proton decoupling implemented during data acquisition. The

acquisition parameters were as follows: The ^{1}H 90° pulse width was set at 5.25 ms, the cross-polarization contact time was 1 ms, the dead time delay was 6.4 ms, and the acquisition time was 45 ms.[30] A recycle delay of 3 seconds between scans was utilized.

In order to analyze copolymer morphologies using solid-state wide-line separation (WISE) NMR spectroscopy was performed using zirconia rotor sleeves, sealed with Teflon™ caps, and spun at rate of 4.0 kHz. The following parameters were utilized in the NMR experiments: ^{1}H 90° pulse width 5.25 ms, the cross-polarization contact time 250 ms, the dead time delay 5.9 ms, and the acquisition time 45 ms. A recycle delay of 3 sec between scans was utilized. To further increase the selectivity of solid state NMR analysis 2D NMR WISE of the chain dynamics by correlating the proton line shape with the carbon chemical shift were conducted at 0 and 7.5 ms contact time.[31, 32] For WISE spectra, the sweep widths in ^{1}H and ^{13}C were 1250 and 301 ppm, respectively. The number of free induction decay (FID) acquired was 128, with 128 scans per FID. Time-proportional phase incrimination (TPPI) phase cycling was used to obtain phase sensitive data, with an additional 384 points added to the indirectly-detected dimension via linear prediction. Both dimensions were zero-filled to 2048 points, with Lorentzian and Gaussian apodization applied prior to Fourier transform.

Microscopic attenuated total reflectance Fourier transform infrared (ATR FT-IR) spectroscopy measurements were conducted on the film-air (F-A) interfaces using a Bio-Rad FTS-6000 FT-IR single beam spectrometer at a 4 cm^{-1} resolution. The surfaces were analyzed using a 2 mm Ge crystal with a 45° angle maintaining constant contact pressure between the crystal and the specimens. All spectra were corrected for spectral distortions using the Urban-Huang algorithm.[33] Internal reflection infrared

imaging (IRIRI) experiments were conducted on a Varian Stingray system. This system consists of a Bio-Rad FTS 6000 spectrometer, a UMA 500 microscope, an Image IR focal plane array (FPA) image detector, and a semispherical germanium IRE. IRIR images were collected using the following spectral acquisition parameters: under sampling ratio 2, step-scan speed 5 Hz, and spectral resolution 8 cm^{-1} and the use of a Ge crystal in contact with the analyzed surface allows spatial resolution in the range of 1 μm.[34] In a typical experiment, spectral data set acquisition time was 2 minutes and image processing was performed using ENVI software (The Environment for Visualizing Images, Research Systems, Inc.) version 3.5. When appropriate, baseline correction algorithms were applied to compensate for baseline deviations which were accomplished by built-in application software supplied by GRAMS/A1 v 7.02 (Galactic Ind.).

Atomic force microscopy (AFM) measurements were conducted on a Nanoscope IIIa Dimension 3000 scanning probe microscope (Digital Instruments). A silicon probe with 125 μm long silicon cantilever, nominal force constant of 40 N/m and resonance frequency of 275 KHz were used in a tapping mode, allowing estimation of surface topography and roughness. Surface tension measurements were obtained using a FTA200 dynamic contact angle analyzer.[35] Zeta potential measurements were conducted on a Malvern Zetasizer nano-ZS using diluted colloidal dispersion in DI water at room temperature.

Bovine serum albumin (BSA), lipopolysacharide (Lipopoly), and fibrinogen (Fib) proteins were purchased from Aldrich Chemical Co. and were dissolved in phosphate buffer saline (PBS) solution (pH 7.0) at a concentration level of 8 mg/ml.

Films containing copolymers p-MMA/nBA/PFS, p-MMA/nBA/PFS/PEG (5% w/w), p-MMA/nBA/PFS/PEG(10% w/w), p-MMA/nBA/PFS/PEG(20% w/w), and p-MMA/nBA/PFS/PEG(30% w/w) were equilibrated in the respective protein solutions by depositing 2 ml solution on the films for 2 hrs at ambient temperature, followed by continuous rinsing the surface for 10 minutes with PBS solution to remove excess protein, followed by drying in a dessicator. Protein adsorptions on polymeric surfaces after drying were evaluated using ATR FT-IR spectroscopy and IRIRI.

Results and Discussions

As stated in the Introduction, the objective of these studies is to develop a new family of colloidal dispersions containing PFS and PEG components copolymerized with MMA and nBA monomers that upon coalescence form films that will repel proteins. The first part of this study will describe synthetic steps involved in the preparation of colloidal dispersions and their solution morphologies, whereas the remaining parts will focus on the particle coalescence and protein adsorption.

Synthesis of p-MMA/nBA/PFS/PEG Colloidal Dispersions

For the purpose of these studies we synthesized p-MMA/nBA/PFS copolymer particles containing 0, 5, 10, 20, and 30 % w/w of PEG. Table V- 1 provides detailed compositions of the dispersions, % solids, and the particle size analysis data. To optimize the glass transition temperature (T_g) of the final compositions, the amount of nBA was varied from 25 to 55% w/w balanced by the equivalent amount of PEG, and their compositions are given in Table V- 1.

To determine if all monomers were copolymerized to form p-MMA/nBA/PFS/PEG copolymer colloidal particles solid-state ^{13}C NMR spectroscopy was utilized. Figure V- 1, A, shows chemical structures of MMA, nBA, PFS, and PEG, while the solid-state ^{13}C NMR spectra of p-MMA/nBA/PFS and p-MMA/nBA/PFS/PEG (30%) are presented in Figure V- 1, B-1 and B-2, respectively. The spectrum labeled B-1 clearly shows the resonances due to MMA, nBA, and PFS copolymer structures and solid-state ^{13}C NMR spectrum of p-MMA/nBA/PFS/PEG (30%) is illustrated in Figure V- 1, B-2 exhibits a large 70.1 ppm resonance due to O-

CH_2 groups, indicating that PEG is copolymerized with MMA, nBA, and PFS monomers.

In an effort to determine the copolymer compositions of the colloidal particles 2D NMR WISE experiments were conducted which allows us to determine the chain dynamics by measuring the ^1H line-width as a function of the pulse contact time. If monomer units are randomly distributed, the ^1H line-width will decrease with the increasing contact time, whereas for block copolymers the band width will remain similar. In view of these considerations the following spectral features are of particular interest: 13.96 ppm due to $-CH_3$ resonance of nBA, 31.4 ppm due to $-CH_2-$ resonance of MMA and nBA, 45.13 ppm resonances due to –CH- resonance of PFS, and 70.1 ppm resonance due to $-O-CH_2-$ resonance of PEG component. Figure V- 2 illustrates the ^1H full width at half height (FWHH) line width of these resonances plotted as a function of mixing time and shows a contour plot for the ^{13}C WISE 2D NMR generated with 0 contact time (A) and contact time set at 7.5ms (B). As seen for 13.96, 31.4, and 45.13 ppm resonances, the corresponding ^1H line-width decreases upon the increased mixing time. However, for 70.1 ppm shown in Figure V- 2, B, the ^1H line-width remains unchanged. Furthermore, when ^1H FWHH line-width is plotted as a function of mixing time, as illustrated in Figure V- 2, C, the ^1H FWHH line widths of 13.96, 31.4, and 45.13 ppm vary as the mixing time increases, and converges to similar values due to ^1H spin diffusion indicating random copolymerization of these monomers. However, the ^1H FWHH for the PEG moiety at 70.1 ppm resonance remains constant and is significantly lower, signifying that PEG is copolymerized, but remains as a phase separated entity.

Table V- 1 also shows that the particle size of colloidal particles increases from 62 to 106 nm as the amount of PEG incorporated into p-MMA/nBA/PFS increases from 0 to 30 wt% and 20% w/w solids was retained. Although it is unlikely that the increase of the particle size with the increase PEG content is attributed to free volume increase since the Tg of both p-nBA and p-PEG are -54 and -42°C, respectively,[36] zeta potential measurements were conducted on the diluted solutions at room temperature. As illustrated in Figure V- 3, as the amount of PEG increases from 0 to 30 % w/w, zeta potential changes from -55 to -32 mV. The linear increase of the zeta potential is attributed to the displacement of surfactant molecules from the surface of the particles, as more PEG is being copolymerized. Initially, MMA, nBA, and PFS being hydrophobic, migrate from monomer droplets to the polymerization site, and copolymerize continuously under monomer starvation conditions to form p-MMA/nBA/PFS random copolymer. Since PEG exhibits significantly greater hydrophilicity and solubility in an aqueous medium, PEG molecules remain in the aqueous phase longer and react at the later stages of polymerization. This is depicted in Scheme 1, A, steps 1 and 2.

p-MMA/BA/PFS/PEG Coalesced Films

The colloidal dispersions listed in Table V- 1 were allowed to coalesce and their surface morphologies at the film-air (F-A) interface were analyzed using AFM. Figure V- 4, A-E shows a series of AFM 5x5 μm phase images of the coalesced films of p-MMA/BA/PFS and p-MMA/BA/PFS/PEG containing 5, 10, 20, and 30% PEG (w/w), respectively. As shown in Image A, a continuous one-phase component is observed and attributed to p-MMA/nBA/PFS at the F-A interface. However, upon introduction of

PEG, the phase separation is observed in Images B-E, which is further enhanced upon higher (B) 5, (C) 10, (D) 20, and (E) 30 % w/w content of PEG incorporated into p-MMA/nBA/PFS particles. The lighter areas of the images are attributed to the p-MMA/nBA/PFS (hard phase), whereas the darker appearance is due to PEG regions (softer phase).

In order to verify chemical compositions at the F-A interface, ATR FT-IR spectra were recorded from the F-A interface. Figure V- 5, Traces A-E illustrates ATR FT-IR spectra recorded from the F-A interface of p-MMA/nBA/PFS (Trace A), p-MMA/nBA/PFS/PEG (5%) (Trace B), p-MMA/nBA/PFS/PEG (10%) (Trace C), p-MMA/nBA/PFS/PEG (20%) (Trace D), and p-MMA/nBA/PFS/PEG (30%) (Trace E) respectively. For reference purposes, Traces F and G illustrate the spectra of PFS and PEG. As expected, the band due to PEG at 1114 cm^{-1} increases as the PEG content increases. It should be pointed out that the same spectral features are observed at the F-S interface, thus showing that PEG distribution is uniform across the film thickness. The same applies to the PFS component of the film, as demonstrated by the unchanged intensities of the bands due to PFS at 1500 and 1520 cm^{-1} (C-F stretching). The 1165 and 1145 cm^{-1} bands due to C-O-C stretching vibrations of nBA and MMA components are also observed for all compositions. However, analysis of the spectra shown in Figure V- 5 also illustrates that SDOSS stratifies near to the F-A interface when PEG is incorporated, and the band at 1046 cm^{-1} due to SO_3Na^+.....H_2O associations increases upon the increasing PEG content (Figure V- 5, Traces A-E) in colloidal dispersions. [35, 37-40] This is not surprising because ionic surfactant-PEG associations are known and result from their hydrophilic properties.[41] Thus, during coalescence, as water

evaporates, PEG retains H_2O molecules for the longest time, and SDOSS solubility in water facilitates environments for SDOSS to remain in the PEG phase.

In order to determine molecular origin of compositional heterogeneities illustrated by AFM images in Figure V- 4, IRIRI measurements were employed. Figure V- 6, A_1 represents the IR image obtained from p-MMA/BA/PFS films by tuning into the 1500 cm^{-1} band due to the C-F stretching vibrations of PFS. As seen, the homogeneous distribution of PFS is observed for p-MMA/nBA/PFS films, which is also confirmed by IR spectra recorded from the Areas 1 and 2. As shown in Figure V- 6, A_2 there are no intensity differences between the 1500 and 1520 cm^{-1} bands. Thus, p-MMA/nBA/PFS colloidal particles exhibit uniform coalescence with no chemical compositional gradients near the interfacial regions. For the films containing p-MMA/nBA/PFS/PEG (5 wt %), IRIR images were obtained by tuning into the 1500 cm^{-1} band due to PFS as well as the 1114 cm^{-1} band due to C-O-C stretching vibrations of PEG. This is illustrated in Figure V- 6, B_1 and B_2. As seen, the phase separation between the PFS and PEG is evident, as manifested by IR spectra recorded from the Areas 1 and 2 (Figure V- 6, B_3), where the spectrum recorded from the Area 1 exhibits higher intensities of the band at 1114 cm^{-1} due to PEG. The phase separation is further enhanced as the amount of PEG is increased to 10, 20, and 30 wt% (Figure V- 6, C_1 to C_3; Figure V- 6, D_1 to D_3; and Figure V- 6, E_1 to E_3). As seen, the domain size of the PEG phase is also significantly enhanced. As noted earlier in the ATR FT-IR analysis, the phase separation between p-MMA/nBA/PFS and PEG is also associated with the presence of the 1046 cm^{-1} band due to SDOSS....H_2O associations where band increases as the amount of PEG incorporated in the colloidal dispersions is increased

(Figure V- 6, A_1-E_3). Thus, the presence of PEG enhances the migration of SDOSS to the F-A interface, thus facilitating mobility of SDOSS molecules to the F-A interface during coalescence. Based on these data, the coalescence mechanism of p-MMA/nBA/PFS/PEG colloidal particles is schematically depicted in Scheme 1, B. Due to the hydrophobic nature of p-MMA/nBA/PFS component containing phase separated hydrophilic PEG component, the two phases upon coalescence form phase-separated films with SDOSS molecules associated with water residing in the PEG phase as illustrated in Scheme 1, B.

Protein Adsorption

Another objective of these studies was to examine protein adsorption properties of p-MMA/nBA/PFS/PEG films. To determine interactions between polymeric films containing p-MMA/nBA/PFS/PEG and proteins we exposed the surfaces of the coalesced films to aqueous solutions containing BSA, Lipopoly, and Fib proteins for 2 hrs, and analyzed their surfaces. To follow the protein adsorption process, ATR FT-IR spectroscopy was utilized. Figure V- 7 (a), (b), and (c) represent a series of ATR FT-IR spectra obtained from p-MMA/nBA/PFS/PEG films exposed to BSA, Lipopoly, and Fib proteins, and Traces B-E correspond to the increasing content of PEG. The amide 1 bands are detected at 1650 and 1550 cm^{-1} and manifest the presence of protein adsorption on the surface. As the PEG content increases, from 5 to 30% (Traces B-E), the intensity of the amide band intensities are reduced, thus inhibiting protein adsorption on the PEG surfaces.

Although it is anticipated that the presence of phase-separated PEG will alter protein adsorption, it is also of interest to identify if and how other components of the

film participate in this process. To determine which phase is most susceptible for protein adsorption, IRIR images were collected from the films after exposure to BSA, Lipopoly, and Fib by tuning into the 1650 cm^{-1} bands due to –CO-NH linkages. The results of the IRIRI analysis are shown in Figure V- 8, A-C series by tuning into the 1650 cm^{-1} band due to amide I. As seen in Figure V- 8, A-1 through A-5 for specimens containing 0, 5, 10, 20 and 30 % w/w PEG incorporated into p-MMA/nBA/PFS/PEG, the surface coverage with BSA is significantly reduced upon the increased PEG content. This is also supported by the analysis of the corresponding spectra recorded from areas 1 and 2 of the image A-4 image. The imaging results observed for Lipopoly (Figure V- 8, B), and Fib (Figure V- 8, C) proteins show similar results. Finally, of particular interest is the location of protein adsorption on the copolymer surfaces. Analysis of the amide I band at 1650 cm^{-1} shows that this band intensity increase parallels the enhanced intensity of the bands at 1500 and 1520 cm^{-1} due to PFS, thus suggesting that the preferential location of the protein adsorption is on the p-MMA/nBA/PFS phase. This is schematically depicted in Scheme 2, A and B.

In summary, these studies showed successful synthesis of stable p-MMA/nBA/PFS/PEG copolymer dispersions using free radical emulsion polymerization process. Up to 30% w/w of PEG can be copolymerized on to the exterior of p-MMA/nBA/PFS particles which upon coalescence form stable films capable of repelling proteins. The compositional heterogeneity between the PEG and PFS phases lead to minimal affinity for proteins adsorption which predominantly occurs on the p-MMA/nBA/PFS surface domains.

Table V-1. Particle Size and Composition of P-MMA/nBA/PFS/PEG Colloidal Dispersions Synthesized With Different Copolymer Compositions.

Composition	p-MMA/nBA/PFS	p-MMA/nBA/PFS/PEG (5%)	p-MMA/nBA/PFS/PEG (10%)	p-MMA/nBA/PFS/PEG (20%)	p-MMA/nBA/PFS/PEG (30%)
Individual Components (w/w%)	(A)	(B)	(C)	(D)	(E)
DDI	79	79	79	79	79
Methyl methacrylate	2.1	2.1	2.1	2.1	2.1
n-butylacrylate	11.6	10.5	9.5	7.4	5.3
PFS	7.4	7.4	7.4	7.4	7.4
PEG	0	1.05	2.1	4.2	6.3
SDOSS	0.63	0.63	0.63	0.63	0.63
VA-044	0.04	0.04	0.04	0.04	0.04
Solids %	21	21	21	21	21
Particle Size (nm)	62	66	70	85	106

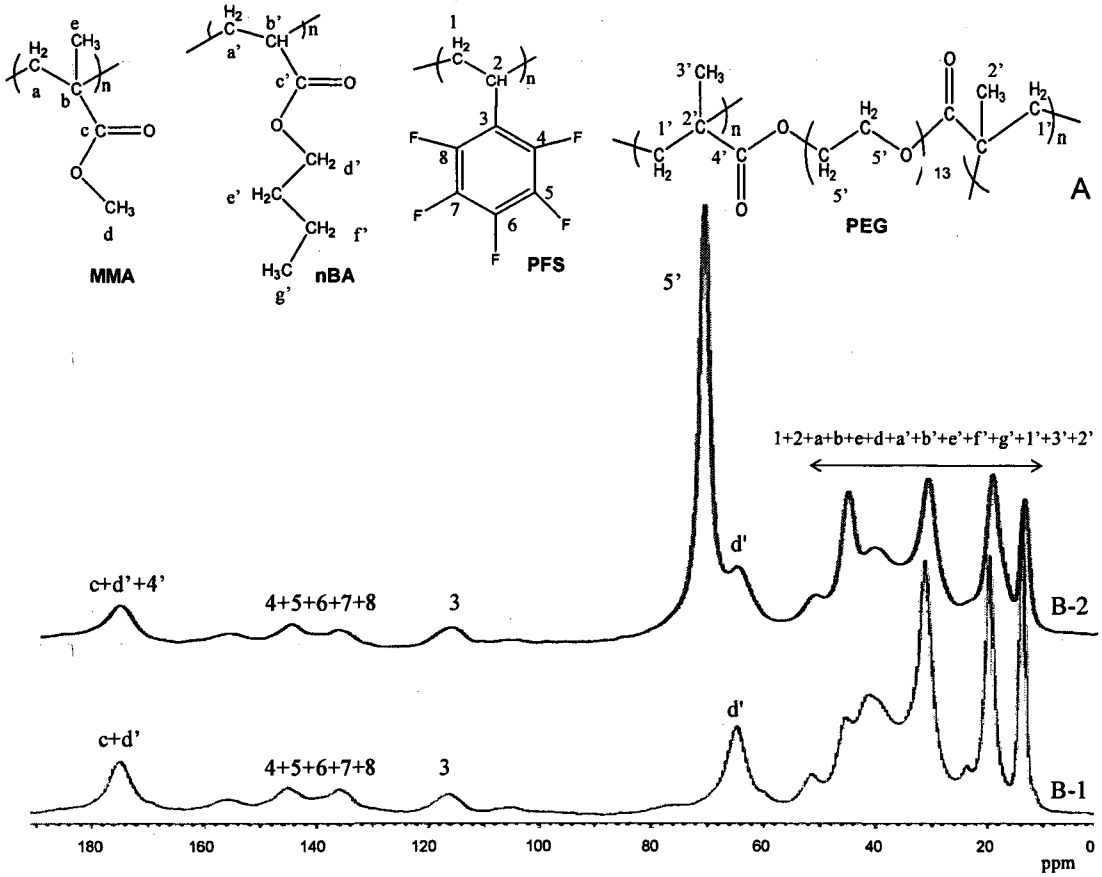

Figure V-1. A- Monomer structures; B- Solid state ^{13}C NMR spectra of p-MMA/nBA/PFS (B-1) and p-MMA/nBA/PFS/PEG (30%) (B-2) colloidal films.

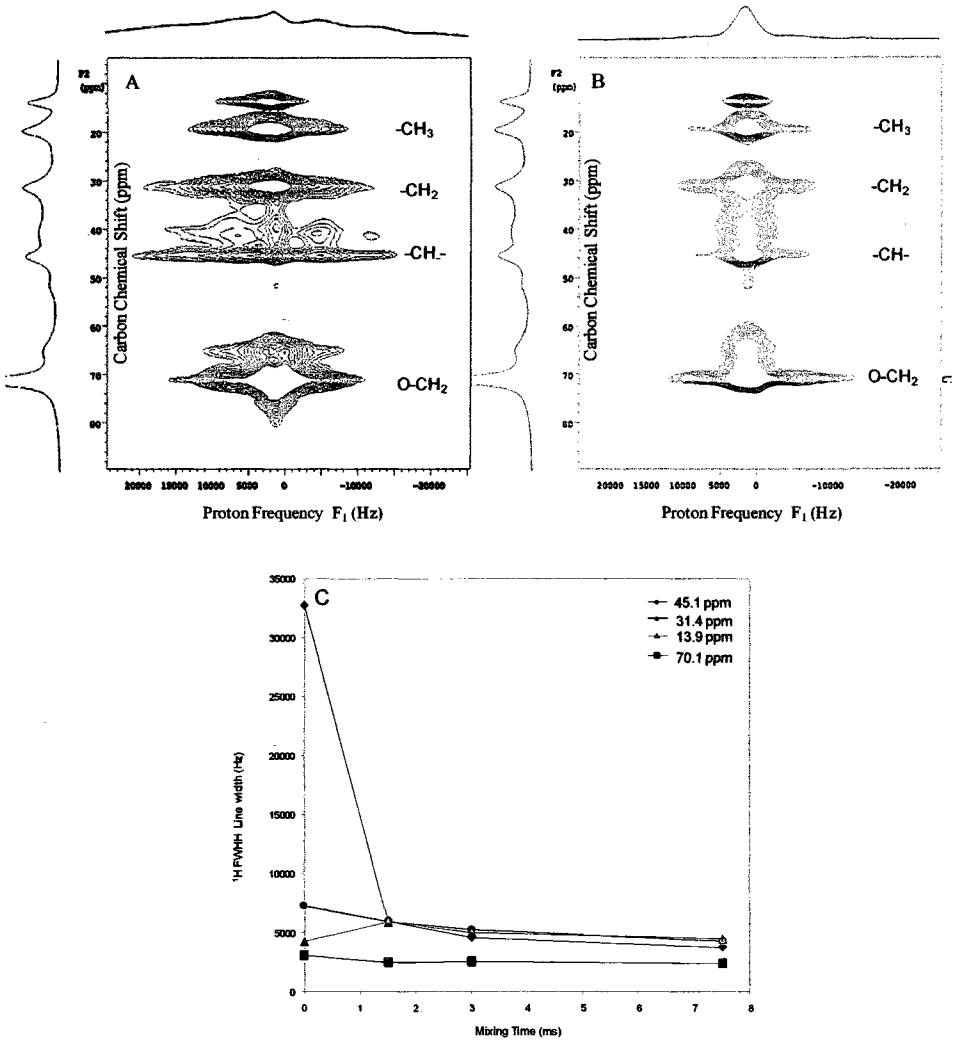

Figure V-2. A contour plot for the ^{13}C WISE 2D NMR of p-MMA/nBA/PFS/PEG (30%) copolymer deduced with 0 ms contact time (A), 7.5 ms contact time (B), and ^{1}H FWHH Line width of various bands with varying mixing time (C).

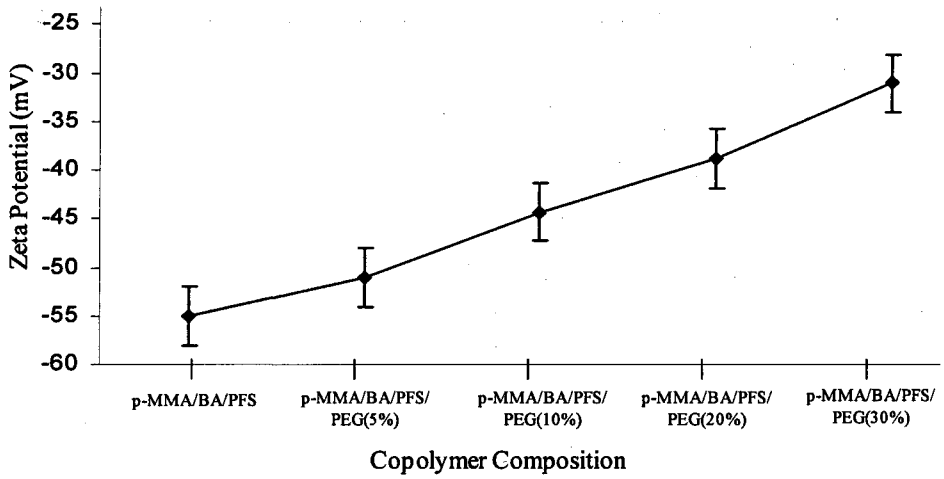

Figure V-3. Zeta potential plotted as a function of copolymer composition of p-MMA/nBA/PFS/PEG colloidal dispersions.

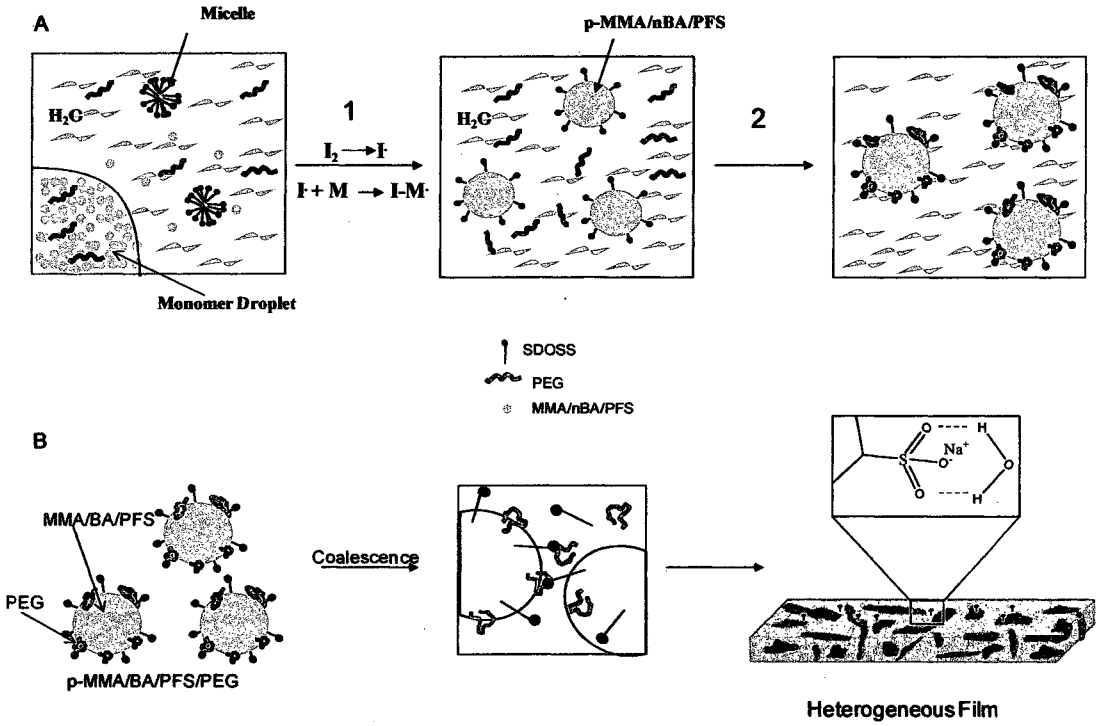

Scheme V-1. Schematic representation of (A) block copolymerization of PEG phase during emulsion polymerization process and (B) coalescence mechanism for p-MMA/nBA/PFS/PEG colloidal dispersions containing SDOSS association with PEG phase.

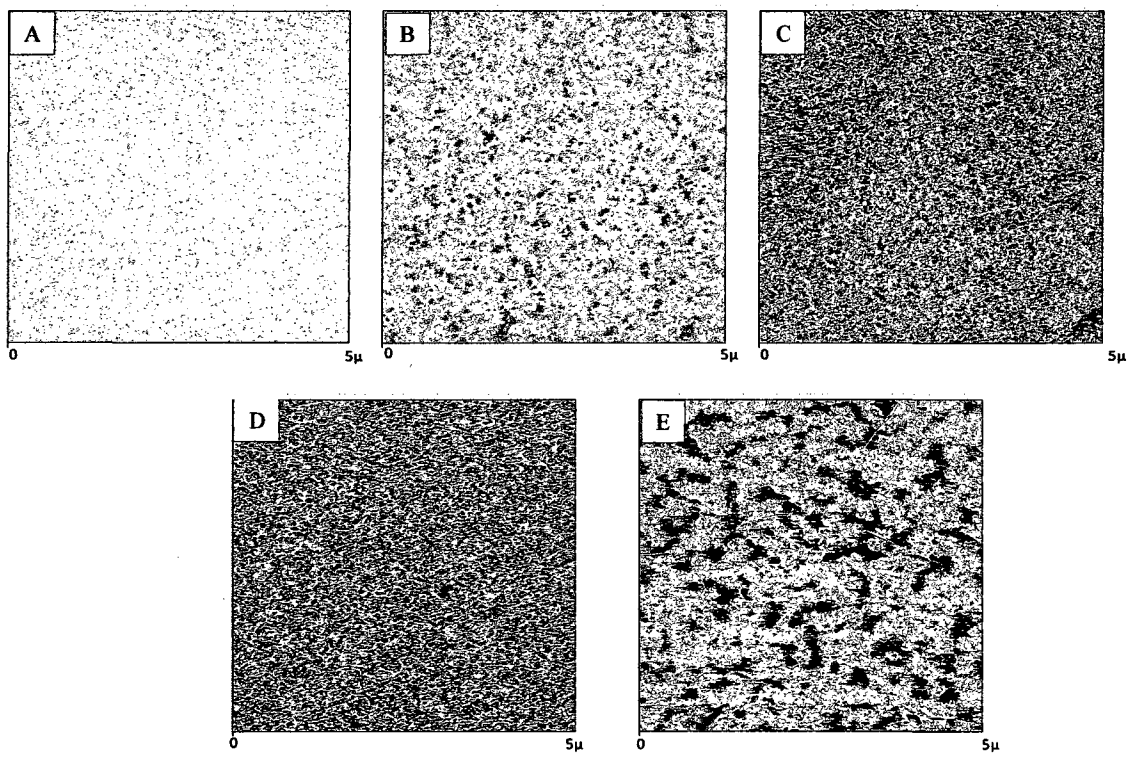

Figure V-4. AFM phase images of (A) p-MMA/nBA/PFS, (B) p-MMA/nBA/PFS/PEG (5%), (C) p-MMA/nBA/PFS/PEG (10%), (D) p-MMA/nBA/PFS/PEG (20%), and (E) p-MMA/nBA/PFS/PEG (30%) copolymer films.

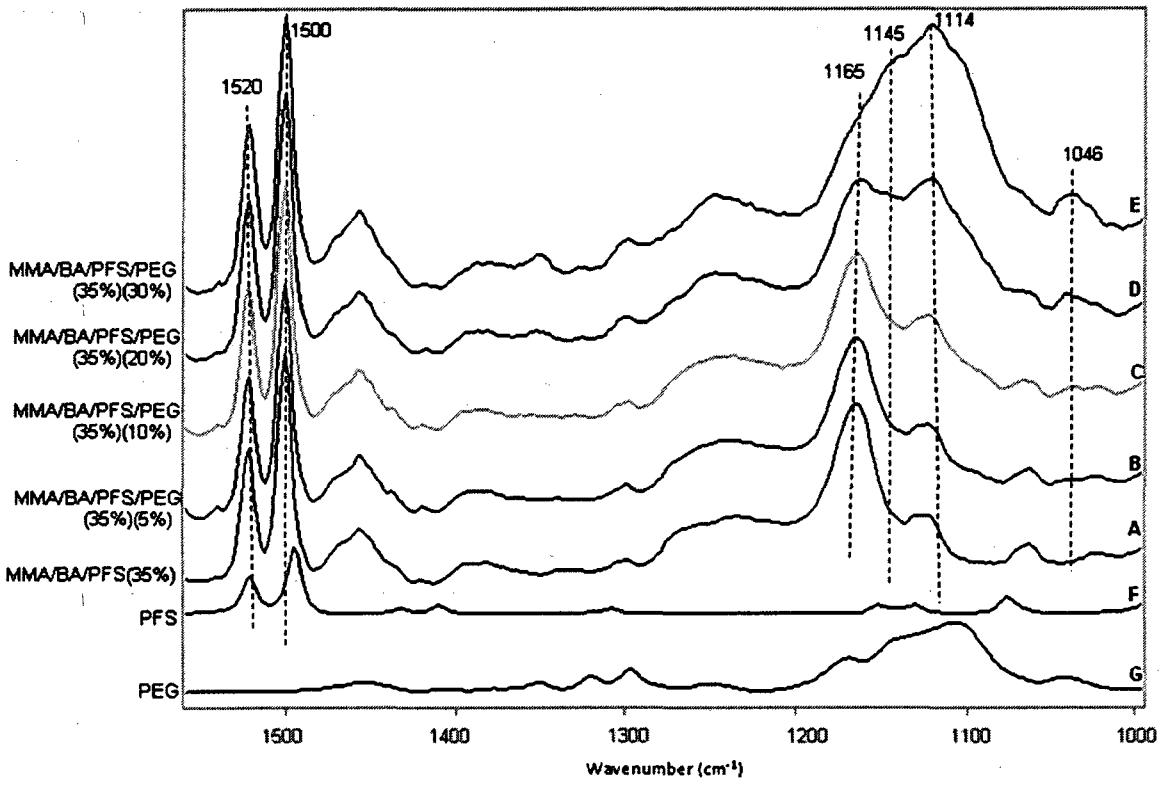

Figure V-5. ATR FT-IR spectra of (A) p-MMA/nBA/PFS, (B) p-MA/nBA/PFS/PEG (5%), (C) p-MMA/nBA/PFS/PEG(10%); (D) p-MMA/nBA/PFS/PEG(20%), (E) p-MMA/nBA/PFS/PEG (30%), (F) PFS monomer, and (G) PEG monomer.

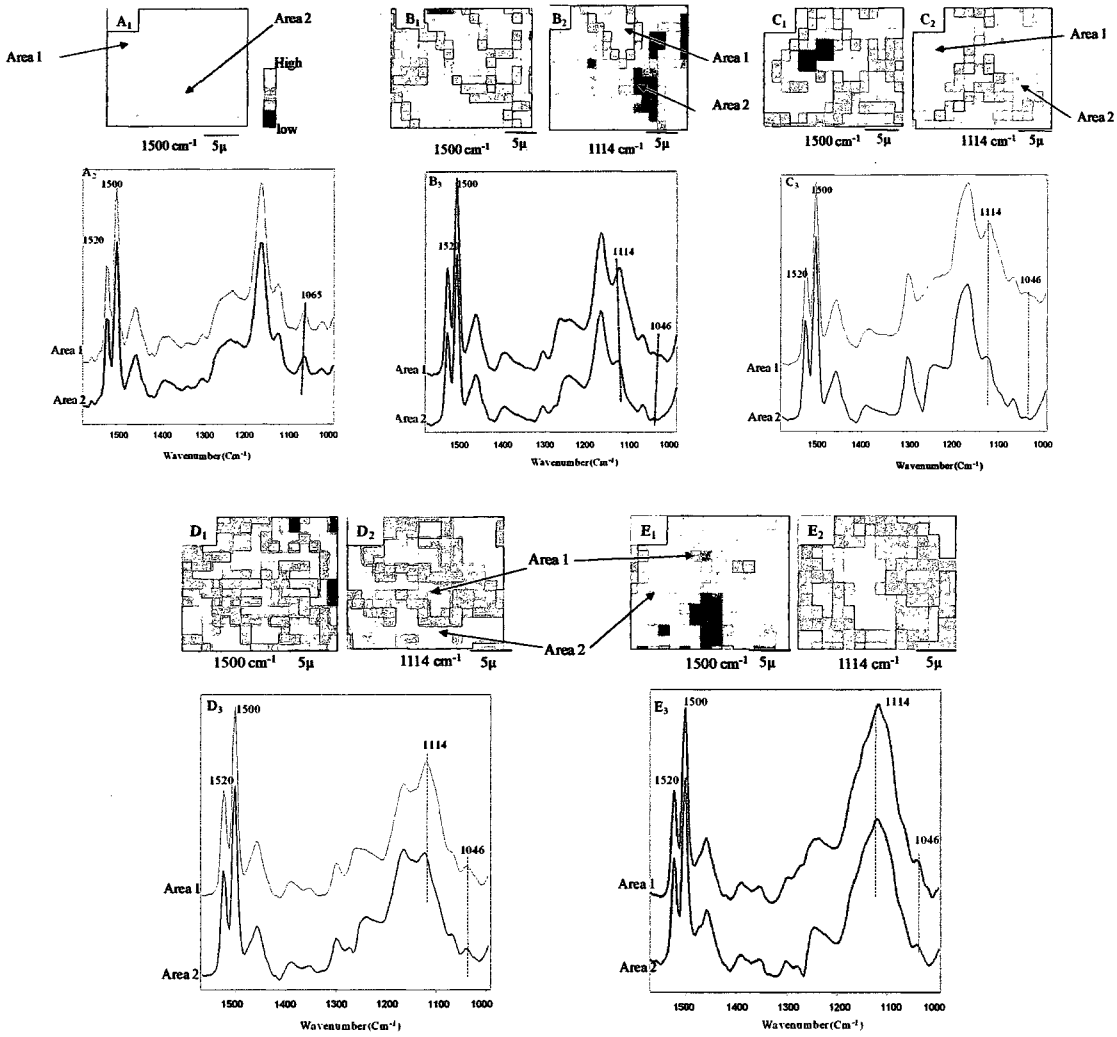

Figure V- 6. IRIR images recorded from the F-A interface of p-MMA/nBA/PFS (A_1), p-MMA/nBA/PFS/PEG (5%) (B_1), MMA/nBA/PFS/PEG (10%) (C_1), MMA/nBA/PFS/PEG (10%) (D_1), and MMA/nBA/PFS/PEG (10%) (E_1) colloidal films upon tuning to 114 and 1500 cm^{-1}; A_2, B_3, C_3, D_3, and E_3 represents IR spectra recorded from areas labeled 1 and 2 from corresponding images.

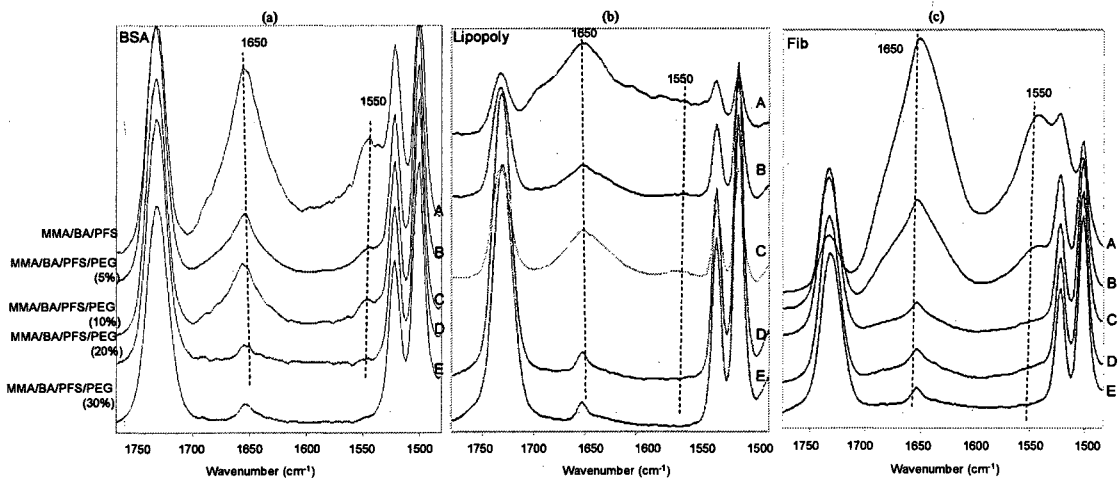

Figure V-7. ATR FT-IR spectra recorded in the 1750-1500 cm^{-1} region of (A) p-MMA/nBA/PFS, (B) p-MMA/nBA/PFS/PEG(5%), (C) p-MMA/nBA/PFS/PEG(10%), (D) p-MMA/nBA/PFS/PEG(20%), (E) p-MMA/nBA/PFS/PEG (30%) films exposed to BSA (a), Lipopoly (b), and Fib (c) proteins. The spectra were recorded after protein adsorption, followed by rinsing each specimen, as described in the Experimental section.

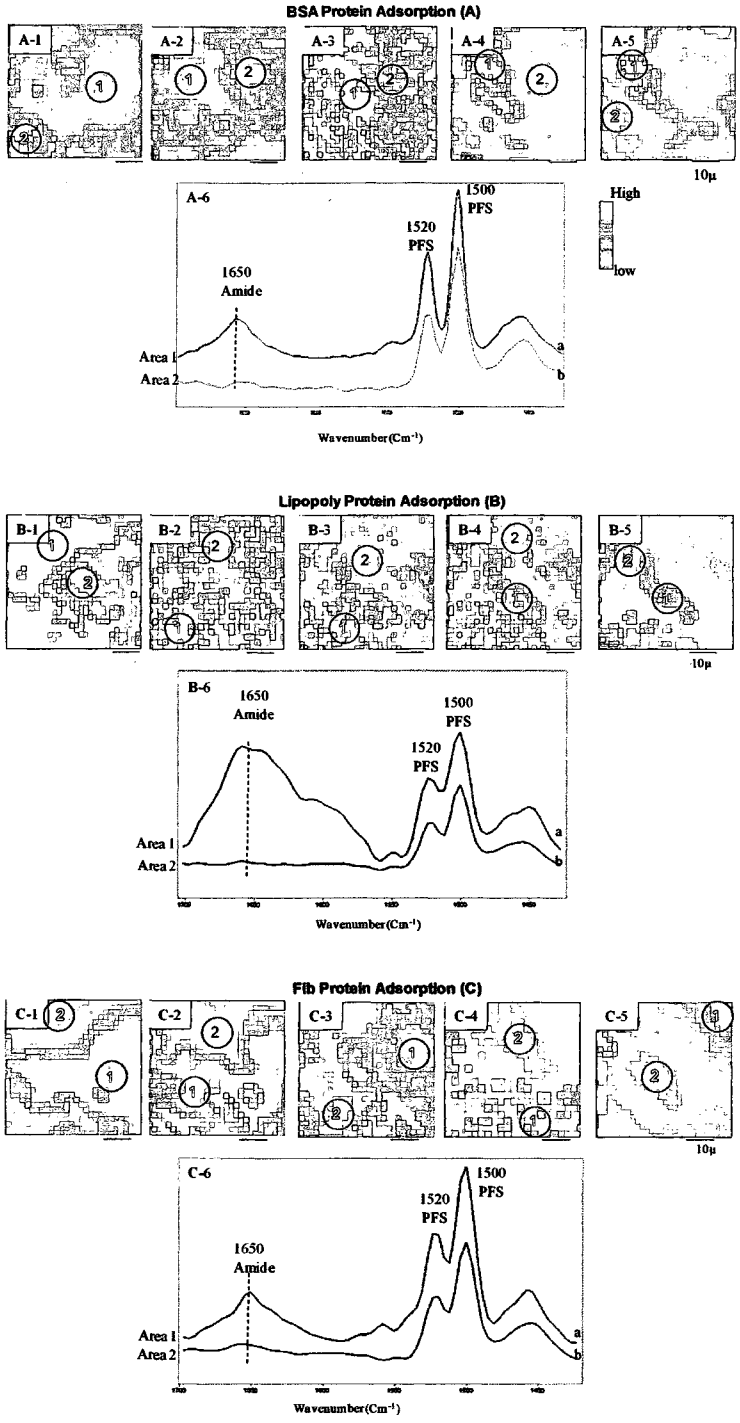

Figure V- 8. IRIR images recorded by tuning into the 1650 cm^{-1} band from the F-A interface of films exposed to BSA (A), Lipopoly (B), and Fib (C) proteins on (A-1, B-1, and C-1) p-MMA/nBA/PFS, (A-2, B-2, and B-2) p-MMA/nBA/PFS/PEG(5%), (A-3, B-3, and B-3) p-MMA/nBA/PFS/PEG(10%), (A-4, B-4, and B-4) p-MMA/nBA/PFS/PEG(20%), ((A-5, B-5, and B-5) p-MMA/nBA/PFS/PEG (30%) copolymer films, and (A-6, B-6, and B-6) IR spectra recorded from areas labeled 1 and 2.

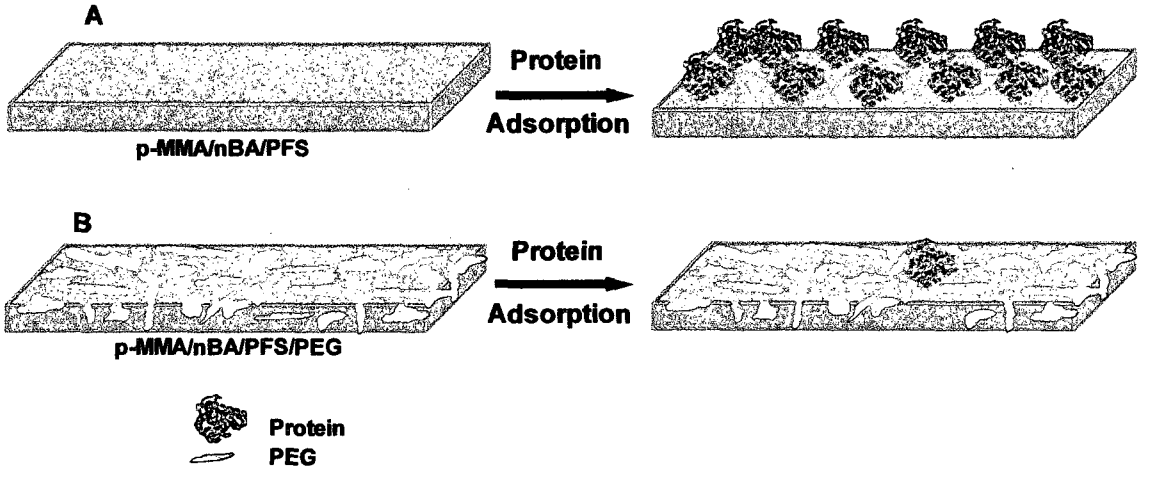

Scheme V-2. Schematic representation of protein adsorption on (A) p-MMA/nBA/PFS and (B) p-MMA/nBA/PFS/PEG films.

References

1. Gudipati, C. S.; Greenlief, C. M.; Johnson, J. A.; Prayongpan, P.; Wooley, K. L. *Journal of Polymer Science, Part A: Polymer Chemistry* **2004,** *42*, 6193.

2. Bartels, J. W.; Cheng, C.; Powell, K. T.; Xu, J.; Wooley, K. L. *Macromolecular Chemistry and Physics* **2007,** *208*, 1676.

3. Brady, R. F. *Biofouling* **2000,** *15*, 73.

4. Chen, Y.; Liu, D.; Deng, Q.; He, X.; Wang, X. *J Polym Sci Part A: Polym Chem* **2006,** *44*, 3434.

5. Misra, A.; Jarrett, W. L.; Urban, M. W. *Macromolecules* **2007,** *40*, 6190.

6. Yarbrough, J. C.; Rolland, J. P.; DeSimone, J. M.; Callow, M. E.; Finlay, J. A.; Callow, J. A. *Macromolecules* **2006,** *39*, 2521.

7. Woodward, I.; Schofield, W. C.; Roucoules, V.; Badyal, J. P. S. *Langmuir* **2003,** *19*, 3432.

8. Youngblood, J. P.; Andruzzi, L.; Ober, C. K.; Hexemer, A.; Kramer, E. J.; Callow, J. A.; Finlay, J. A.; Callow, M. E. *Biofouling* **2003,** *19*, 91.

9. Vermette, P.; Meagher, L. *Colloidds Surf. B- Biointerfaces* **2003,** *28*, 153.

10. Morra, M. *J. Biomater. Sci.- Polym. Ed.* **2000,** *11*, 547.

11. Leckband, D.; Sheth, S.; Halperin, A. *J. Biomater. Sci.- Polym. Ed.* **1999,** *10*, 1125.

12. Kingshott, P.; Griesser, H. J. *Curr. Opin. Solid State Mater. Sci.* **1999,** *4*, 403.

13. McPherson, T.; Kidane, A.; Szleifer, I.; Park, K. *Langmuir* **1998,** *14*, 176.

14. Efremova, N. V.; Sheth, S. R.; Leckband, D. E. *Langmuir* **2001,** *17*, 7628.

15. Malmsten, M.; Emoto, K.; Van Alstine, J. M. *J. Colloid Interface Sci.* **1998,** *202*, 507.

16. Pasche, S.; De Paul, S. M.; Voros, J.; Spencer, N. D.; Textor, M. *Langmuir* **2003,** *19*, 9216.

17. Otts, D. B.; Pereira, K. J.; Jarret, W. L.; Urban, M. W. *Polymer* **2005,** *46*, 4776.

18. Otts, D. B.; Cueva-Parra, L. A.; Pandey, R. B.; Urban, M. W. *Langmuir* **2005,** *21*, 4034.

19. Otts, D. B.; Urban, M. W. *Polymer* **2005,** *46*, 2699.

20. Powell, K. T.; Cheng, C.; Wooley, K. L.; Singh, A.; Urban, M. W. *J Polym Sci Part A: Polym Chem* **2006,** *21*, 3044.

21. Gudipati, C. S.; Finlay, J. A.; Callow, J. A.; Callow, M. E.; Wooley, K. L. *Langmuir* **2005,** *21*, 3044.

22. Gan, D.; Mueller, A.; Wooley, K. L. *Journal of Polymer Science, Part A: Polymer Chemistry* **2003,** *41*, 3531.

23. Finlay, J. A.; Krishnan, S.; Callow, M. E.; Callow, J. A.; Dong, R.; Asgill, N.; Wong, K.; Kramer, E. J.; Ober, C. K. *Langmuir* **2008,** *24*, 503.

24. Yarbrough, J. C.; Rolland, J. P.; DeSimone, J. M.; Callow, M. E.; Finlay, J. A.; Callow, J. A. *Macromolecules* **2006,** *39*, 2521.

25. Sharma, S.; Johnson, R. W.; Desai, T. A. *Biosensors & Bioelectronics* **2004,** *20*, 227.

26. Popat, K. C.; Sharma, S.; Desai, T. A. *Journal of Physical Chemistry B* **2004,** *108*, 5185.

27. Sharma, S.; Johnson, R. W.; Desai, T. A. *Langmuir* **2004,** *20*, 348.

28. Dreher, W. R.; Jarrett, W. L.; Urban, M. W. *Macromolecules* **2005,** *38*, 2205.

29. Davis, S. D.; Hadgraft, J.; Palin, K. J., *Encyclopedia of Emulsion Technology.* Marcel Dekker: New York, 1985; Vol. 2.

30. Schaefer, J.; Stejskal, E. O.; Buchdahl, R. *Macromolecules* **1977,** *10*, 384.

31. Schmidt-Rohr, K.; Clauss, J.; Spiess, H. W. *Macromolecules* **1992,** *25*, 3273.

32. Tekely, P.; Palmas, P.; Mutzenhardt, P. *Macromolecules* **1993,** *26*, 7363.

33. Urban, M. W., *Attenuated Total Reflectance Spectroscopy of Polymers - Theory and Practice*. 1989; Vol. Vol. 2.

34. Otts, D.; Zhang, P.; Urban, M. W. *Langmuir* **2002,** *18*, 6473.

35. Evanson, K. W.; Thortenson, T. A.; Urban, M. W. *J. Appl. Polym. Sci.* **1991,** *42*, 2309.

36. Brandrup, J.; Immergut, E. H., *Polymer Handbook.* 2nd ed.; Johnwiley & Sons: New York, 1966.

37. Zhao, Y.; Urban, M. W. *Macromolecules* **2000,** *33*, 7573.

38. Niu, B. J.; Urban, M. W. *J. Appl. Polym. Sci.* **1996,** *62*, 1903.

39. Thortenson, T. A.; Evanson, K. W.; Urban, M. W. *Polym. Mater. Sci. Eng.* **1991,** *64*, 195.

40. Niu, B.-J.; Urban, M. W. *J. Appl. Polym. Sci.* **1996,** *60*, 371.

41. Dreher, W. R.; Urban, M. W. *Langmuir* **2003,** *19*, 10254.

CHAPTER VI

ACORN-SHAPE POLYMERIC NANO-COLLOIDS: SYNTHESIS AND SELF-ASSEMBLED FILMS

Abstract

These studies show for the first time synthesis of phase separated two distinct phases within one colloidal particle which consist of p-methylmethacrylate (MMA)/n-butylacrylate (nBA) and p-nBA/pentafluorostyrene (PFS) phases and exhibit a unique acorn-shaped morphologies. These colloidal particles are capable of self-assembling on surfaces, and depending upon the surface energy of a substrate, create hydrophobic or hydrophilic film-air (F-A) interfaces. When the particles coalesce on high surface tension substrates, the p-PFS phase expresses itself near the F-A interface, whereas for low surface energy substrates the p- PFS phase dominates the film-substrate (F-S) interface. Using a number of spectroscopic and morphological analytical approaches combined with the contact angle measurements as well as thermodynamic modeling morphologies of acorn-shaped particles and their film formation are examined. These studies show that in an effort to create stable heterogeneous morphologies it is essential to provide desirable interfacial energies during polymerization and utilize monomers that exhibit similar phase transition temperature (Tg).

Introduction

As Mother Nature mastered formation of various heterogeneous entities that interactively and collectively are responsive to many biological functions, mimicking this behavior in a controllable fashion using synthetic materials has been quite challenging. One of the features that make polymer synthesis particularly exigent is how two chemically distinct phases can be affixed to form reproducible heterogeneous morphologies at nano and micro scales. Although recent advances in microfluidics,[1-4] where two distinct polymer solutions combined to form polymer/polymer interfaces of biphasic particles of dumbbell or ellipsoidal shapes, represent innovative examples of heterogeneous synthesis, one would like to control synthetic efforts by chemical means. Other approaches have employed templating,[5, 6] lithographic,[7, 8] and nanomolding[9] techniques in which polymeric phases were processed to create desired heterogeneous morphologies.

Although emulsion polymerization represents an attractive way of creating high molecular weight water dispersible particles, most synthetic efforts resulted in spherical homolithic shapes and compositions. Aside from core-shell morphologies[10] and various speculations regarding interfacial forces leading to heterogeneous morphologies,[11, 12] there are virtually only a few experimental protocols that resulted in stable water-dispersible non-spherical morphologies. Utilizing phospholipids as stabilizing agents, hollow polystyrene particles and cocklebur-shape non-spherical particles were obtained,[13, 14] but particularly challenging is combining monomers with low or high surface tension properties into one stable heterogeneous phase-separated particle. Previous studies[15-18] on fluoroacrylates and p-MMA/nBA colloidal particles showed

that fluoro-containing polymer shell can be produced around the p-MMA/nBA core, but the main limiting factor was that the amount of the fluoropolymer phase (up to 15% w/w) and limited control of heterogeneity.

These studies depart from the previous approaches and utilize pentafluorostyrene (PFS) as well as MMA and nBA monomers in a simple two-step synthetic process that generated acorn-shaped stable colloidal particles, where one side of the particle consists of the PFS phase, and its opposite counterpart is the p-MMA/nBA phase. The TEM images of these particles are illustrated in Figure VI-1, A, and for comparison Figure VI- 1, B shows a photograph of acorns.[19] Another uniqueness of these particles which will be explored in this study is their ability to form films with the surface energies dependent upon the surface energy of a substrate.

Experimental

MMA, nBA, PFS, and sodium dioctylsulfosuccinate (SDOSS) were purchased from Aldrich Chemical Co. Water soluble initiator 2,2'-Azobis[2-(2-imidazolin-2-yl)propane] dihydrochloride (VA-44) was purchased from Wako Pure Chemicals Ind. Ltd. Bio-Rad AG® 501-X8 cation-anion resin was purchased from Bio-Rad laboratories, Inc. and PTFE substrate was purchased from Electron Microscopy Sciences.

p-MMA/nBA (P_1) and p-nBA/PFS (P_2) primary colloidal solutions were synthesized using a semicontinuous process outlined elsewehere,[17, 20] and adapted for small-scale polymerization. The reaction flask was placed in a water bath set at 50°C, purged with N_2 gas, charged with 30 ml of DDI water under continuous stirring at 300 rpm. SDOSS surfactant was utilized and Table VI- 1 provides ratio of all dispersions prepared for the purpose of these studies. SDOSS was dissolved in water under high agitation followed by addition of monomers to produce a semi-stable pre-emulsion. The pre-emulsion was fed continuously over the period of 4 hrs while the initiator solution was added for 4.5 hrs. Upon completion of the initiator feed, polymerization was allowed to continue for another 10 hrs. After synthesis of first step P_1 and P_2 second step synthesis involved taking the primary particles P_1 and P_2 and copolymerizing MMA and nBA monomers on P_1, and nBA and PFS monomers on P_2, detailed composition is given in Table VI- 1. The particle size analysis was obtained using a Microtrac UPA 250 instrument. Morphologies of colloidal particles were determined using a Zeiss EM 109-transmission electron microscope (TEM) in which colloidal dispersions were diluted to a 10,000:1 vol. ratio (DDI H_2O: dispersions) and deposited on a formvar coated copper TEM grid (Ted Pella, Inc.).

Molecular weight was determined using gel permeation chromatography (GPC) system which consisted of a Waters Alliance 2695 Separation Module, a Waters 2410 interferometric refractometer, and two polymer labs hexafluoroisopropanol (PL HFIP) gel (Polymer Laboratories Inc.), with GPC columns connected in series. Freshly distilled HFIP serves as the mobile phase with a flow rate of 1.0 mL/min. Sample concentrations were 10-12 mg/mL in freshly distilled HFIP, with an injection volume of 50 micro liters. The detector signals were recorded using Empower 2 Chromatography Data Software (Waters Corporation) and molecular weight were determined relative to narrow molecular weight p-MMA standards and is listed in Table VI- 1. ^{13}C NMR spectra were acquired using the Varian Mercury 300 MHz NMR spectrometer. Typical measurement conditions involved a 90° pulse, 0 s relaxation delays, and the acquisition time of 1.815 s. The spectrum represents co-addition of 256 scans. In a typical experiment, 5% (w/v) of the copolymer was dissolved in deuteriated chloroform ($CDCl_3$).

The resin exchange experiments were performed on colloidal solutions containing P_1, P_2, P_1–S_2 and P_2-S_1 utilizing Bio-Rad AG® 501-X8 cation-anion resins from Bio-rad laboratories, Inc. In a beaker 2 gm of resin was taken and added 5 ml colloidal solution, let it stir overnight followed by filtering colloidal solutions from the resin. This procedure was repeated twice to completely remove ionic species from the system. After the resin exchange, colloidal solutions were diluted to a 1000:1 vol. ratio (DDI H_2O: dispersions), followed by coalescence on glass and PTFE substrates by drop deposition method to form a thin film of approximately 100 to 200 nm thickness.

Atomic force microscopy (AFM) measurements were conducted on a Nanoscope IIIa Dimension 3000 scanning probe microscope (Digital Instruments). A silicon probe with 125 μm long silicon cantilever, nominal force constant of 40 N/m and resonance frequency of 275 KHz were used in a tapping mode, allowing estimation of surface topography and roughness. Differential scanning calorimetry (DSC) measurements were performed on a TA Instruments Q Series DSC Q800 instrument, and the heating rate was 10°C/min from -20 to 200 °C.

Grazing angle attenuated total reflectance Fourier transform infrared (GATR FT-IR) spectroscopy measurements were conducted on the film-air (F-A) interfaces using a Bio-Rad FTS-6000 FT-IR single beam spectrometer at a 4 cm^{-1} resolution. The surfaces were analyzed using a 2 mm Ge crystal with a 65° angle maintaining constant contact pressure between the crystal and the specimens. All spectra were corrected for spectral distortions using software for the Urban-Huang algorithm.[21]

Static and dynamic contact angle measurements were conducted using a sessile drop technique using a ramè-hart goniometer coupled with DROPimage® data analysis software. 10μl drops of water were placed onto a flat surface and image of the drop was captured. Dynamic and receding contact angle were measured by using the tilting plate technique with a tilting degree of 35°. An average of 5 different measurements was taken and all the values were within ±2°. Surface energy was calculated utilizing the Fowkes et al.[22] and Owens-Wendt[23] method and measuring the contact angle between the sample surface and deionized water as well as the sample surface and methyl iodide.

Quantum mechanical semi-empirical calculations were conducted using Material Studio software (Accerlrys Inc., version 4.1). Computer modeling simulations

were performed using a classical (Newton) molecular dynamics theory combined with the COMPASS force field conditions. In the first step, we created an alternate polymeric unit of MMA and nBA consisting of twelve monomer units of each, followed by block copolymerization of fluoropolymer (two monomer units). In an effort to determine thermodynamic response of molecular segments, a 25 x 25 x 25 Å periodic unit cell was constructed at 298 K using eight polymeric chains of block copolymerized fluoropolymers with p-MMA/nBA units. After amorphous cell construction first the control parameter were number, volume, and temperature (NVT) (298 K, 25 ps dynamic time, 25000 number of steps, and frame output at every 1000 steps), and second step was to control number, pressure, temperature (NPT) (298K, 50 ps dynamic time, 50000 number of steps, and frame output at every 5000 steps) to determine the most favorable conformation of copolymer chains.

Results and Discussion

Synthesis of Acorn-Shaped Particles

To synthesize morphologies shown in Figure VI- 1, A that resemble acorn shapes illustrated in Figure VI- 1, B, a two-step emulsion polymerization reaction was conducted. The first step involved copolymerization of n-BA with PFS and nBA with MMA in two independent processes. As a result, two primary p-nBA/PFS and p-MMA/nBA particles designated as P_1 and P_2 listed in Table VI- 1 were produced. The second step involved taking P_1 and P_2 colloidal precursors and copolymerizing MMA/nBA on P_1 and nBA/PFS on P_2 particles in two separate synthetic batches. Newly formed species are designated as P_1-S_2 and P_2-S_1, and their feed compositions are listed in Table VI- 1. Figure VI- 2 illustrates the TEM images of P_1, P_2, P_1-S_2, and P_2-S_1 particle morphologies. As shown in Figure VI- 2A, the synthesis of p-nBA/PFS copolymers leads to uniform spherical colloidal particles with an average particle size of 75 nm. When the primary p-nBA/PFS (P_1) structure was further reacted by feeding p-MMA/nBA monomers, an acorn morphology shown in Figure VI- 2A' was obtained. The high electron density phase containing F-component exhibits significantly darker appearance whereas lighter areas are due to p-MMA/nBA phase. When p-MMA/nBA (P_2) was utilized as the seed, followed by the PFS and nBA monomer copolymerization, also acorn-shaped particle morphologies were obtained. This is shown in Figures VI-2, B and B'. Using TEM images illustrated in Figure VI- 2 we estimated an average particle size of the synthesized particles and compared with the results of the light scattering (LS) measurements which are shown in Figure VI- 3. The TEM and LS results are in good agreement, and the average particle size increases from 75 nm for P_1

to 105 nm for P_1-S_2 (Figure VI- 3, A), and from 95 nm for P_2 to 115 nm for P_2-S_1 (Figure VI- 3, B) compositions. The significance of the LS experiments is further amplified by measuring the particle size as a function of the reaction time during the second P_1-S_2 and P_2-S_1 polymerization stage. As shown in Figure VI- 3, A, unimodal distributions of particles during the second step synthesis for P_1-S_2 is observed, and the particle size increases as a function of time to level off at the later stages (Figure VI- 3, A'). Similar results are observed for P_2-S_1 colloidal dispersions, which are shown in Figure VI- 3, B and B'. These data also show that during the second stage of the polymerization monomer polymerizes on the primary particles and there is no secondary nucleation, thus retaining the monomodal distribution of the particle size during all the stages. The direct visual evidence that supports the above conclusions is shown in Figure VI-4, A-F for P_1-S_2 and A'-F' for P_2-S_1, which illustrates morphology changes detected by TEM as a function of time. As seen, TEM images were collected at various time intervals during polymerization by taking snapshots of aliquots. As polymerization proceeds, the primary P_1 seed particles, initially form an eye-ball like morphologies (Figure VI-4, B and C), followed by the formation of a moon-like (Figure VI-4, D and E) shapes. The final polymerization stages lead to acorn-shaped morphologies. The mirror image morphology evolution is obtained when the primary P_2 seeds are utilized, but the events begin with the low electron density seed that contains p-MMA/nBA copolymer, followed by the formation of P_2-S_1 particles. This is shown in Figure VI-4, A'-F' which illustrates TEM images of aliquots taken during the P_2-S_1 synthesis.

While the above data undeniably supports the formation of acorn morphologies, the ^{13}C NMR evidence of copolymer compositions of P_1, P_2, P_1-S_2, and P_2-S_1 copolymers, were collected and are shown in Figure VI- 5. For P_1 composition all structural components of nBA and PFS (Figure VI- 5, A) are detected and labeled. The second step resulting in P_1-S_2 compositions by copolymerization of MMA and nBA generates MMA resonances due to quaternary carbon (Trace A') at 48 ppm along with -0-CH_3 group at 55 ppm (Figure VI- 5, A'). Also, for P_1-S_2, structural carbons due to PFS and nBA are detected. Similarly for P_2 and P_2-S_1 compositions, all the structural components are observed, with the primary step containing p-MMA/nBA (Figure VI- 5, B) and upon the second step, the resonances due to PFS (Figure VI- 5, B') are detected at 118 and 130 to 150 ppm. ^{13}C-NMR data confirm the structural composition of P_1, P_2, P_1-S_2, and P_2-S_1. Although acorn-shape morphologies are observed, the main question is what are the driving forces behind the development of these morphologies. Taking into account the reactivity ratios calculated from the Q and e values of MMA, nBA, and PFS monomers,[24-26] MMA reactivity with respect to nBA is 2.46 whereas nBA against MMA is 0.31. In contrast, the nBA values against PFS is 0.44 and PFS with respect to nBA is 2.23. Thus, the reactivity ratio differences favor the formation of random copolymers. Also, the solubility parameters of the monomers in an aqueous environment (δ_{water} = 23.4 $(cal/cm^3)^{1/2}$)[24] favor the formation of MMA/nBA or nBA/PFS random copolymers under monomer starvation conditions (δ_{MMA} and δ_{nBA} = 8.8 $(cal/cm^3)^{1/2}$, δ_{PFS} = 8.2 $(cal/cm^3)^{1/2}$). While neither reactivity ratios nor solubility considerations suggest the formation of acorn morphologies, it should be pointed out that similar sequential synthetic steps have led to core-shell morphologies for high T_g

core and low T_g shell copolymerizations.[10, 27] Furthermore, when a low Tg polymer is polymerized first, followed by a high T_g monomer reactions, the phase inversion between the core and the shell occur.[10] In contrast, the P_1-S_2 and P_2-S_1 particles do not exhibit this behavior which is not related to solubilities and reactivity ratios. Let us thus measure the surface energies of P_1 (p-nBA/PFS) and P_2 (p-MMA/nBA) seeds. For that purpose we "disinfected" both dispersions by removing all ionic species using the resin exchange (Experimental Section) and such dispersions were allowed to coalesce. Using the Young's equation[24] ($W_A = \gamma_{LV}(1+\cos\theta)$; where γ_{LV}, γ_{SV} are liquid-vapor, solid-vapor interfacial tension, respectively, and θ is the contact angle), the polar (γ^p_{SV}) and dispersive (γ^d_{SV}) contributions to the surface energies were determined ($W_A = 2[\{\gamma^d_{LV} * \gamma^d_{SV}\}^{1/2} + \{\gamma^p_{LV} * \gamma^p_{SV}\}^{1/2}]$[22, 23] by measuring the contact angles of water and methyl iodide solvents. Table VI- 2 summarizes the results of these experiments. As seen, the values of interfacial tensions for P_1 and P_2 copolymers are 19.8 and 44.6 mN/m which indicate that the phase-separated domains within one particle are likely to occur due to substantial surface energy differences between the two phases. In contrast, for nBA and p-styrene (p-Sty) which form core-shell morphologies,[10] their respective surface energy values are 33.7 mN/m for p-nBA and 35 mN/m for p-Sty.[24]

Postponing temporarily the effect of the Tg and considering that the driving force for the acorn shape formation is the interfacial energy between the two phases, let us examine the morphologies illustrated in Figure VI-6: a - core-shell, b - inverted core-shell, c - hemisphere, and c'- acorn-shape. All phases exhibit the same volume and the values used to estimate the surface-to-volume ratios were taken from dimensions of the TEM images. The calculated surface-to-volume (S/V) ratios for each shape illustrate

that the acorn-shape exhibits the highest ratio of $29.13*10^{-4}$ nm^{-1} compared to $29.02*10^{-4}$ nm^{-1} for other morphologies illustrated in Figure VI-6. However, to estimate the most energetically favorable morphologies one also needs to take into account the contact between the phases which diminishes significantly from $91.02*10^3$ nm^2 to $33.55*10^3$ nm^2 for hemisphere and from $91.02*10^3$ nm^2 to $30.15*10^3$ nm^2 for acorn-shape morphologies. Thus, the contact area between the two phases is the lowest for acorn-shape morphologies, and thermodynamic simulations in which we used packing energy minimized polymer chains under 3D periodic boundary conditions (the details of the computational analysis are provided in the Experimental Section) predict very distinct phases of p-MMA/nBA and p-nBA/PFS copolymers. This is shown in Figure VI-7 showing phase separated particles within the unit cell, which is in agreement with the TEM and contact angle measurements.

In view of these considerations there is an aspect of the P_1-S_2 and P_2-S_1 morphologies: the shape retention. As indicated above, the surface interfacial energy difference between p-nBA and p-Sty favors their core-shell morphologies, but has an opposite effect on P_1-S_2 and P_2-S_1 formation. What favors core-shell phase inversion are significant differences between p-Sty and p-nBA Tg's. Specifically, for core-shell morphologies, the core exhibits a high Tg and the shell has low Tg polymer, such as shown in Figure VI-6, B. However, when a two phases such as P_1 and P_2 have similar Tg's and high enough with respect to the experimental conditions, both phases cannot easily flow, thus morphologies produced during the synthesis will be retained. As shown in the Figure VI-8, the Tg's of P_1 and P_2 are 20 and 16°C, thus their flow will be limited. This is schematically depicted in Figure VI-6, B (c/c').

In summary, polymerization process of acorn-shape particles can be described as follows. Upon the synthesis of P_1 or P_2 precursors with spherical morphologies and the sequential polymerization during the second step occurs on the precursors instead of the nucleation of new particles. Figure, 6 B summarizes the formation of morphologies during the second synthetic step for all the morphologies whereby to attain a minimum contact between the two phases acorn-shape is produced.

Film Formation

The formation of acorn shape colloidal particles provides an opportunity for self-assembly on substrates with various surface energies. The premise behind these experiments is to be able to create polymeric coatings that, depending upon the substrate surface energy, will result in hydrophobic or hydrophilic surfaces. For that reason we deposited approximately one particle thick films on PTFE ($\gamma = 18.5$ mN/m)[24] and glass ($\gamma = 70$ mN/m)[24] substrates. Upon coalescence of the particles, the water contact angle measurements were performed which are summarized in Table VI- 4. While the water contact angle for glass and PTFE substrates are 35° and 120°, respectively, static, advancing and receding contact angles for films coalesced on a glass substrate are 95°, 100° and 87°, respectively. In contrast, when the same films were allowed to coalesce on a PTFE substrate, the contact angles were reduced to 68°, 74°, and 62°, respectively. These data show preferential alignment of the acorn particles in such a way that the p-nBA/PFS rich phase is near the film-substrate (F-S) interface when the particles are coalesced on low surface tension substrates. In contrast, for films coalesced on higher surface tension substrates, the p-MMA/nBA rich phase is directed towards the F-S interface, while the p-nBA/PFS phase is oriented outward. These

observations are further supported by the AFM analysis shown in Figure VI- 9 which illustrates phase (A), height (A'), and 3-D (A") images of the coalesced films on a glass substrate. As seen, distinct p-nBA/PFS phase (light regions) is imbedded into a softer p-nBA/MMA matrix shown as darker regions. In contrast, when the same films are deposited on a PTFE substrate, significantly less distinguished particles are observed indicating higher degree of coalescence near the surface due to slightly lower Tg of the p-MMA/nBA phase.

In order to further justify a chemical makeup of the top surface layers, we also employed GATR FT-IR spectroscopy. Figure VI-10, Traces a and b, illustrate IR spectra recorded from the top surface of the films deposited on glass and PTFE substrates, respectively. For reference purposes, Traces c, d, and e are the spectra of PFS, nBA, and MMA. Comparisons of Traces a and b in the range of 3050 to 2850 cm^{-1} clearly illustrates increased intensities of the 2965, 2935, and 2875 cm^{-1} bands due to CH_2 stretching vibrations of the p-MMA/nBA component. However, in the 1500 to 1100 cm^{-1} region, for films coalesced on a glass substrate, the intensities of the 1500 and 1520 cm^{-1} bands due to PFS increase, whereas the 1165 and 1145 cm^{-1} bands due to C-O-C stretching vibrations of p-nBA and p-MMA are reduced. Again, these data indicate self-assembly of the acorn particles driven by the surface tension of the substrate which appear to be a competing process between the surface energies of the acorn-shaped particles and the surface of a substrate. A schematic diagram depicting this process for high and low energies of substrates is shown in Figure VI-11.

Conclusions

Utilizing a two-step emulsion polymerization process these studies show for the first time the synthesis of particles consisting of the p-MMA/nBA and p-nBA/PFS distinct phases within one particle. Unique acorn-shape colloidal particles were obtained which consists of fluorinated and non-fluorinated phase-separated entities. The colloidal particles self-assembly on surfaces, and depending upon the surface energy of the substrate, are able to create hydrophobic or hydrophilic surfaces.

Table VI-1. Composition, Particle Size, and Molecular Weight of P_1, P_2, P_1-S_2, And P_2-S_1 Colloidal Dispersions Synthesized With Different Compositions.

Composition (w/w%)	p-nBA/PFS (P_1)	p-MMA/nBA (P_2)	p-nBA/PFS p-MMA/nBA (P_1-S_2)	p-MMA/nBA p-nBA/PFS (P_2-S_1)
p-nBA/PFS seed (P_1)	-	-	50	-
p-MMA/nBA seed (P_2)	-	-	-	50
DDI	54.8	54.8	27.4	27.4
MMA	-	21.9	10.9	-
nBA	21.9	21.9	10.9	10.9
PFS	21.9	-	-	10.9
SDOSS	1.32	1.32	0.66	0.66
VA-44	0.08	0.08	0.04	0.04
Particle Size (nm)	75	104	95	115
Molecular Weight (gm/mol)	$9.1 * 10^4$	$7.2 * 10^4$	$12.8 * 10^4$	$13.2 * 10^4$

Table VI-2. Contact Angle and Surface Energy of Copolymer Films of P_1 and P_2 Containing Films after Resin Exchange.

Copolymer	Static Water Contact Angle (°)	Static Methyl Iodide Contact Angle (°)	γ (mN/m)	γ^d_{sv} (mN/m)	γ^p_{sv} (mN/m)
p-MMA/BA	65	54	44.6	32.0	12.6
p-BA/PFS	103	78	19.8	18.5	1.3

Table VI-3. Water Contact Angle of Glass and PTFE Substrate, and Static, Advancing, and Receding Water Contact Angle on Glass and PTFE Substrate after Film Deposition.

Substrate	Water Contact Angle (°)	Static Water Contact Angle (°) after Coating with Acorn Particles	Advancing Water Contact Angle (°) after Coating with Acorn Particles	Receeding Water Contact Angle (°) after Coating with Acorn Particles
Glass	35	95	100	89
PTFE	120	68	74	62

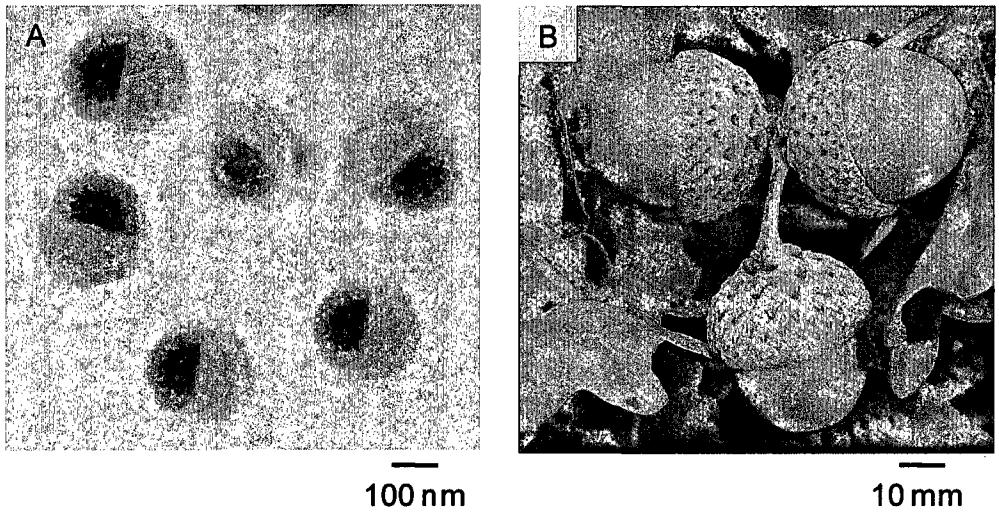

Figure VI-1. TEM micrograph of acorn-shaped morphology of synthesized colloidal particles (A) and optical image of acorns from nature[19] (B).

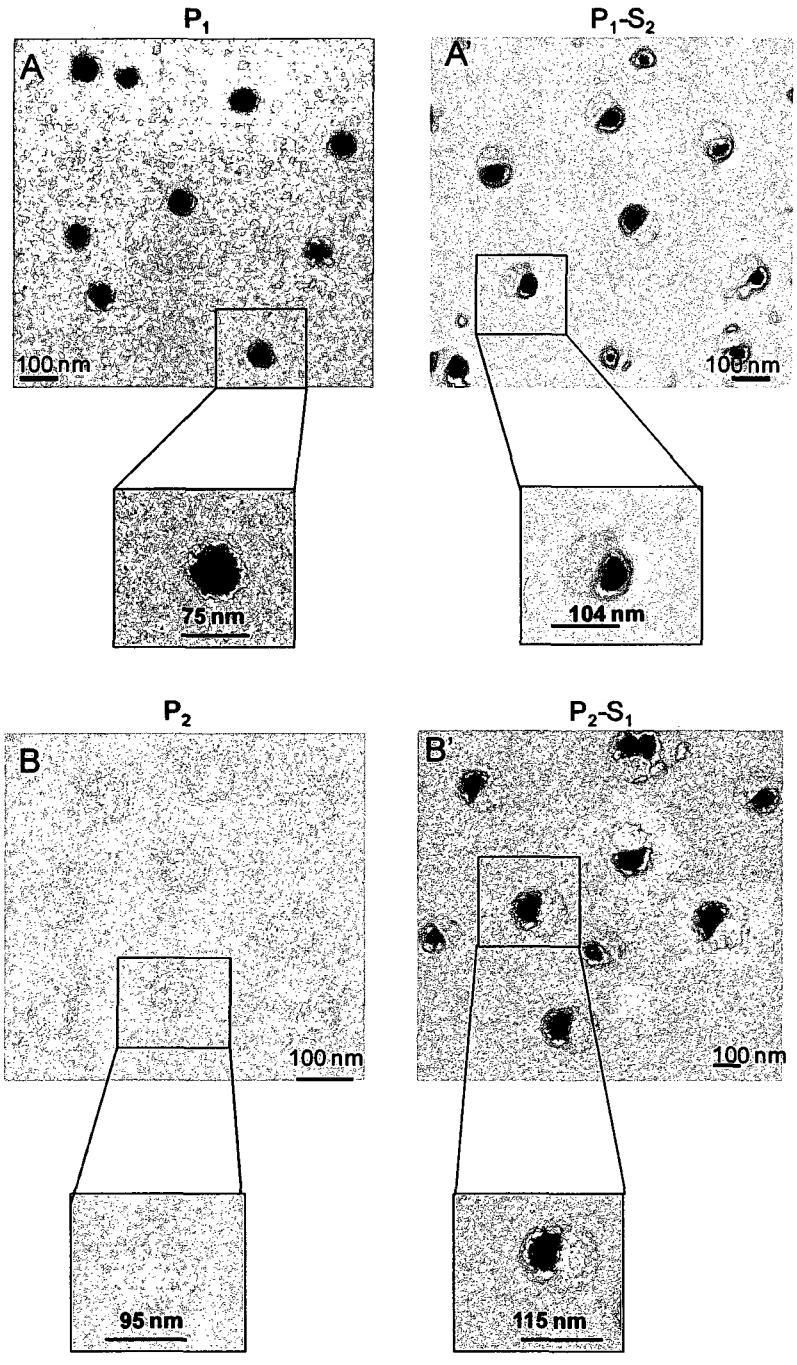

Figure VI-2. TEM micrographs of colloidal particles containing (A) p-nBA/PFS (P_1); (A') p-nBA/PFS and p-MMA/nBA (P_1-S_2); (C) p-MMA/nBA (P_2); and (D) p-MMA/nBA and p-nBA/PFS (P_2-S_1).

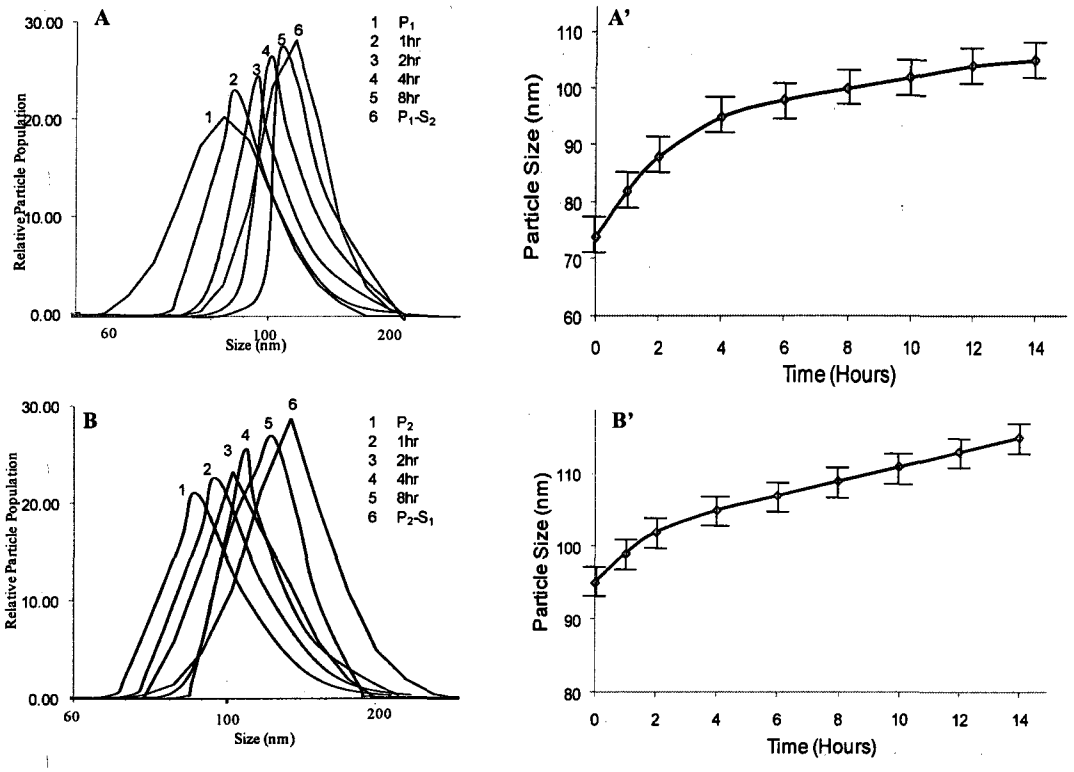

Figure VI-3. Particle size and particle size distribution curve for (A)- Particle size distribution as a function of reaction time for P_1-S_2 synthesis; (A')- Particle size plotted as a function of time during second step polymerization of P_1- S_2; (B)- Particle size distribution as a function of reaction time for P_2-S_1 synthesis; and (B')- Particle size plotted as a function of time during second step polymerization of P_2- S_1.

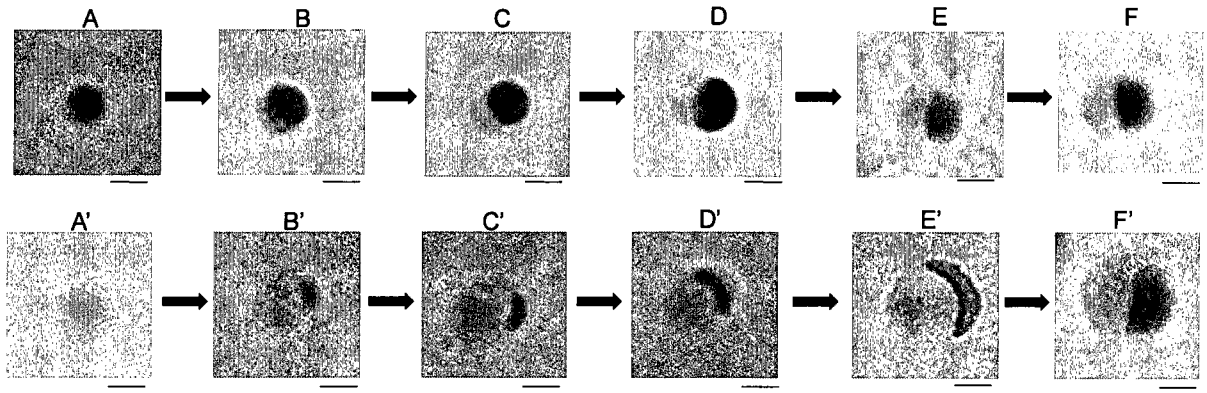

Figure VI-4. TEM micrographs of P_1 (A) and P_2 (A') seed followed by second step polymerization at intervals: (B and B') 1 hr, (C and C') 2hr, (D and D') 4hr, (E and E') 8 hrs, (F) P_1-S_2, and (F') P_2-S_1; the scale on the images is 50 nm.

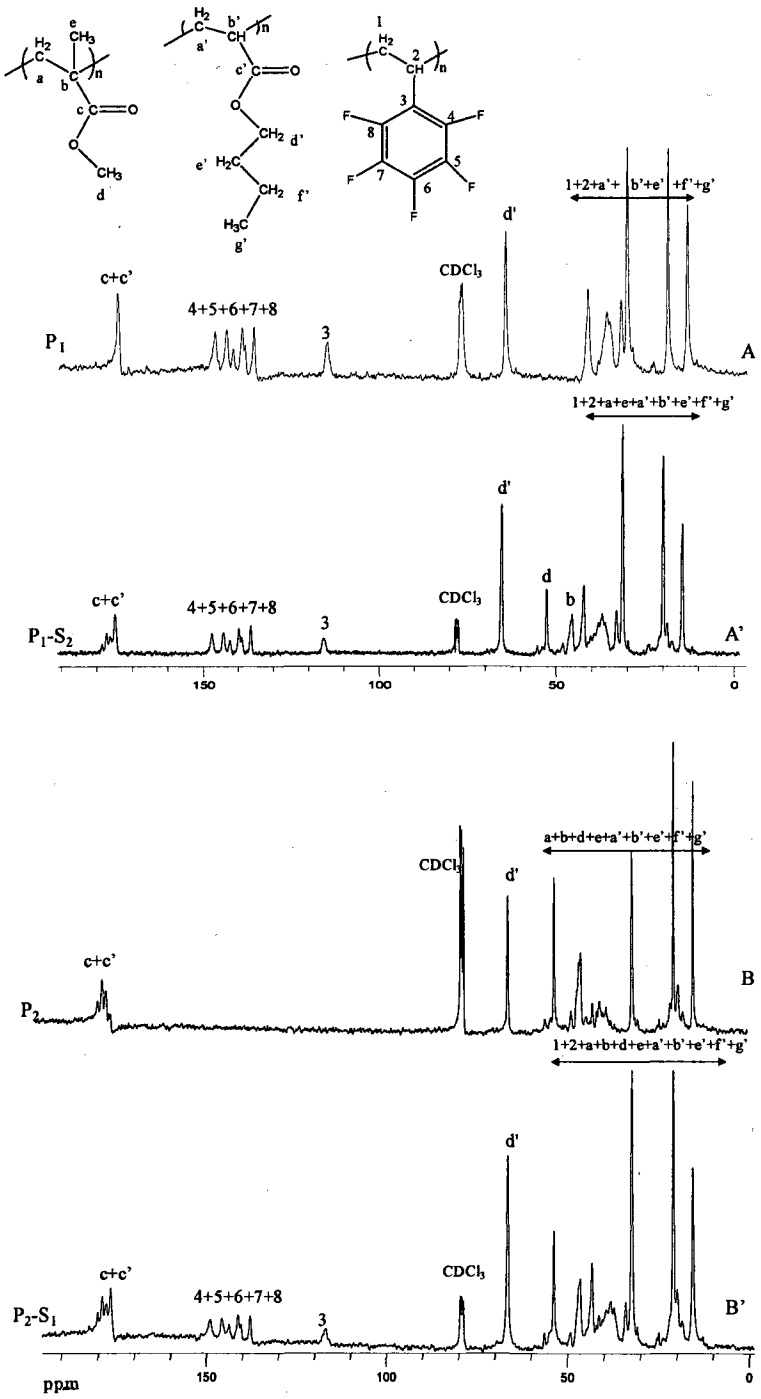

Figure VI-5. ^{13}C NMR spectra of: (A) p-nBA/PFS (P_1); (A') p-nBA/PFS and p-MMA/nBA (P_1-S_2); (B) p-MMA/nBA (P_2); and (B') p-MMA/nBA and p-nBA/PFS (P_2-S_1) colloidal dispersions.

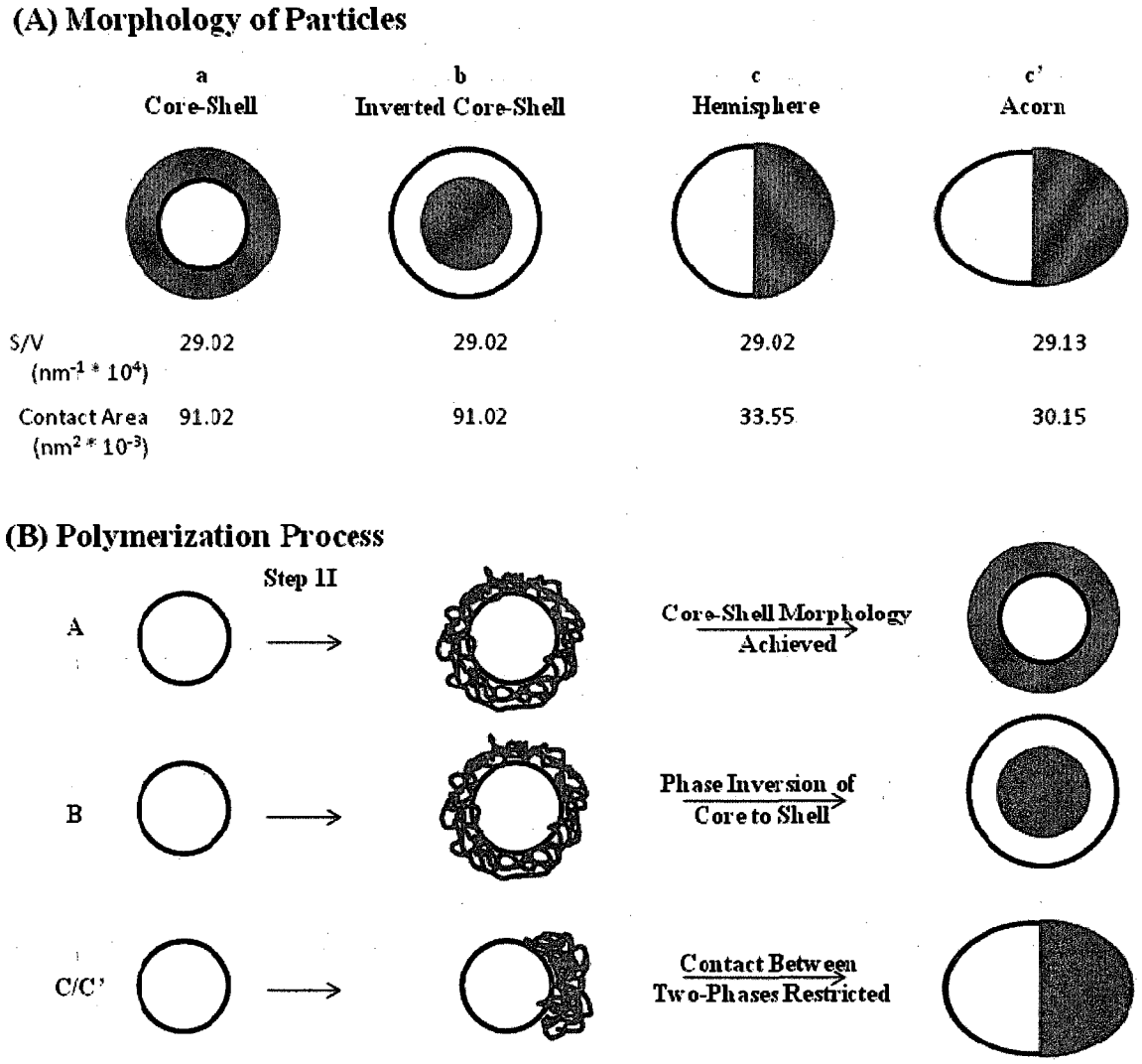

Figure VI-6. Schematic representation of (A) various possible morphologies, surface to volume ratio (S/V), and contact area and (B) Polymerization process for different morphologies.

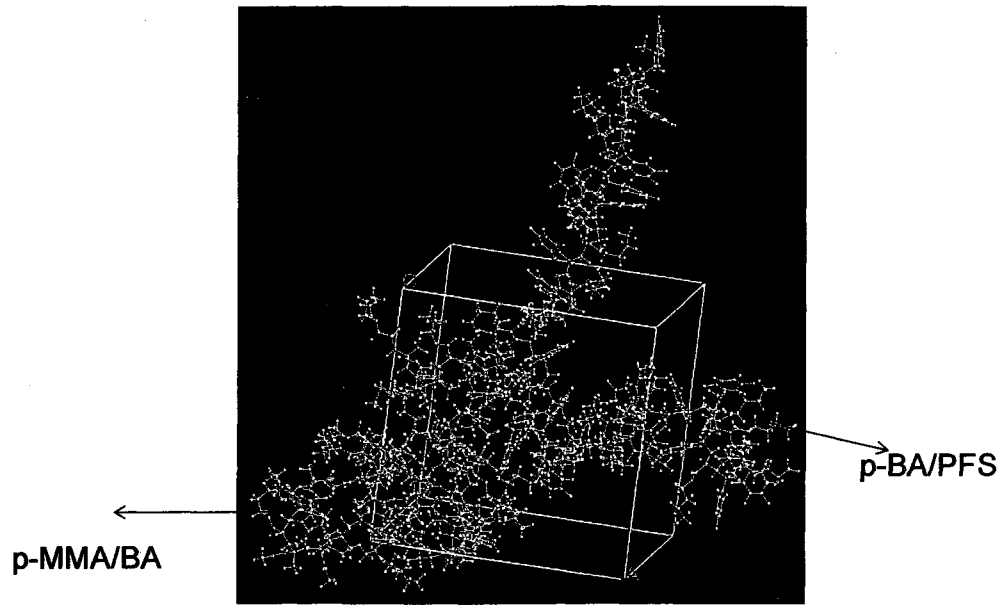

Figure VI-7. Results of computational simulations leading to conformational changes for P_1-S_2 or P_2-S_1 copolymer structure.

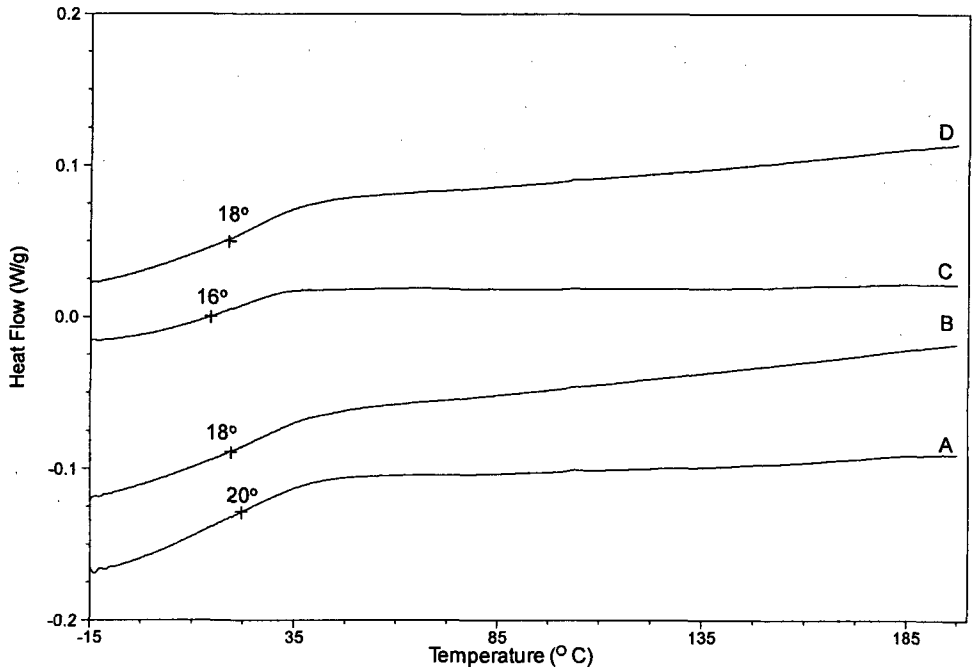

Figure VI-8. Differential scanning calorimetry (DSC) of (A) P_1, (B) P_1-S_2, (C) P_2, and (D) P_2-S_1 copolymer films. The Tg values are acquired at mid point.

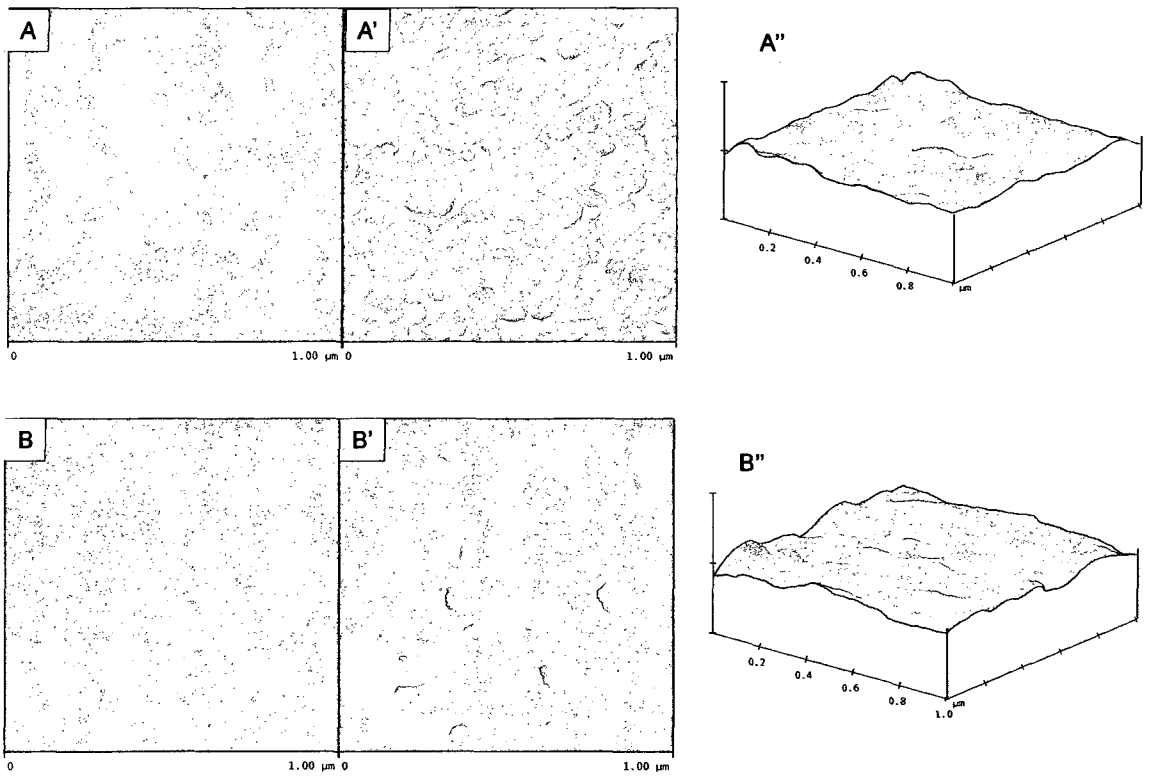

Figure VI-9. AFM phase images (A, B), height images (A', B'), and 3-D images of acorn particles coalesced on glass (A) and PTFE (B) substrate.

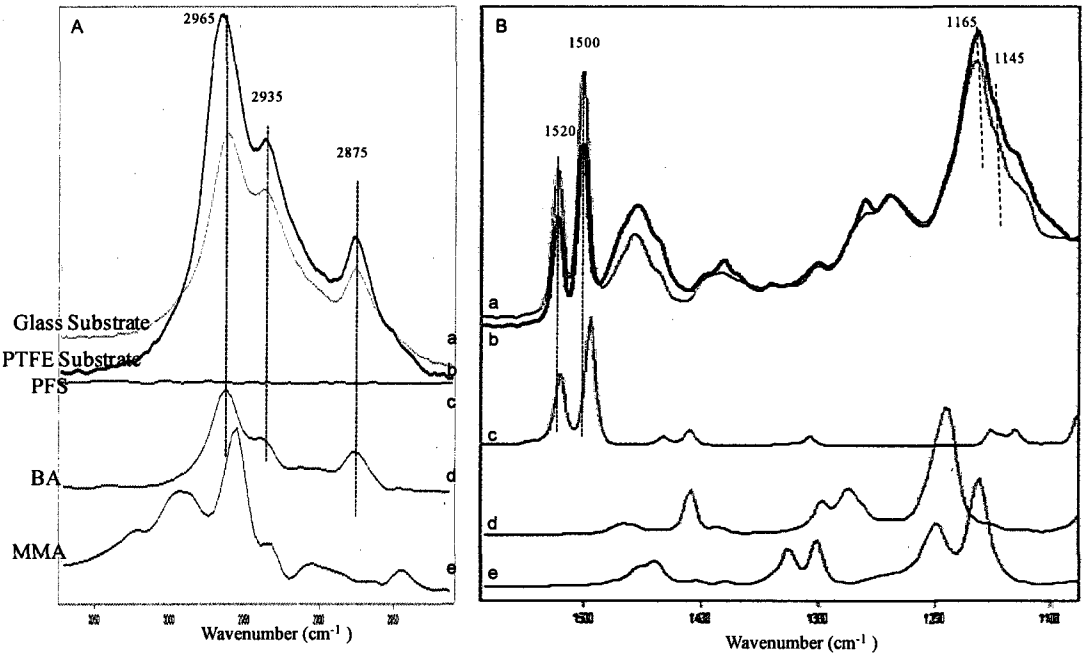

Figure VI-10. GATR-FTIR spectra recorded from the F-A interface in the 3050-2850 cm^{-1} (A) and 1550-1100 cm^{-1} region of acorn particles coalesced on glass (Trace a) and PTFE (Trace b) substrate; and IR spectrum of (c) PFS, (d) nBA, and (c) MMA monomers for reference purposes.

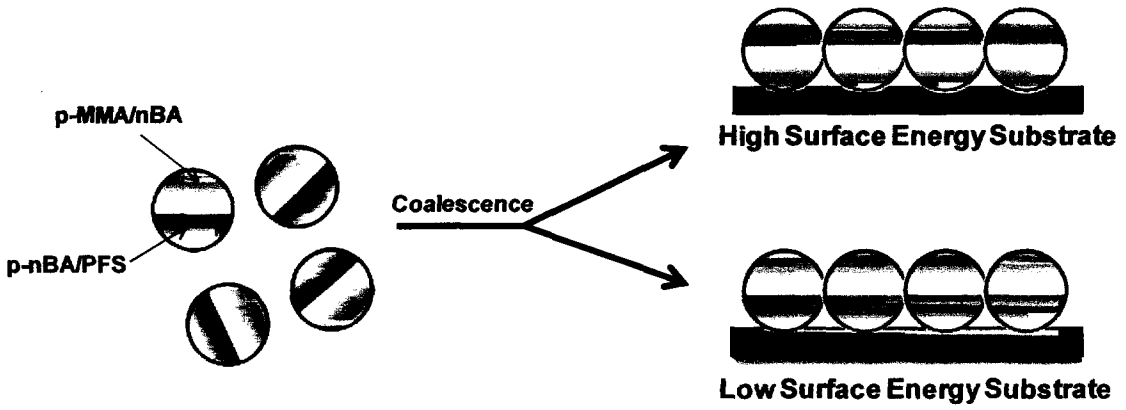

Figure VI-11. Schematic representation of orientation of acorn-shaped colloidal particles on high and low surface energy substrates.

References

1. Dendukuri, D.; Hatton, T. A.; Doyle, P. S. *Langmuir* **2007,** 23, 4669.

2. Xu, S.; Nie, Z.; Seo, M.; Lewis, P.; Kumacheva, E.; Stone, H. A.; Garstecki, P.; Weibel, D. B.; Gitlin, I.; Whitesides, G. M. *Angew. Chem., Int. Ed.* **2005,** 44, 724.

3. Roh, K.-H.; Martin, D. C.; Lahann, J. *Nature Materials* **2005,** 4, 759.

4. Nie, Z.; Xu, S.; Seo, M.; Lewis, P. C.; Kumacheva, E. *J. Am. Chem. Soc.* **2005,** 127, 8058.

5. Moon, S. I.; McCarthy, T. J. *Macromolecules* **2003,** 36, 4253.

6. Park, S.; Lim, J.-H.; Chung, S.-W.; Mirkin, C. A. *Science* **2004,** 303, 348.

7. Badaire, S.; Cottin-Bizonne, C.; Woody, J. W.; Yang, A.; Stroock, A. D. *J. Am. Chem. Soc.* **2007,** 129, 40.

8. Hernandez, C. J.; Mason, T. G. *J. Phys. Chem.* **2007,** 111, 4477.

9. Kelly, J.; DeSimone, J. M. *J. Am. Chem. Soc.* **2008,** 130, 5438.

10. Zhao, Y.; Urban, M. W. *Macromolecules* **2000,** 33, 7573.

11. Duda, Y.; Vazquez, F. *Langmuir* **2005,** 21, 1096.

12. Torza, S.; Mason, S. G. *J. Colloid Interface Sci.* **1970,** 33, 67.

13. Lestage, D. J.; Urban, M. W. *Langmuir* **2005,** 21, 4266.

14. Lestage, D. J.; Urban, M. W. *Langmuir* **2005,** 21, 10253.

15. Misra, A.; Jarrett, W. L.; Urban, M. W. *Macromolecules* **2007,** 40, 6190.

16. Singh, A.; Dreher, W. R.; Urban, M. W. *Langmuir* **2006,** 22, 524.

17. Dreher, W. R.; Jarrett, W. L.; Urban, M. W. *Macromolecules* **2005,** 38, 2205.

18. Dreher, W. R.; Singh, A.; Urban, M. W. *Macromolecules* **2005,** 38, 4666.

19. Finlay, J. A.; Krishnan, S.; Callow, M. E.; Callow, J. A.; Dong, R.; Asgill, N.; Wong, K.; Kramer, E. J.; Ober, C. K. *Langmuir* **2008,** 24, 503.

20. Davis, S. D.; Hadgraft, J.; Palin, K. J., *Encyclopedia of Emulsion Technology*. Marcel Dekker: New York, 1985; Vol. 2.

21. Urban, M. W., *Attenuated Total Reflectance Spectroscopy of Polymers - Theory and Practise*. 1989; Vol. Vol. 2.

22. Fowkes, F. M.; Kaczinski, M. B.; Dwight, D. W. *Langmuir* **1991,** 7, 2464.

23. Owens, D. K.; Wendt, R. C. *J. Appl. Polym. Sci.* **1969,** 13, 1741.

24. Brandrup, J.; Immergut, E. H., *Polymer Handbook*. 4th ed.; Johnwiley & Sons: New York, 1966.

25. Odian, G., *Principles of Polymerization*. John Wiley & Sons: New York, 2004.

26. Granville, A. M.; Boyes, S. G.; Akgun, B.; Foster, M. D.; Brittain, W. J. *Macromolecules* **2004,** 37, 2790.

27. Lestage, D. J.; Urban, M. W. *Langmuir* **2004,** 20, 6443.

CHAPTER VII

SELF-HEALING POLYMERIC COATINGS OBTAINED FROM PHOSPHOLIPID-ASSISTED COLLOIDAL DISPERSIONS

Abstract

Poly(methyl methacrylate/n-butyl acrylate/heptadecafluorodecyl methacrylate) (p-MMA/nBA/FMA) colloidal dispersions containing 15 % w/w of pFMA were synthesized in the presence of biologically active phospholipid (PL) 1,2-dilauroyl-sn-glycero-3-phosphocholine (DLPC) and ionic surfactants, sodium dodecyl sulfate (SDS) and phosphoric acid bis(tridecafluoro-octyl) ester ammonium salt (FSP). Upon coalescence, the particles form films which exhibit surface self-healing properties. Such films, upon mechanical damage to form a 30 x 3 (length x depth) μm scratch shown in photograph (A), self-heal within a 30 min. timeframe (B). This behavior is attributed to multi-layered skin-like stratification of the colloidal particle components. Using internal reflection infrared imaging (IRIRI) and mechanical nano-indentation these studies demonstrate that upon mechanical damage, the wound area is filled with the low Tg p-MMA/nBA component. This process is driven by the surface tension difference of vertically stratified p-FMA and p-MMA/nBA bi-layer film components, resulting in p-MMA/nBA scar in the wound area, thus resembling the skin healing process.

Introduction

The unique ability of biological systems to self-heal inspired novel ideas and avenues of research in an attempt to develop materials that exhibit remendable characteristics mimicking Mother Nature. However, mimicking integrated and sophisticated nano or microstructures, and mechanisms leading to self-repairing processes, are intrinsically challenging and complex. Among notable attempts, the fusion of broken surfaces with a 57% recovery after heating was identified as one of the approaches,[1] whereas a two phase system in which a polymer matrix served as a host to another phase on which upon heating, diffused to the damaged area and repaired the damage [2,3] is another example. A biological "bleeding" approach was also examined which involves imbedding microcapsules[4] or hollow fibers[5,6] containing reactive components, which upon rapture, release reactive monomers and the catalyst, thus restoring the matrix within the damage area through crosslinking reactions. Another studies explored a tri-layer films, [7] which consisted of a liquid layer sandwiched between two elastic layers. Most recently, the use of hydrogen-bonding to form chains and cross-links were proposed which were designed for creating self-healing materials.[8] In view of these advances and the recent perspective,[9] which eloquently outlined advantages and disadvantages of these and other extensionally related self-healing mechanisms, the importance of compartmentalization and multi-layered stratified skin-like features of self-healing inspired these studies.

These studies report the development of self-healing fluorine-containing polymeric coatings which were produced by coalescence of aqueous colloidal dispersions of poly-methylmethacrylate/n-butyl acrylate/fluoromethacrylate (p-

MMA/nBA/FMA) colloidal particles containing 15 w/w% of phase-separated pFMA phase. While the synthesis and film formation of these dispersions were described in Chapter II,[10] the presence of biologically active phospholipids (PL), such as 1,2-dilauroyl-sn-glycero-3-phosphocholine (DLPC), facilitated otherwise difficult to obtain copolymerization process that resulted in non-spherical particles.[10,11] The interior of the particles consists of p-MMA/nBA random copolymer, whereas the exterior is decorated by the p-FMA homopolymer phase. During the synthesis of these species PLs serve as "phase transport vehicle" for fluoromonomer to diffuse to the polymerization site, thus allowing copolymerization on the surface of p-MMA/nBA particles.[10] While these aqueous dispersions exhibit unique non-spherical morphologies, the most intriguing feature is their film formation as well as remendable surface characteristics. Atomic force microscopy (AFM) as well as internal reflection infrared imaging (IRIRI) experiments revealed that these particles coalescence to form vertically stratified films in which the pFMA component phase separates near the film-air (F-A) interface, and the p-MMA/nBA phase resides near the film-substrate (F-S) interface.[10] As a result, their interfacial properties are significantly different as manifested by low values of static and kinetic coefficients of friction at the F-A interface (0.145 and 0.042, respectively). These values are significantly lower compared to that of p-MMA/nBA films (0.78 and 0.38, respectively) and compare favorably with polytetrafluoroethylene (PTFE) (0.2 and 0.04, respectively).[12]

Experimental

Experimental details regarding preparation and characterization of colloidal dispersions and their films are described in Chapter II.[1, 2] Colloidal particle solutions were allowed to coalesce on a polyvinyl chloride (PVC) substrate for 72 hrs in a controlled environment at 23 °C temperature and 60% relative humidity to form approximately 10μm thick films. Optical micrographs of film surfaces were acquired using a Nikon Optical biological microscope. Internal reflection infrared imaging (IRIRI) experiments were conducted on a Varian Stingray system. This system consists of a Bio-Rad FTS 6000 spectrometer, a UMA 500 microscope, an Image IR focal plane array (FPA) image detector, and a semispherical germanium IRE. IRIR images were collected using the following spectral acquisition parameters: under sampling ratio 2, step-scan speed 5 Hz, and spectral resolution 8 cm^{-1}. The use of a Ge crystal in contact with the analyzed surface allows spatial resolution in the range of 1 μm.[3] In a typical experiment, spectral data set acquisition time was 2 minutes and image processing was performed using ENVI software (The Environment for Visualizing Images, Research Systems, Inc.) version 3.5. When appropriate, baseline correction algorithms were applied to compensate for baseline deviations which was accomplished by built-in application software supplied by GRAMS/A1 v 7.02 (Galactic Ind.).

Nano-indentation experiments were performed on triboindenter (Hysitron, Minneapolis, MN) operated with a three-sided diamond (Berkovich type) tip calibrated on a fused silica. The experiments were performed under a closed loop with load control using a compliance method, in which the force displacement curves were obtained during loading and unloading cycles. In a typical experiment, as the indenter

was pressed into the surface, the displacement was recorded continuously as a function of the applied load at the loading rate of 20 μN/s, whereas unloading rate was maintained at 20, 10, 5, 1, and 0.5μN/s with a 10 s hold time at the maximum force of 200μN. In addition, the load displacement curve with the loading and unloading rates of 20 μN/s and 1μN/s, respectively was performed after 2 hrs on the same spot. Table S-1 summarizes experimental conditions.

Results and Discussions

As noted earlier, coalescence of these colloidal dispersions results in vertical stratification of p-FMA and p-MMA/nBA components, [10] and this communication reports the ability of such stratified films to self-repair upon surface mechanical damage. In an effort to examine this feature we created a 30 (width) x 3 (deep) μm scratch illustrated in Figure VII-1, A. After 30 min., which is shown in Figure VII-1, B, the damage disappears and the surface becomes smooth again, notably containing a small scar. The Supplemental Documents show the video recorded during the self-healing process. To determine the origin of this phenomenon IRIRI with spatial resolution of 1μ[13] was performed on p-MMA/nBA/FMA films before and after the damage at various time intervals of the recovery process. Since the top surface layer consists of p-FMA phase, we monitored the band at 1203 cm^{-1} due to C-F stretching vibrations before and after the damage and during the recovery. Figure VII-2, Images A-D, illustrates IRIR images recorded from the F-A interface recorded at the area of damage. While Image A was collected before the damage, Images B, C, and D were collected during the recovery over a 30 min. period. As seen in Images A, which is consistent with the previous studies, heterogeneous distribution of the p-FMA (Red area) and p-MMA/nBA (Blue area) phases (depth of penetration of IR is 0.7μ) is observed. This is confirmed by the IR spectra recorded from areas 1 and 2 at various locations of the damaged area. After creating the damage (Figure VII-2, B) the 1203 cm^{-1} band reduces its intensity, while the bands due to MMA at 1145 cm^{-1} due to C-O-C stretching and the 1165 cm^{-1} due to C-O-C stretching modes of n-BA increase. These data indicate the presence of p-MMA/nBA matrix in the damaged area which during the 30 min recovery period

(Figure VII-2-1, C, D) becomes the major component of the surface. This is also confirmed by the 1165 and 1145 cm^{-1} bands which increase in intensity during the recovery. Furthermore, the presence of the 1300 and 1265 cm^{-1} bands due to DLPC and p-MMA/nBA associations [14] indicate that DLPC also participates in the recovery. Similar observations were made for the 1078 cm^{-1} band due to S-O stretching vibrations of sodium dodecyl sulfate (SDS) in the same areas, thus indicating that the damage area is filled by the low Tg p-MMA/nBA component and the dispersing agents utilized in the synthesis of p-MMA//nBA/FMA colloidal particles. To illustrate spectroscopic changes before and after the damage we averaged all IR spectra collected from a 30x30μm area (average of 900 IR spectra) and the resulting IR spectra are shown in Figure VII-2-2. As seen, before the damage, a strong band at 1203 cm^{-1} band due to p-FMA along with 1145 and 1165 cm^{-1} bands due to MMA and nBA dominate the region. However, as self-healing occurs, the p-FMA band disappears and p-MMA/nBA bands dominate the spectral region. At the same time, the bands at 1265 and 1300 cm^{-1} bands due to DLPC-p-MMA/nBA associations are detected. While these experiments show that the wound area is filled with the p-MMA/nBA phase, if this is indeed the case, mechanical properties should be affected.

In order to determine composition of the wound and establish self-healing mechanisms we conducted nano-indentation experiments in which we examined the % of polymer recovery resulting from controlled force application and its release as a function of time. The % recovery is determined by rationing of the recovered depth of nano-indentation penetration to the initial displacement at a given force. Figure VII-3 illustrates the force plotted as a function of nano-indentation displacement as a function

of loading/unloading force rates, thus allowing determination of the % recovery upon the damage. Initially, a 200 μN contact force was applied to the surface of p-MMA/nBA/FMA film at the rate of 20 μN/s (Figure VII-3, Curve A, 1-2), which was held for 10 sec (Curve 2-3), and released with the unloading force rate of 1 μN/s (Curve 3-4). When the force is applied (Curve 1-2), the tip displacement at the p-MMA/nBA/FMA surface is 2.0 μm. Upon holding it, the loading force at 200 μN is retained for 10s (Curve 2-3), the tip displacement is increased to 2.4 μm. Upon releasing the force, while sensing the surface recovery, the % recovery is 71% (Curve 3-4). Thus, during 220 s time frame p-MMA/nBA/FMA % recovery was 71%.

As IRIRI measurements showed, the area of recovery consists primarily of p-MMA/nBA phase. If this is indeed the case, nano-indentation experiment conducted on the same area that was shown in Figure VII-3, Curve A after 2 hrs of recovery time should result in the same force-displacement curves as for p-MMA/nBA. The force vs Displacement curve is shown in Figure VII-3, Curve B. As seen during the hold time (Curve 2^1-3^1), the displacement increases from 2.42 μ (point 3) to 2.53 μ (point 3^1), thus indicating that the surface at the recovery area contains elastic component. Also, upon unloading the force, the recovery point for both measurements is the same, as illustrated by the same ending point at 0.7 μm (point 4). Since the depth of penetration during indentation increased, but the recovery point is same, the % recovery increases from 71% to 75% during second run. These results indicate that there is a change in the surface composition after the damaged area by the nano-indentation has been allowed to recover after the first run (Curve A).

The results of experiments conducted on p-MMA/nBA control films are shown in Figure VII-3, Curves C and D. As seen during the force loading (Curve 1-2^2), hold time (Curve 1-3^2), and unloading (Curve 1-4) in the initial run and after 2hrs are same. A comparision of the second run on p-MMA/nBA/FMA films (Curve B) approaches towards the p-MMA/nBA control which indeed shows that the p-MMA/nBA phase provides self-healing component during the recovery.

Both optical microscopy and video of the recovery process shown in the Supplement Documents illustrate that the recovery is a transient effect. For that reason, nano-indentation experiments were performed at various unloading force rates in order to determine transient effects of recovery. Figure VII-4-1 shows the force vs displacement curves for p-MMA/nBA/FMA films with 200μN loading force at the rate of 20 μN/s (Figure VII-4-1, Curve 1-2), hold time of 10 s (Curve 2-3), and with the unloading rates of 20, 10, 5, 1, and 0.5 μN/s. This is shown in Figure VII-4-1, Curves A (3-4), B (3-4^1), C (3-4^2), D (3-4^3), and E (3-4^4). Upon releasing the load, while sensing the surface recovery, the % recovery for 20μN/s is 56% (Curve 3-4), for 10μN/s is 62% (Curve 3-4^1), for 5μN/s is 68% (Curve 3-4^2), for 1μN/s is 71% (Curve 3-4^3) and for 0.5μN/s is 75.5% (Curve 3^1-4^4). Similar control experiments were conducted on p-MMA/nBA films and results are shown in Figure VII-4-2. First 200μN loading force at the rate of 20 μN/s (Figure VII-4-2, Curve 1-2) was applied; hold time of 10 s (Curve 2-3). Upon releasing the force, while sensing the surface recovery (line 3-4), the % recovery for 20μN/s is 44%, for 10 μN/s is 52% (line 3-4^1), for 5μN/s is 61% (line 3-4^2), for 1μN/s is 75% (line 3-4^3) and for 0.5μN/s is 77% (line 3-4^4). It should be noted here that for p-MMA/nBA/FMA % recovery is more at 20, 10, and 5 μN/s unloading rate

compare to p-MMA/nBA films. Thus p-MMA/nBA/FMA films heal faster compare to p-MMA/nBA films.

In summary, these experiments show that upon damage of stratified p-MMA/nBA/FMA films the wound area is filled with the low Tg p-MMA/nBA component. To illustrate the sequence of events based on the experimental evidence discussed above Figure 5 was constructed and illustrates a schematic diagram of the mending process. As we recall, this is vertically self-stratified film and the F-A interface consists of the p-FMA phase with the Tg of 172°C, whereas the F-S interface is the pMMA/n-BA copolymer (Tg=10°C) and its minimum film formation temperature (MFFT) is 14°C. The $Tg_{p\text{-}MMA/nBA}$ – FMMT difference facilitates particle coalescence at 23°C, the temperature at which the coalescence was conducted. It should be noted that the choice of 1,2-dilauroyl-sn-glycero-3-phosphocholine/sodium dodecyl sulfate (DLPC) as the bioactive dispersing agent was dictated by the fact that combining this PL with SDS/ phosphoric acid bis(tridecafluoro-octyl) ester ammonium salt (FSP) surfactants results in the reduction of the overall surface tension of an aqueous phase from 72 mN/m to about 1-5 mN/m,[15,16] thus facilitating the synthesis of non-spherical particles. After coalescence, the dispersing agents occupy interfacial regions between the lower (p-FMA) and higher (p-MMA/n-BA) surface tension stratified layers. When the p-FMA phase is mechanically damaged, such as shown in Figure VII-5, C-1, DLPC/SDS/FSP species residing at the p-FMA and p-MMA/nBA interfacial regions, in order to compensate for an access of the interfacial energy, diffuse to the damaged area (Figure VII-5, C-2) enhancing the flow of the low Tg pMMA/nBA phase into the damaged area (Figure VII-5, C-3). As a consequence, the damaged area is filled

(Figure VII-5, C-4) due to the ability to flow of the p-MMA/n-BA phase (Tg < MFFT). This self-healing behavior illustrates the importance of stratification and compartmentalization with multi-layered features which appear to be the key features in designing remendable polymeric films.

Table VII-1. Maximum loading rate, unloading rate, hold time, and total time for p-MMA/nBA/FMA and p-MMA/nBA films during nano-indentation experiments.

Curve Description	Loading Rate (μN/s)	Unloading rate (μN/s)	Hold Time (s)	Total time (s)
A	20	20	10	30
B	20	10	10	40
C	20	5	10	60
D	20	1	10	220
E	20	0.5	10	420

Table VII-2. Reduced modulus and hardness of the p-MMA/nBA/FMA, p-MMA/nBA/FMA; recovery time 2hrs, p-MMA/nBA, and p-MMA/nBA; recovery time 2hrs.

Sample	Reduced Modulus (MPa)	Hardness (MPa)
p-MMA/nBA/FMA	17.4	3.45
p-MMA/nBA/FMA; recovery time: 2 hrs	16.1	3.2
p-MMA/nBA	15.61	3.05
p-MMA/nBA; recovery time: 2 hrs	15.48	2.95

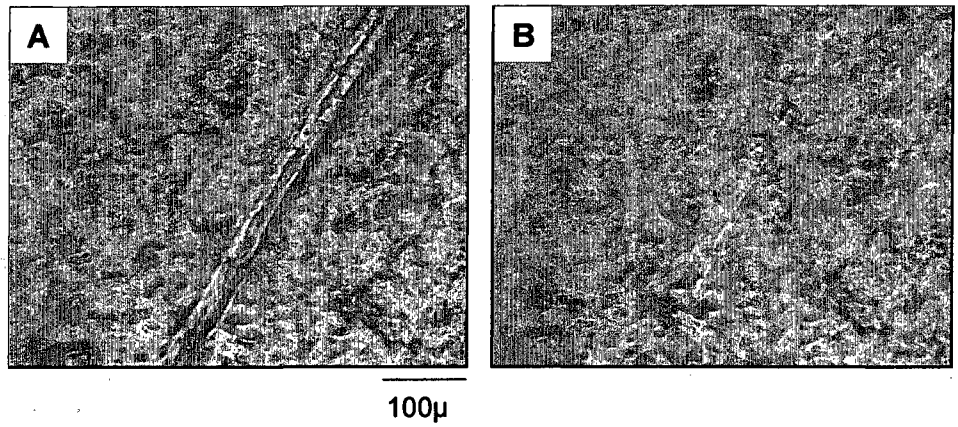

Figure VII-1. A - Optical image obtained immediately after the surface was subjected to 30 x 3 (length x depth) μm mechanical damage; B – Optical image of the same area 30 minutes later.

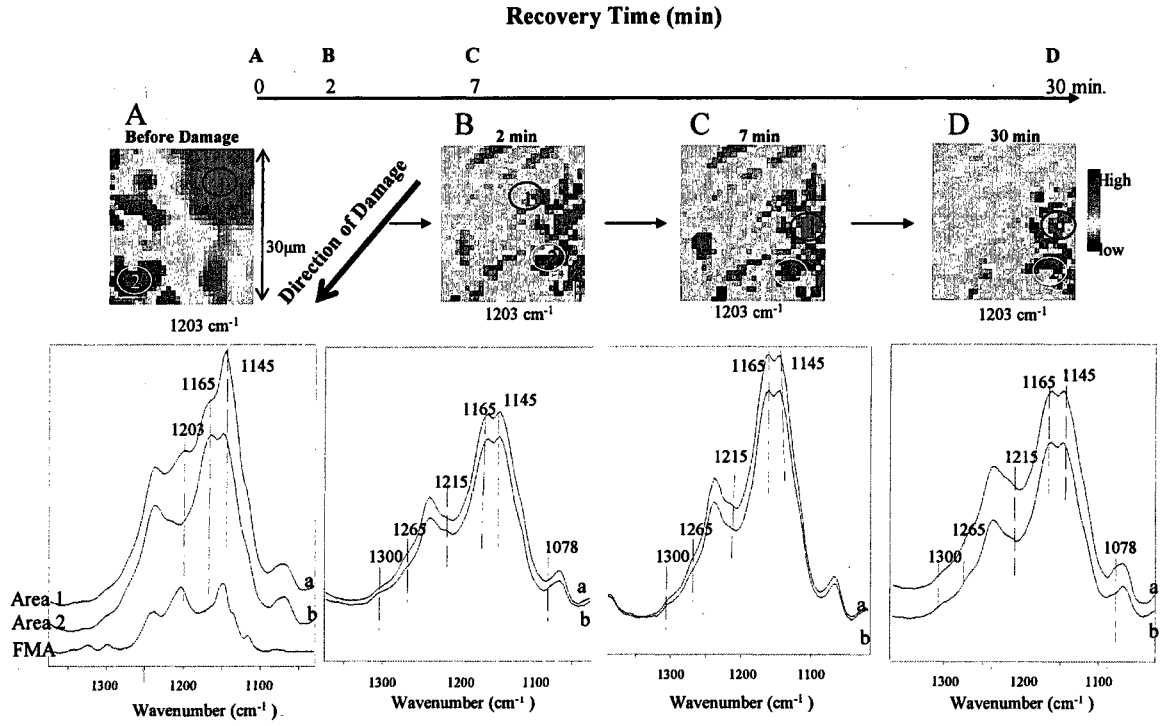

Figure VII-2-1. Internal reflection IR images (IRIRI) of the 1203 cm^{-1} band due to C-F stretching vibrations recorded from the surface area before the damage (A) and 2 min (B), 7 min (C), and 30 min (D) after. Traces a and b represent IR spectra recorded from areas 1 and 2 and Trace FMA represents the IR spectrum of poly(fluoromethacrylate).

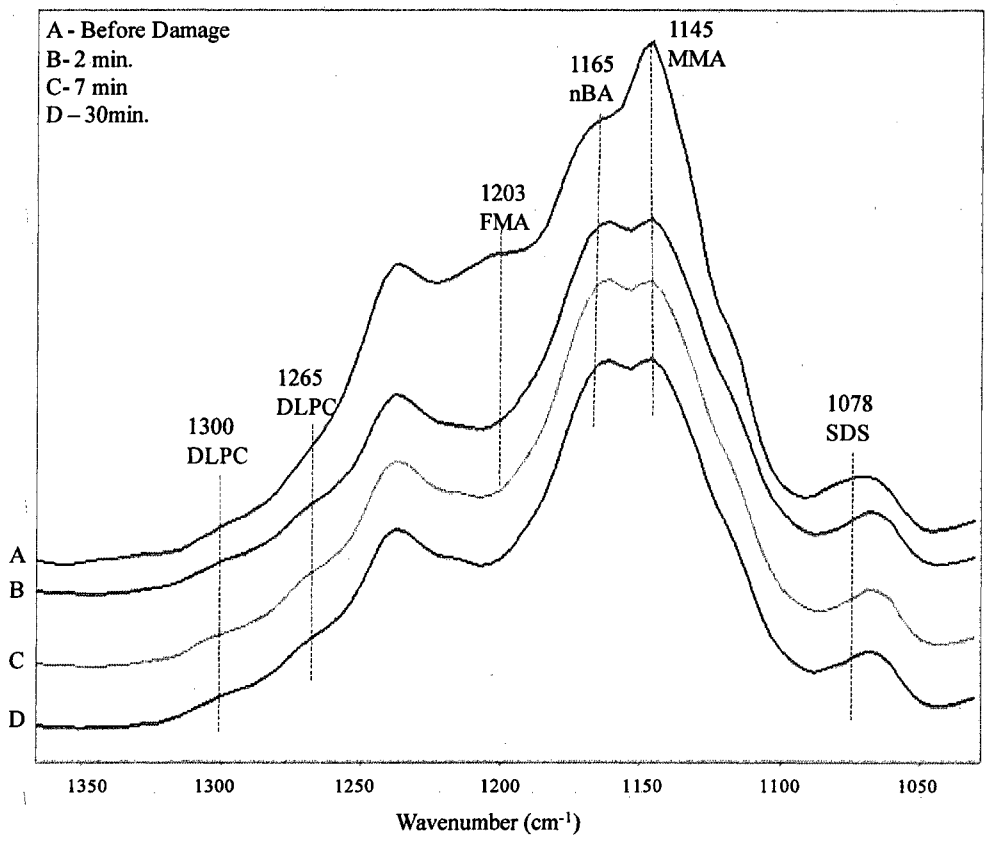

Figure VII-2-2. Average IR spectra recorded from 30x30 μm area: A- before damage; B – 2 min; C – 7 min; and D – 30 min of the recovery.

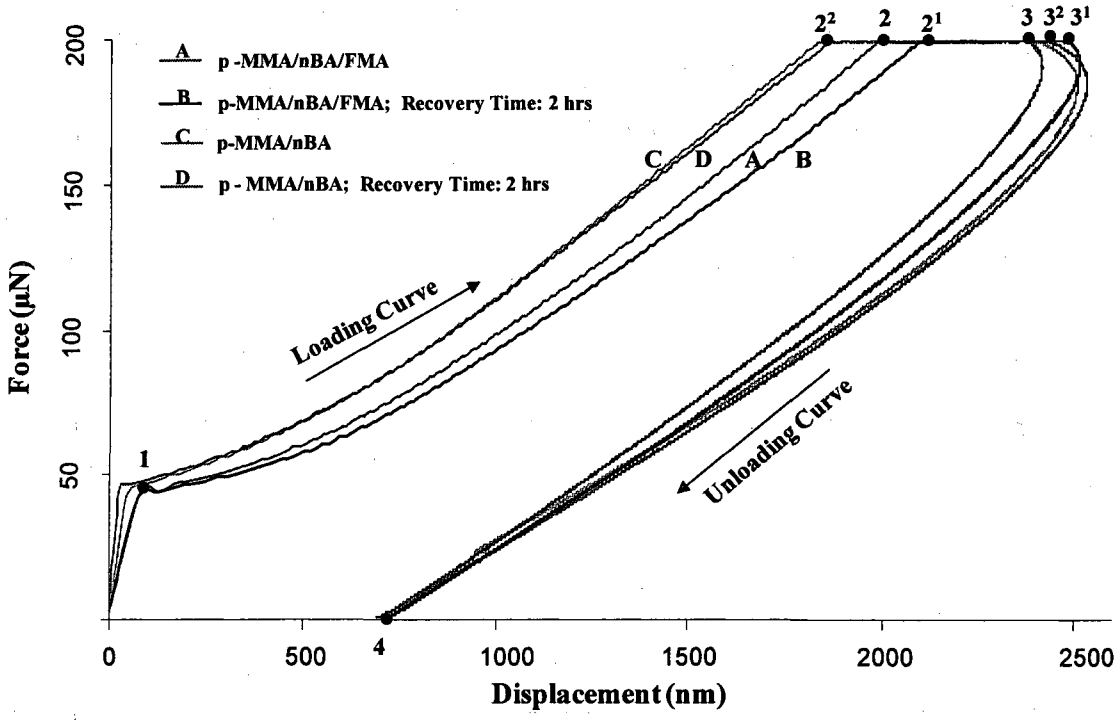

Figure VII-3. Nano-indentation force vs displacement curves for p-MMA/nBA/FMA (Trace A and B) and p-MMA/nBA (Trace C and D) copolymer films recorded using a maximum load of 200 μN at the loading rate of 20 μN/sec and unloading at 1 μN/sec and after 2 hrs.

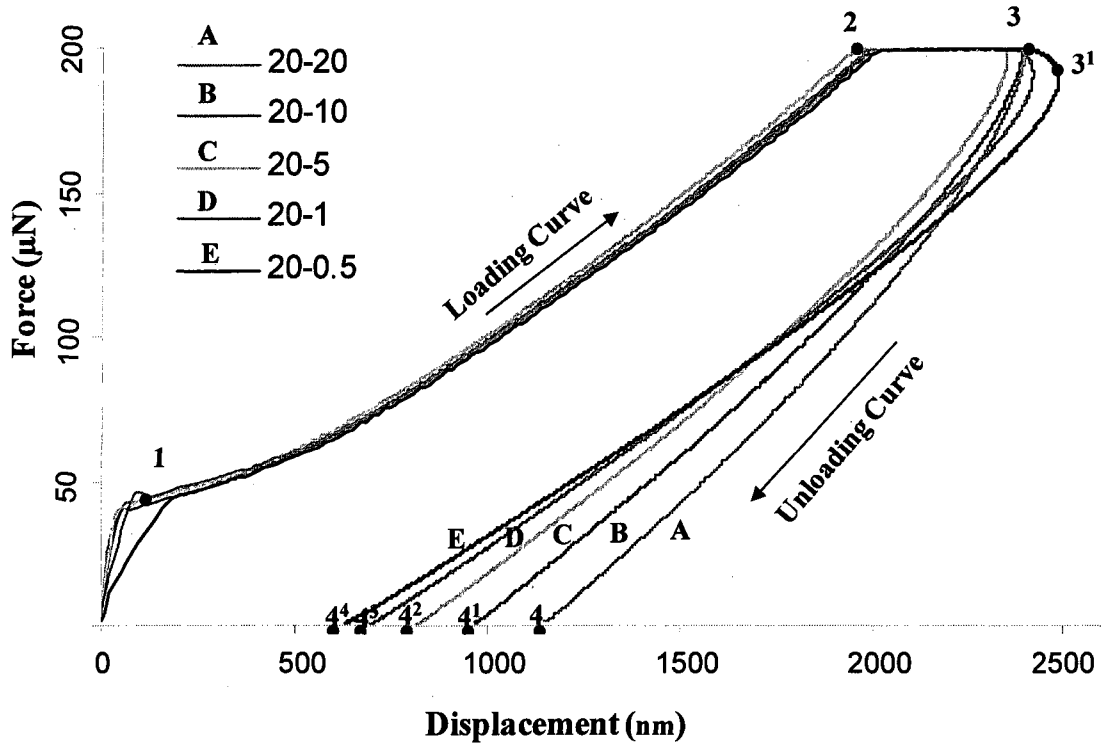

Figure VII-4-1. Nano-indentation force vs displacement curves for p-MMA/nBA/FMA copolymer films recorded using a maximum load force of 200 μN at the loading rate of 20 μN/sec and unloading rates at 20 (A), 10 (B) , 5 (C), 1 (D), and 0.5 (E) μN/sec.

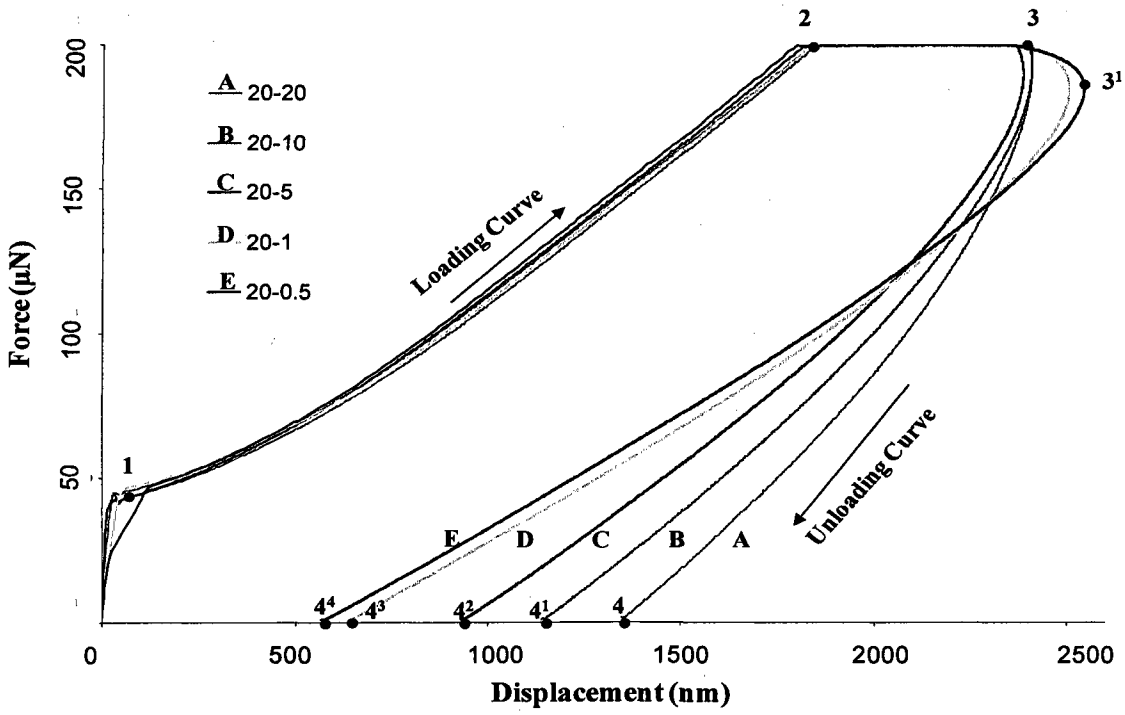

Figure VII-4-2. Nano-indentation force vs displacement curves for p-MMA/nBA copolymer films recorded using a maximum load force of 200 μN at the loading rate of 20 μN/sec and unloading rates at 20 (A), 10 (B) , 5 (C), 1 (D), and 0.5 (E) μN/sec.

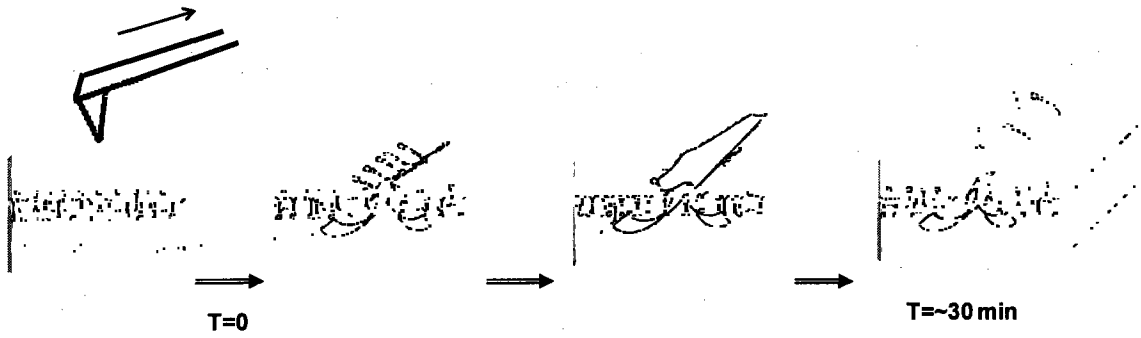

Figure VII-5. Schematic depiction of the proposed self-healing mechanism: 1 - mechanical surface damage; 2 – formation of groove and exposure of dispersing agents; 3 – diffusion and flow of low Tg pMMA/n-BA copolymer; 4 – self-repairing of the damage.

References

1. X. Chen, M.A. Dam, K. Ono, A.K. Mal, S.R. Nutt, K. Sheran, and F. Wudl, *Science*, 2002, 295, 1698.

2. M. Zako and N. Takano, *J. Int. Mater. Syst. Struct.*, 1999, 10, 836.

3. S.A. Haynes, F.R. Jones, K. Marhiya, W. Zhang, Proc. 15th Int. Conf. Composite Materials, Durban, June 27-July 1, 2005.

4. S.R. White, N.R. Sottos, P.H. Geubelle, J.S. Moore, M.R. Kessler, S.R. Sriran, E.N. Brown, S. Viswanathan, *Nature*, 2001, 409, 794.

5. S.M. Bleay, C.B. Loader, V.J. Hawyes, L. Humberstone, P.T. Curtis, *Composites*, 2001, A32, 1767.

6. M.R. Kessler, N.R. Sottos, S.R. White, *Composites*, 2003, 34A, 743.

7. P. Sonntag, P. Hoerner, A. Cheymol, G. Argy, G. Riess, and G. Reiter, *NatureMaterials*, 2004, 311.

8. P. Cordier, F. Tournilhac, C. Soulie′-Ziakovic, L. Leibler, *Nature*, 2008, 451, 977.

9. R.S. Trask, H.R. Williams, and I.P. Bond, *Bioinsp. Biomim.*, 2007, 2, 1.

10. A. Singh, W.R. Dreher, M.W. Urban, *Langmuir*, 2006, 22, 524.

11. A. Misra and M.W. Urban, *Macromolecules*, 2007, 40, 6190.

12. C. Pooley, D. Tabor, Proceedings of the Royal Society of London. Series , *Mathematical and Physical Sciences*, 1972, 329, 251.

13. D. Otts, P. Zhang, M. W. Urban, *Langmuir* 2002, 18, 6473.

14. D. J. Lestage, M. Yu, M. W. Urban, *Biomacromolecules* 2005, 6, 1561.

15. T. Nii, F. Ishii, *Colloids Surf. B: Biointerfaces* 2004, *39*, 57.

CHAPTER VIII

CONCLUSIONS AND FUTURE RECOMMENDATIONS

Due to their unique physical and chemical properties fluoropolymers (FPs) are highly useful materials. As outlined in Chapter I, numerous studies focus on synthesis of these materials which utilizes chlorofluorocarbons (CFCs), fluorine-containing surfactants, and other detailed synthetic and processing techniques. There are various avenues in fluorine containing colloidal particles which can be further explored, such as green synthesis of FPs without use of CFCs or fluorine-containing surfactants. Increasing the amount of FPs that can be incorporated in the colloidal dispersions, exploring bio-active dispersing agents and polymerization under environmentally benign conditions. Although synthesis is one aspect, applying colloidal dispersions on surface is major factor contributing to new applications. Ideally, one would like to synthesize fluorine containing colloids which can be directly deposited as coatings materials to obtain mechanically stable films with desired surface properties of FPs.

With this in mind, this research has explored numerous scientific issues regarding the development of stable colloidal dispersions and copolymer matrix affecting mechanism governing their film formation. By utilizing bio-active dispersing agents phospholipids (PLs), amount of heptafluorobutylmethacrylate (FBMA), heptafluorobutylacrylate (FBA), heptadecafluorodecylmethacrylate (FMA), and heptadecafluorodecylacrylate (FA) monomers can be increased from 8.5% w/w to 15% w/w which was otherwise not possible. Furthermore, upon incorporating PLs fluorine-containing dispersing agent was not required during synthesis. Colloidal dispersions containing fluoromonomers were observed to be non-spherical in which p-FP phase

exists on the p- methyl methacrylate/n-butyl acrylate (p-MMA/nBA) core, which was confirmed by utilizing various microscopic tools such as transmission electron microscopy (TEM), spectroscopically via solid state 2D nuclear magnetic resonance (NMR), and thermodynamic molecular modeling simulation.

Upon further investigation of the origin of non-spherical colloidal morphologies by copolymerizing MMA/FMA, nBA/FMA, and MMA/nBA/FMA with varying ratios of MMA:nBA, these studies showed that for p-MMA/FMA spherical morphologies are obtained due to random copolymerization of MMA and FMA. Further incorporations of nBA compositional heterogeneity began to appear at 50:50 MMA: nBA ratio and complete heterogeneous particles are formed for p-nBA/FMA copolymer colloids. During film formation the FP phase migrates preferentially to the film-air (F-A) interface and surface property gradients are achieved, with low friction coefficients and high water contact angle films. Surface properties were found to be directly related to the perfluoroalkylside chain length of fluoromonomers, with longer perfluoroalkyl side chain length provides more coverage of FPs at F-A interface leading to low friction properties. Due to low surface energy of FP phase thermo-responsiveness of films were observed leading to further migration of FP to the F-A interface. Further advances in this field can be achieved by applying the same synthetic process to the gaseous state monomers.

Another class of styrenics fluoromonomers were also investigated in these studies compare to fluoroacrylates and methacrylates fluorinated styrenes is less hydrophobic, as fluorine atom is dispersed on the aromatic ring. Upon copolymerizing pentafluorostyrene (PFS) with MMA, nBA, and poly (ethylene glycol) dimethacrylate

(PEG) monomers stable colloidal dispersions containing upto 30% w/w PEG was obtained. PEG was observed on the surface of p-MMA/nBA/PFS colloids. Upon coalescence heterogeneous films containing islands of PEGylated and p-MMA/nBA/PFS components were obtained and this heterogeneity and presence of PEG on the surface repels protein adsorption.

Other unique approach utilized in these studies is a two-step synthetic process in which first p-nBA/PFS was copolymerized as precursor and, in second-step, p-MMA/nBA was polymerized on the precursor particles. Uniform acorn-shaped particle morphologies were observed in which one phase consists of fluorinated segments and other phase consists of carbon-based segments. These acorn-shaped colloids are able to preferentially align in such a way that for high surface energy substrate (glass) p-MMA/nBA phase is towards the substrate and p-nBA/PFS phase is aligned towards the F-A interface and vice versa for low surface energy substrates (PTFE). Furthermore, by exploiting the advantages of heterogeneity at nano level, these acorn-shape colloids have potential in directed assembly, attachment of proteins or drugs on one side of colloidal particles with either on fluorinated or non-fluorinated phase and can be utilized in number of applications.